

2
2007

This is to certify that the
thesis entitled

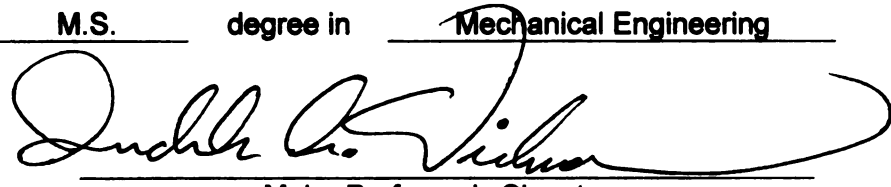
DROPLET EVAPORATION IN A QUIESCENT, MICRO-
GRAVITY ATMOSPHERE

presented by

Paul Raphael Cole

has been accepted towards fulfillment
of the requirements for the

M.S. degree in Mechanical Engineering



Major Professor's Signature

November 21, 2006

Date

MSU is an Affirmative Action/Equal Opportunity Institution

LIBRARY
Michigan State
University

PLACE IN RETURN BOX to remove this checkout from your record.
TO AVOID FINES return on or before date due.
MAY BE RECALLED with earlier due date if requested.

DATE DUE	DATE DUE	DATE DUE

DROPLET EVAPORATION IN A QUIESCENT, MICRO-GRAVITY ATMOSPHERE

By

Paul Raphael Cole

A THESIS

Submitted to
Michigan State University
in partial fulfillment of the requirements
for the degree of

MASTER OF SCIENCE

Department of Mechanical Engineering

2006

ABSTRACT

DROPLET EVAPORATION IN A QUIESCENT, MICRO-GRAVITY ATMOSPHERE

By

Paul Raphael Cole

Droplet evaporation is important in many applications and spans numerous research topics ranging from rocket fuel to crystal growth. In this thesis, the author gives a detailed analysis of the sensitivity of the droplet surface temperature and the droplet radius-squared to various physical parameters of common hydrocarbon fuels. Furthermore, the author has provided a brief optimization analysis in which the physical parameters are optimized in such a way that the time required for the droplet to completely evaporate is minimized. Due to the nonlinearity of the governing equations, a numerical algorithm was developed so that these analyses might be conducted.

Ad Matris Sapientia quod est non factum

ACKNOWLEDGEMENTS

First, I wish to thank the Mechanical Engineering department for its financial and academic support. Second, I wish to thank Mr. DeVon Washington for his many useful comments and suggestions. Third, I wish to thank Dr. Ronald Averill for introducing me to the power of the HEEDS© software.

And last but by no means least, I wish to thank Dr. Indrek S. Wichman, without whose knowledge and guidance this thesis would not have been possible.

TABLE OF CONTENTS

LIST OF TABLES.....	viii
LIST OF FIGURES.....	ix
Chapter 1: Introduction	1
1.1. Background	1
1.2. Motivation	1
1.3. Methodology	2
Chapter 2: Literature Survey	4
2.1. Overview	4
2.2. Survey	4
Chapter 3: The Governing Equations.....	9
3.1. Overview	9
3.2. The Ideal Gas Law	11
3.3. The Clausius–Clapeyron Relationship.....	12
3.4. General Governing Equations	14
3.5. Derivation of the Dimensionless Governing Equations.....	21

3.6.	Solutions for a Propane Droplet.....	23
Chapter 4: The Sensitivity Analysis.....		25
4.1.	Overview	25
4.2.	Computational Methodology	26
4.3.	Results and Discussion.....	27
4.3.1.	Sensitivity to the Gas Constant	27
4.3.2.	Sensitivity to the Latent Heat of Vaporization.....	31
4.3.3.	Sensitivity to the Boiling Temperature	36
4.3.4.	Sensitivity to the Ambient Temperature	40
4.3.5.	Sensitivity to the Initial Temperature.....	44
4.3.6.	Sensitivity to the Specific Heat of the Droplet Vapor.....	47
4.3.7.	Sensitivity to the Specific Heat of the Liquid Comprising the Droplet	51
4.3.8.	Sensitivity to the Lewis Number of the Fuel	55
4.3.9.	Sensitivity to the Ambient Mass Fraction.....	59
4.3.10.	Sensitivity to the Mass Fraction above the Evaporated Surface	63
4.3.13.	Final Conclusions for the Sensitivity Analysis	67

Chapter 5: The Optimization Study	71
5.1. Overview	71
5.2. Computational Methodology	72
5.3. Results and Discussion.....	76
5.3.1. Optimization of the Gas Constant, the Latent Heat of Vaporization, the Boiling Temperature, the Vapor Specific heat, the Droplet Specific Heat, the Vapor Thermal Conductivity, and the Droplet Density.....	76
5.3.2. Optimization of the Gas Constant, the Latent Heat of Vaporization and the Boiling Temperature.....	79
5.4. Final Conclusions.....	81
Chapter 6: The Asymptotic Analysis	83
Chapter 7: Notes concerning the Computational Algorithms	91
Bibliography.....	93

LIST OF TABLES

Table 1. Parameter ranges for those that are varied.....77

Table 2. Top – ranking designs.....77

Table 3. Parameter ranges for those that are varied.....79

Table 4. Top – ranking designs.....80

LIST OF FIGURES

Figure 1. The solution for the surface temperature and for the radius-squared for a propane droplet.....	24
Figure 2. The sensitivity of the surface temperature to the gas constant.....	29
Figure 3. The surface temperature solution.....	29
Figure 4. The sensitivity of the radius-squared to the gas constant.....	30
Figure 5. The radius-squared solution.....	30
Figure 6. The sensitivity of the surface temperature to the latent heat of vaporization.....	33
Figure 7. The surface temperature solution.....	33
Figure 8. The sensitivity of the radius-squared to the latent heat of vaporization.....	34
Figure 9. The radius-squared solution.....	34
Figure 10. Variation of the surface temperature sensitivity with the latent heat at select instances of time.....	35
Figure 11. Variation of the radius-squared sensitivity with the latent heat at select instances of time	35
Figure 12. The sensitivity of the surface temperature to the boiling temperature.....	38
Figure 13. The surface temperature solution.....	38

Figure 14. The sensitivity of the radius-squared to the boiling temperature.....	39
Figure 15. The radius-squared solution.....	39
Figure 16. The sensitivity of the surface temperature to the ambient temperature.....	42
Figure 17. The surface temperature solution.....	42
Figure 18. The sensitivity of the radius-squared to the ambient temperature.....	43
Figure 19. The radius-squared solution.....	43
Figure 20. The sensitivity of the surface temperature to the initial surface temperature..	45
Figure 21. The surface temperature solution.....	45
Figure 22. The sensitivity of the radius-squared to the initial surface temperature.....	46
Figure 23. The surface temperature solution.....	46
Figure 24. The sensitivity of the surface temperature to the specific heat of the droplet vapor.....	49
Figure 25. The surface temperature solution.....	49
Figure 26. The sensitivity of the radius-squared to the specific heat of the droplet vapor.....	50
Figure 27. The radius-squared solution.....	50
Figure 28. The sensitivity of the surface temperature to the droplet specific heat.....	53
Figure 29. The surface temperature solution.....	53

Figure 30. The sensitivity of the radius-squared to the droplet specific heat.....	54
Figure 31. The radius-squared solution.....	54
Figure 32. The sensitivity of the surface temperature to the fuel Lewis number.....	57
Figure 33. The surface temperature solution.....	57
Figure 34. The sensitivity of the radius-squared to the fuel Lewis number.....	58
Figure 35. The radius-squared solution.....	58
Figure 36. The sensitivity of the surface temperature to the ambient mass fraction.....	61
Figure 37. The surface temperature solution.....	61
Figure 38. The sensitivity of the radius-squared to the ambient mass fraction.....	62
Figure 39. The radius-squared solution.....	62
Figure 40. The sensitivity of the surface temperature to the evaporated mass fraction....	65
Figure 41. The surface temperature solution.....	65
Figure 42. The sensitivity of the radius-squared to the evaporated mass fraction.....	66
Figure 43. The radius-squared.....	66
Figure 44. A plot of eqn. (11.i) for contours of constant latent heat.....	70
Figure 45. A close-up of Figure 44 in the vicinity of the contour intersections.....	70

Figure 46. Burn-out time per design evaluation. The horizontal line represents the burn-out time for a propane droplet, i.e., the baseline design.....	77
Figure 47. Burn-out time per design evaluation. The horizontal line represents the burn-out time for a propane droplet, i.e., the baseline design.....	80
Figure 48. Solutions for the surface temperature, the radius-squared and the χ -parameter for a large latent heat. Note χ is 10 times larger for illustration purposes.....	84
Figure 49. Asymptotic solutions for the interval of increasing surface temperature and radius-squared.....	86
Figure 50. Asymptotic solution for the surface temperature in the vicinity of the maximum radius-squared.....	89
Figure 51. Asymptotic solution for the radius-squared in the vicinity of the maximum radius-squared.....	89
Figure 52. Asymptotic solution for the χ -parameter in the vicinity of the maximum radius-squared.....	90

Chapter 1: Introduction

1.1. Background

In the study of a physical system described by mathematical relationships it is essential to pare the system down to its most important elements, while at the same time retaining that system's essential nature. Then its behavior can be described in terms of those elements. In theoretical analysis the elements are the dimensionless parameters that appear in the equations describing the problem. The number of parameters may range from only one (e.g. the Reynolds number in laminar, incompressible fluid mechanics), to dozens (as in combined fluid mechanics/combustion/heat transfer studies). A theoretical or mathematical model is commonly understood to be optimized for the description of a particular process when the number of parameters is minimal. How this minimization is to be accomplished has been a subject of discussion since the dawn of the scientific age. On a historical note, Antoine de Saint-Exupery (French writer and aviator, 1900–1944) said “A designer knows he has achieved perfection not when there is nothing left to add, but when there is nothing left to take away.”

1.2. Motivation

This thesis examines an evaporating droplet in a quiescent atmosphere. This problem was chosen for two reasons. First, as a pseudo-combustion problem it has relevance to the huge and growing discipline of research into the combustion of fuel

droplets in oxidizing gas flows. This is a mainstay topic of combustion research on which many lengthy articles and reviews have been written. Furthermore, evaporation is not limited to fuels but is also important in other sciences such as cloud physics and biological crystal growth [10].

The second reason is that this problem can be simplified to eliminate all combustion and flow quantities while still retaining a fairly large number of dimensionless parameters in the governing equations. Hence, the relatively simple physical problem of an evaporating quiescent droplet can be extremely difficult to examine from the standpoint of running sufficient numbers of cases to encompass the phenomenon or even to make reliable generalizations and predictions. It is difficult to run a one-parameter flow system within a specified range of operating Reynolds numbers; one can imagine the difficulty of operating a system with approximately ten parameters that must be specified and controlled to remain within specified intervals.

1.3. Methodology

The first goal of this thesis is to examine the influence of a large number of parameters on droplet evaporation. The influence must be examined in a careful, rational way even for this relatively simple example. The procedure outlined here exemplifies the need for even more careful considerations of complicated problems that may, in addition, involve chemical reactions, non-symmetric flows and other difficulties which were removed at the outset from our model. If it is difficult to sort out the importance of

parameters when there are few, it will be correspondingly more difficult to accomplish this sorting when there are many.

Sensitivity analyses related to this thesis have been systematized for large systems of chemical reaction equations. These studies benefit from the qualitatively identical mathematical structure of the chemical kinetic equations. Their response to temperature is functionally the same, and the sensitivity analysis reduces to one of sorting out areas in the temperature spectrum where certain groups of reactions dominate other groups of reactions. In the problem considered here, by contrast, there is a set of “physical” processes that lead to a set of equations, each of which describes a different physical process. The problem is then not one of sorting out the dominant members of a certain class (e.g. among a large set of reactions) but rather one of sorting out the important and dominant physical terms in the equations themselves before any approximations were made. This is an altogether different approach with an altogether different goal.

The second goal of this thesis is to study the results of parameter optimization so that droplet lifetime is minimized. This is something of a novel approach to studies in combustion although the importance of evaporation cannot be disregarded: the evaporation process can be the slowest process, which consequently determines the overall burning rate [19].

Chapter 2: Literature Survey

2.1. Overview

There are relatively few studies devoted to pure evaporation; rather, the majority of archival research on droplets seems to be in the actual combustion process and/or flame behavior. This is somewhat surprising in light of the fact that evaporation would seem to constitute the simpler “model” problem which should be solved first. However, the papers that are described in the following section seem to be relevant to this study in that they offer commensurate computational and experimental results. The following section seeks to highlight the important aspects of the corresponding works.

2.2. Survey

J. Hegseth *et al.* [10] experimentally demonstrated to show that when a droplet evaporates sufficiently fast, it exhibits a vigorous flow in the interior; a flow that is driven by surface tension gradients. The D^2 -law theory formulated by Maxwell assumed that the evaporation process is controlled by a mass diffusion process exterior to the droplet. If there is no convection, then the liquid interior of the evaporating droplet must supply the heat to the surface for vaporization. In this thesis, we have assumed that the motion inside the droplet is negligible and that Marangoni effects are negligible.

Vai-meng Ha *et al.* [9] intended to investigate the onset and physical mechanisms of the Marangoni instability of an evaporating droplet. Generally, evaporation at the surface of a liquid is an unsteady process involving heat and mass transport. Additionally, the process of evaporation also leads to a local reduction in the temperature of the bulk liquid near the surface. The Marangoni instability may then be induced by surface temperature reduction and the consequent variation in surface tension. With the quasi-steady approximation (i.e., the regression of the droplet is negligible during evaporation), the surrounding gas motion is asymptotically steady and the temperature distribution of the droplet is temporarily frozen at each specified instant. Thus, the authors derived a lower limit of the onset of Marangoni instability via a linear stability analysis. Although the evaporation of a droplet is never a steady process since the radius, surface temperature, and hence the evaporation rate decrease during evaporation, the time scales of the gas phase are two orders of magnitude smaller than the time scale of heat diffusion in the liquid phase. Therefore, when the interest is mainly on the liquid phase, the gas phase can be treated as asymptotically steady since its response time is so much faster than that of the liquid phase. For this thesis we use the assumption of a negligible regression rate to simplify the boundary conditions.

T. Elperin *et al.* [7] numerically investigated the evaporation of a spherical droplet immersed in a stagnant, sub-critical, radiative gaseous mixture. Here, heat flux from the high temperature surrounding conducts to the droplet causing the droplet to evaporate. The authors showed that, in the case of sub-critical evaporation, neglecting the liquid volumetric expansion causes underestimation of the evaporation rate at the initial stage and overestimation of the evaporation rate at the final stage of the evaporation process.

Furthermore, the authors demonstrated the significance of liquid thermal expansion during the evaporation process. Some of the oversimplifying assumptions used in this work were: (1) the quasi-steady behavior for the gaseous phase heat and mass transfer, (2) the thermo-physical properties were evaluated at some reference condition, (3) the “1/3” rule was used for averaging the thermo-physical properties, (4) liquid thermal expansion and radiation effects were negligible. However, the quasi-steady assumption for droplet evaporation is valid when thermal (t_T) and diffusion relaxation (t_D) times are much smaller than the droplet lifetime. The authors demonstrated that evaporation of highly volatile droplets in a hot gaseous medium cannot be assumed quasi-steady. Additionally, liquid volumetric expansion is significant. For this thesis, the temperature of the ambient, i.e., the gaseous medium, is taken as room temperature thereby allowing the quasi-steady assumption.

R. Digilov *et al.* [5] showed that Trouton’s empirical rule for the entropy of vaporization follows from the similarity of the potential function of molecular interaction, thus illustrating that the rule is associated with the law of corresponding states. Frederick Thomas Trouton (1863-1922) developed an empirical rule that makes the following statement: for most liquids at atmospheric pressure, the ratio of latent heat of vaporization to normal boiling point has a value between 75 and 80 kJ/kmol-K for a large number of different pure substances. If one wishes to obtain a dimensionless result, Trouton’s rule can be formulated to read:

$$\frac{L_v}{RT_b} \sim O(10)$$

Water and alcohols do not follow this rule exactly – in fact, only for elemental liquids whose molecules are quasi-spherical and non-polar does this rule hold reasonably well. Furthermore, the authors showed that Trouton’s empirical rule should be reformulated to read “constant within a family of similar substances alone, and possibly differing for substances from different groups.”¹ For this thesis, we have restricted possible fuels to hydrocarbons, thus appreciably maintaining Trouton’s rule.

Kozyrev *et al.* [15] examined a diffusion model for droplet evaporation which considered the reduction in the droplet temperature and vapor pressure near its surface. The evaporation of a single spherical droplet can be regarded as classical; in its simplest form, it was solved by Maxwell in 1877. However, Maxwell assumed the vapor above the droplet surface was always saturated, which is generally not true. Furthermore, the concentration of saturated vapor at the surface is determined by the droplet temperature rather than the ambient temperature. In their study of the vapor and heat fluxes, the authors confined themselves to the simplest assumptions, viz., the linear diffusion of molecules and the supply of energy to the evaporating droplet by heat conduction. Overall, the model allowed estimation of the condensation coefficient of the vapor molecules from the experimental form of this dependence. For this thesis, we have not assumed that the vapor above the droplet is a function of the ambient temperature; on the contrary, the droplet temperature is one of the variables sought.

Zhu *et al.* [27] investigated the evaporation of fuel droplets (n-heptane) in high-pressure environments where the thermodynamic conditions exceed the critical state of

¹ Pg. 20

the fuel. Droplet gasification in such surroundings is important for diesel engines and liquid rockets. To model such conditions is no simple task since the conventional “low–pressure” models generally break down in high–pressure situations; in high–pressure surroundings, mass transport within the droplet interior cannot be neglected. To make matters more complex, as the droplet surface approaches the critical state, the latent heat of vaporization, as well as the surface tension, goes to zero. For this thesis, it has been assumed that the droplet evaporates under atmospheric conditions.

Ghassemi *et al.* [8] experimentally investigated the evaporation characteristics of single and multi–component droplet which were suspended from the tip of a quartz fiber in normal gravity conditions. In this study, the authors varied the environment pressure from atmospheric to 25 times atmospheric; the temperature, 400–700 °C. For single droplets, the authors observed the classical D^2 –law in the last stages of the evaporation process. They also observed that an increase in ambient temperature would act to decrease the total droplet lifetime. From their experiments, they found that when the ambient temperature is not too high (relative to the boiling temperature), the interior temperature is not uniform. Under this condition, the evaporation process does not exactly follow the D^2 –law. For this thesis, there is a large enough difference between the ambient and the boiling temperature to allow a linear evaporation process.

Chapter 3: The Governing Equations

3.1. Overview

The equations and boundary conditions for an evaporating droplet in a quiescent atmosphere are derived in the following sections. These include the conservation equations for the liquid phase and the gas phase. For the liquid phase, the domain is $0 < r < r_s(t)$; for the gas phase (i.e., the vapor above the surface of the droplet, which is assumed to be an ideal gas), the domain of interest is $r_s(t) < r < \infty$. The surface temperature and square of the droplet radius (i.e., the surface area) are both functions of time. The physical parameters are as follows: R (the gas constant), L_v (the latent heat of vaporization), T_b (the boiling temperature), T_∞ (the ambient temperature), T_0 (the initial droplet temperature), C_p (the constant-pressure specific heat of the vapor), C_L (the constant-pressure specific heat of the liquid), Le_F (the fuel Lewis number), $Y_{F\infty}$ (the ambient fuel mass fraction), Y_{Fb} (the fuel mass fraction that exists at the boiling temperature), k_g (the thermal conductivity of the droplet vapor), and ρ_L (the density of the droplet).

A relevant quantity in this analysis is ε , which is a ratio of gas and liquid densities. This parameter is defined in equation (1).

$$\varepsilon = \rho_g / \rho_L \quad (1)$$

Here the subscript “g” refers to the vapor above the droplet surface (assumed to obey the ideal gas law) and the subscript “L” refers to the liquid comprising the droplet. Under atmospheric conditions, $\varepsilon \sim O(10^{-3})$. At high pressure, ε increases and achieves a value of unity at the critical point. The parameter ε relates to the derivation of appropriate boundary conditions and also serves as an indication of suitable “disperse” conditions.

A major assumption in this study is that the gas-phase analysis is quasi-steady, i.e., at any instant in time, the process can be treated as if the gas phase were at steady state. It can be shown that the characteristic response time of the gas is much shorter than the vaporization time, i.e., $t_g \ll t_v$ where

$$t_v \sim \frac{r_0 / v_{g,0}}{\varepsilon}$$

and

$$t_g \sim \left(\frac{3r_0^2}{\alpha_{T,g\infty}} \right)$$

Clearly, as ε diminishes, t_v becomes large. This means that evaporation is a faster process relative to the thermal equilibration of the gas. Hence, it is not unreasonable to expect a nearly uniform droplet temperature throughout the vaporization process.

3.2. The Ideal Gas Law

The “gas” under consideration is the vapor around the droplet surface as well as the surrounding gas phase. The ideal gas law (IGL) is typically written in the following form:

$$pV = mRT$$

where $m = MN$, i.e., ($mass [kg] = (molar\ mass [kg/kmol]) \times (number\ of\ moles [kmol])$), p is the pressure in kPa , V is the volume in m^3 , R is the particular gas constant for the gas under consideration in $kJ/kg-K$ and T is the temperature in K . Note that the IGL can also be written in the following form:

$$p = \rho RT$$

where ρ is the density in kg/m^3 of the gas at the pressure p and temperature T . It has been assumed that atmospheric pressure exists at the surface of the droplet, i.e., $p = p_{atm} = 101.325\ kPa$. So, at the droplet surface toward the gas side, we can write the following expression:

$$\rho_s(t) = \frac{p_{atm}}{RT_s(t)}$$

For the purposes of this study, we write the following:

$$\rho_g = \frac{p_{atm}}{RT_b}$$

Now, we shall test equation (1); for ethane, $\rho_g \approx 1.986 \text{ kg/m}^3 \rightarrow \varepsilon \approx 0.0036$ thus equation (1) seems to be satisfied for this hydrocarbon. In terms of the IGL, we can describe the ε -term in the following way:

$$\varepsilon = \frac{P_{atm}}{\rho_L R T_b}$$

3.3. The Clausius–Clapeyron Relationship

In this section, a method for expressing the Clausius–Clapeyron relationship in terms of mass fraction rather than pressure is given. Such a form will allow this relationship to be used as a boundary condition.

A detailed derivation of this relationship is usually found in most thermodynamics textbooks. The conventional form is written as:

$$\ln\left(\frac{p_2}{p_1}\right)_{sat} \approx \frac{L_v}{R} \left(\frac{1}{T_1} - \frac{1}{T_2} \right)_{sat}$$

The subscripts “1” and “2” refer to the states under consideration. Specifically, the derivation considers two thermodynamic states, 1 and 2, for the same chemical species. One of the assumptions associated with this relationship is that the change in volume (induced by evaporation) is equal to the volume of the vapor produced. Another assumption is that the latent heat of vaporization is constant over the temperature range from state 1 to state 2.

The mass fraction of species j is defined as the ratio of the mass of species j to the total mass, i.e.,

$$Y_j = \frac{m_j}{m}$$

This means the IGL can be written as $pY_j = m_jRT$. For an ideal gas mixture at constant volume, we can define the gas phase mole fraction as

$$y_j = \frac{p_j}{p}$$

where p_j is the partial pressure of species j and p is the total pressure. Alternatively, we can write

$$y_j = \frac{N_j}{N}$$

where N_j is the number of moles of species j and N is the number of moles of the mixture.

Since $m = MN$, we can write the relationship between y_j and Y_j as

$$Y_j = y_j \frac{M_j}{M}$$

Finally, we can say

$$\frac{p_2}{p_1} = \frac{y_2}{y_1} = \frac{M_1}{M_2} \frac{Y_2}{Y_1} = \frac{Y_2}{Y_1}$$

Note that $M_1 = M_2$ since there is just one specie under consideration, viz., the fuel vapor.

Hence, the Clausius–Clapeyron relationship can be written as follows:

$$Y_2 = Y_1 \exp\left(\frac{L_v}{R} \left\{ \frac{1}{T_1} - \frac{1}{T_2} \right\}\right)$$

For this study, state 2 exists at the droplet surface; state 1 exists at the boiling condition.

In [9], the authors used a similar form of this relationship for a boundary condition at the liquid/vapor interface.

3.4. General Governing Equations

The spherically symmetric conservation equations of mass, species, and energy are given by equation (2). The initial conditions are given by equation (3) and the boundary conditions are given by equation (4).

$$\frac{\partial \rho_g}{\partial t} + \frac{1}{r^2} \frac{\partial}{\partial r} \left(\rho_g V_g r^2 \right) = 0 \quad (2.i)$$

$$\begin{aligned} \frac{\partial}{\partial t} \left(\rho_g Y_i \right) + \frac{1}{r^2} \frac{\partial}{\partial r} \left(\rho_g V_g r^2 Y_i \right) \\ = \frac{1}{r^2} \frac{\partial}{\partial r} \left(\rho_g D_i r^2 \frac{\partial Y_i}{\partial r} \right) \end{aligned} \quad (2.ii)$$

$$\begin{aligned} \frac{\partial}{\partial t}(\rho_g C_p T_g) + \frac{1}{r^2} \frac{\partial}{\partial r}(\rho_g V_g C_p r^2 T_g) \\ = \frac{1}{r^2} \frac{\partial}{\partial r} \left(\rho_g C_p Le D_F r^2 \frac{\partial T_g}{\partial r} \right) \end{aligned} \quad (2.iii)$$

$$r_s(t=0)=r_0 \quad (3.i)$$

$$T(r,t=0)=T_0 \quad (3.ii)$$

$$T(r \rightarrow \infty, t)=T_\infty \quad (4.i)$$

$$T(r=r_s, t)=T_s(t) \quad (4.ii)$$

$$Y_{F_s}(r=r_s, t)=Y_{F_b} \exp \left(\frac{L_v}{R} \left\{ \frac{1}{T_b} - \frac{1}{T_s(t)} \right\} \right) \quad (4.iii)$$

$$\rho_g (V_g - \dot{r}_s) = \dot{m}'' = -\rho_l \dot{r}_s \quad (4.iv)$$

$$\rho_g (V_g - \dot{r}_s) Y_F - \rho_g D_F \frac{\partial Y_F}{\partial r} = \dot{m}'' \quad (4.v)$$

$$\rho_g (V_g - \dot{r}_s) Y_{Ox} - \rho_g D_{Ox} \frac{\partial Y_{Ox}}{\partial r} = 0 \quad (4.vi)$$

$$\rho_g (V_g - \dot{r}_s) L_v + \dot{q}_l'' = \dot{q}_g'' \quad (4.vii)$$

Equation (4.iii) is the Clausius-Clapeyron equation which is discussed in section 3.3. Equation (4.v) and (4.vi) are mass-conservation equations for the fuel and oxidizer, respectively [19]; they are also the classic boundary conditions in mass diffusion problems [25]. Equation (4.vii) is an energy balance at the liquid-vapor interface, i.e., this equation equates the difference in conductive fluxes to the energy required for

vaporizing the liquid at the surface [19]. Note that the vapor and the liquid heat fluxes can be expressed according to equation (5).

$$\dot{q}_l'' = k_l \frac{\partial T_l}{\partial r} \quad (5.i)$$

$$\dot{q}_g'' = k_g \frac{\partial T_g}{\partial r} \quad (5.ii)$$

Note that equation (5.i) describes the heat flux entering the liquid interior, and equation (5.ii) describes the heat entering the vapor above the droplet surface.

The droplet regression rate is considered negligible insofar as the gas-phase response is concerned [9]. This can be exploited when we examine the relative velocity term, i.e. $\left(V_g - \dot{r}_s \right)$. If we make the following definitions:

$$V_g^* = V_g / V_{g,0}, \quad r_s^* = r_s / r_0, \quad t^* = t / t_v$$

then we can obtain an estimate for the relative velocity, viz.,

$$V_g - \dot{r}_s = V_{g,0} \left(V_g^* - \frac{r_0 / V_{g,0}}{t_v} \frac{dr_s^*}{dt^*} \right)$$

Recalling the magnitude of the vaporization response time, we can write the following expression:

$$V_g - \dot{r}_s \sim V_{g,0} \left(V_g^* - \varepsilon \frac{dr_s^*}{dt^*} \right).$$

Clearly, as the value of ε diminishes, then the term $\varepsilon \frac{dr_s^*}{dt^*}$ becomes negligible.

This means that the regression rate of the droplet can be neglected in the boundary conditions in comparison with the vapor velocity. Similarly, since $t_l \ll t_v$, the droplet temperature during most of the burning process is essentially uniform, as already mentioned.

The heat flux entering the liquid interior (multiplied by the surface area) must be equal to the volumetric heat capacity of the liquid droplet (multiplied by the transient rate of temperature rise), i.e.,

$$\left(\dot{q}_l'' \right) \left(4\pi r_s^2 \right) = \left(\frac{4\pi}{3} r_s^3 \rho_l C_l \right) \left(\frac{\partial T_l}{\partial t} \right)$$

where $\frac{\partial T_l}{\partial t} = \frac{dT_s}{dt}$ since the droplet temperature is spatially uniform [19].

Now equations (2.i–iii) need to be integrated under the boundary conditions (equations (4.i–vii)) and the quasi-steady assumption for the gas phase i.e., the partial derivatives with respect to time are zero. On integrating equation (2.i), we obtain an expression of the mass flow rate.

$$\rho_g V_g r^2 = \frac{\dot{m}}{4\pi} = \dot{M} \quad (6.i)$$

Using this result in conjunction with a negligible regression rate, we can re-cast equations (4.v-vi) as

$$\dot{M} Y_F - \rho_g D_F r^2 \frac{\partial Y_F}{\partial r} = \dot{M} \quad (6.ii)$$

$$\dot{M} Y_{Ox} - \rho_g D_{Ox} r^2 \frac{\partial Y_{Ox}}{\partial r} = 0 \quad (6.iii)$$

Equation (2.iii) will be evaluated via integration, substitution of the \dot{M} term, then utilizing equations (4.ii) and (5.ii) to evaluate the integration constant. For convenience, equation (5.ii) will be expressed in terms of the Lewis number and mass diffusivity term.

$$\left(\rho_g V_g C_p r^2 T_g \right) = \left(\rho_g C_p Le D_F r^2 \frac{\partial T_g}{\partial r} \right) + C_0$$

$$\dot{M} C_p T_g = \rho_g C_p Le D_F r^2 \frac{\partial T_g}{\partial r} + C_0$$

$$T_g(r=r_s, t) = T_s(t)$$

$$\rho_g C_p Le D_F \left(r^2 \frac{\partial T_g}{\partial r} \right)_{r_s, T_s} = r_s^2 \dot{q}_g''$$

$$C_0 = \dot{M} C_p T_s - r_s^2 \dot{q}_g''$$

Thus, we arrive at the following equation for the gas-phase energy equation:

$$\dot{M} C_p \left(T_g(t, r) - T_s(t) \right) + r_s^2 \dot{q}_g'' = \rho_g C_p Le D_F r^2 \frac{\partial T_g(t, r)}{\partial r}$$

This equation must be integrated again. We say that $T_g(t, r \rightarrow \infty) - T_s(t) = T_\infty$, which yields equation (7).

$$T_g(r, t) - T_s(t) + \frac{r_s^2 \dot{q}_g^*}{\dot{M} C_p} = \left(T_\infty - T_s(t) + \frac{r_s^2 \dot{q}_g^*}{\dot{M} C_p} \right) \exp \left(-\frac{\dot{M} C_p}{k_g r} \right) \quad (7)$$

Now we examine equation (6.ii), which can be re-arranged to read as follows:

$$\dot{M} (Y_F - 1) = \rho_g D_F r^2 \frac{\partial Y_F}{\partial r},$$

On integration under the limits $Y_F(r = r_s) = Y_{Fs}$ and $Y_F(r \rightarrow \infty) = Y_{F\infty}$, we obtain the following solution (for $k_g/C_p = \rho_g D_F Le_F$):

$$\frac{\dot{M} C_p}{k_g r_s} Le_F = \ln \left(\frac{1 - Y_{F\infty}}{1 - Y_{Fs}} \right)$$

Later on, it will prove convenient to define the following surface parameter given in equation (8):

$$\chi = \frac{\dot{M} C_p}{k_g r_s} = \frac{1}{Le_F} \ln \left(\frac{1 - Y_{F\infty}}{1 - Y_{Fs}} \right) \quad (8)$$

If now we evaluate equation (7) at the droplet surface, i.e., at $r = r_s$, we can make the following statement:

$$\dot{q}_g'' = \frac{\dot{M} C_p}{r_s^2} \left(T_\infty - T_s(t) + \frac{r_s^2 \dot{q}_g''}{\dot{M} C_p} \right) e^{-\chi} = \frac{\dot{M} C_p}{r_s^2} (T_\infty - T_s(t)) e^{-\chi} + \dot{q}_g'' e^{-\chi}$$

or

$$\dot{q}_g'' = \frac{\dot{M} C_p (T_\infty - T_s(t))}{r_s^2} \frac{e^{-\chi}}{1 - e^{-\chi}}$$

$$\Rightarrow \dot{q}_g'' = \frac{k_g (T_\infty - T_s(t))}{r_s} \left(\frac{\chi}{e^\chi - 1} \right)$$

On recalling equation (4.vii) and the expression for the heat flux entering the liquid, we can use the above result to obtain the following expression:

$$\frac{k_g (T_\infty - T_s(t))}{r_s} \left(\frac{\chi}{e^\chi - 1} \right) = \dot{M} L_v + \frac{l}{3} r_s \rho_l C_l \frac{dT_s}{dt}$$

This expression can be re-arranged to yield equation (9.i).

$$\frac{dT_s}{dt} = \frac{\chi}{\left(\frac{r_s^2}{\bar{\alpha}_T} \right)} \left(\frac{(T_\infty - T_s(t))}{e^\chi - 1} - \frac{L_v}{C_p} \right) \quad (9.i)$$

where $\bar{\alpha}_T = \frac{3k_g}{\rho_L C_L}$ is a particular and convenient definition of a combined gas/liquid thermal diffusivity.

From equation (4.iv) we can extract an equation for the radius-squared of the droplet which is given in equation (9.ii).

$$\frac{d r_s^2}{d t} = - \lambda \bar{\alpha}_T \chi \quad (9.ii)$$

In this equation, $\lambda = \frac{2 C_L}{3 C_p}$, i.e., λ is a ratio of liquid/gas specific heats. Equations (9.i–ii) constitute the governing equations of the droplet evaporation process.

3.5. Derivation of the Dimensionless Governing Equations

The governing equations are rendered dimensionless since such equations are typically easier to program. The dimensionless variables and parameters are given in equations (10.i–vii). This method of non–dimensionalization is adapted from [7].

$$\tau = \left(\frac{T_s(t)}{T_\infty} \right) \quad (10.i)$$

$$\xi^2 = \frac{r_s^2(t)}{r_0^2} \quad (10.ii)$$

$$\tau_0 = \left(\frac{T_s(t=0)}{T_\infty} \right) \quad (10.iii)$$

$$\tau_b = \left(\frac{T_b}{T_\infty} \right) \quad (10.iv)$$

$$s = t/t_0 \quad (10.v)$$

$$t_0 = \frac{r_0^2}{\bar{\alpha}_T} \quad (10.vi)$$

$$l_v = L_v / RT_\infty \quad (10.vii)$$

$$\Omega = \frac{l_v (\gamma - 1)}{\gamma} \quad (10.viii)$$

Note that γ is the ratio of specific heats which is usually tabulated in thermodynamics tables and that $\tau_0 \neq 0$. From these definitions the governing equations take the following form:

$$\frac{d\tau}{ds} = \frac{\chi}{\xi^2} (\mu - \Omega) \quad (11.i)$$

$$\frac{d\xi^2}{ds} = -\lambda \chi \quad (11.ii)$$

Here, we have used

$$Y_{Fs} = Y_{Fb} \exp \left(l_v \left\{ \frac{1}{\tau_b} - \frac{1}{\tau} \right\} \right) \quad (12.i)$$

$$\theta = \frac{1 - Y_{F\infty}}{1 - Y_{Fs}} \quad (12.ii)$$

$$\chi = \frac{\ln(\theta)}{Le_F} \quad (12.iii)$$

$$\mu = \frac{1 - \tau}{e\chi - 1} \quad (12.iv)$$

The initial conditions for the coupled, non-linear equations (11.i–ii) are

$$\tau(0) = \tau_0 \quad (13.i)$$

$$\xi^2(0)=1 \quad (13.ii)$$

An interesting quantity is the transfer number B [24]. Qualitatively, this transfer number represents the ratio of an impetus for inter-phase transfer to a resistance opposing the transfer. For a vaporizing droplet, the gas-phase diffusion of the fuel is the primary impetus for vaporization, as opposed to the heat conduction. Thus the transfer number takes the following form:

$$B = \theta - 1$$

3.6. Solutions for a Propane Droplet

Figure 1 describes a representative solution for the evaporation process of a propane droplet. The plot will describe the dimensionless surface temperature solution and the dimensionless radius-squared solution, i.e., equations (11.i–ii). The representative hydrocarbon is propane, so the parameters assume the following values:

$$R = 0.1885 \text{ kJ/kg-K}; L_v = 427.8 \text{ kJ/kg}; T_b = 231.05 \text{ K}; T_\infty = 300.15 \text{ K}; T_0 = 100.15 \text{ K};$$

$$C_p = 1.6794 \text{ kJ/kg-K}; C_L = 2.25 \text{ kJ/kg-K}; Le_F = 1.0; Y_{F\infty} = 0.010;$$

$$Y_{Fb} = 0.9; k_g = 0.0151 \times 10^{-3} \text{ kW/m-K}; \rho_L = 581 \text{ kg/m}^3$$

Hence, the dimensionless variables (equations (10.iii–viii)) are as follows:

$$\tau_0 = 0.3337; \tau_b = 0.7698; l_v = 7.5612; \Omega = 0.8487;$$

$$\gamma = 1212.1; \bar{\alpha}_T = 1212.1; \lambda = 12121.0; t_0 = 7.2144 \text{ seconds};$$

For a propane droplet under these conditions, the burn-out time is $s_b = 4.304158$, i.e., $t_b = 0.64202$ seconds. Qualitatively, the solutions shown in Figure 1 agree very closely with the results from several sources, viz., [3], [7], [8], [9], and [26]. However, the actual numerical quantities differ mainly because of differences in fuels, initial conditions, and non-dimensionalization techniques.

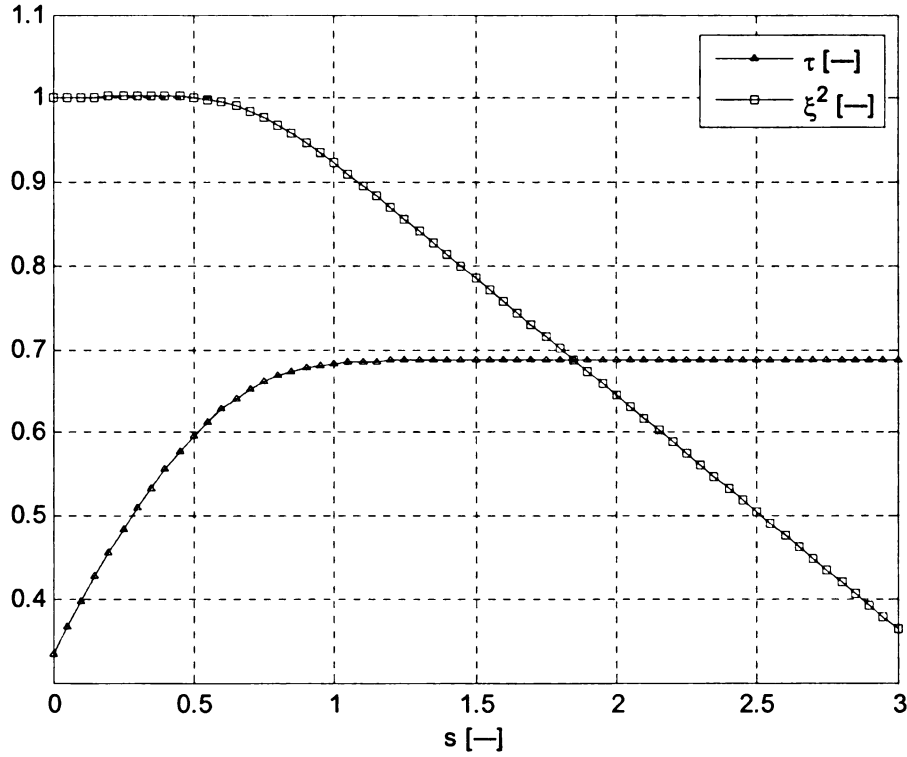


Figure 1. The solution for the surface temperature and for the radius-squared for a propane droplet.

Chapter 4: The Sensitivity Analysis

4.1. Overview

The approach to the sensitivity analysis for this study is to induce small changes in the vicinity of a set of representative values in the relevant physical parameters. This seems to be a very intuitive way of conducting a sensitivity analysis since such an approach will aid in determining the influence of the physical parameters on the droplet vaporization rate and the droplet surface temperature.

For this thesis, when a parameter is varied, the other parameters are maintained at their representative values for propane. Also, in each section, there are a total of four plots; two plots for the surface temperature and two plots for the radius-squared. One plot is the actual sensitivity, which contains five contours to show how the value of the parameter itself affects the sensitivity. The other plot is the solution, which also contains five contours in order to show how the value of the parameter itself affects the solution. An interesting characteristic of the solution for surface temperature is that the surface temperature is always less than unity as well as less than the boiling temperature. In fact, the surface temperature converges to a wet-bulb temperature [25].

It has been found that the derivatives of the surface temperature and the radius-squared (equations (11.i–ii)) play an important role in the sensitivity behavior. The derivatives under consideration are those taken with respect to time. In equations (11.i–ii), the derivatives are taken with respect to s , which is a dimensionless time.

4.2. Computational Methodology

The majority of sensitivity work was conducted in MATLAB®. The methodology for inspecting the sensitivity of τ (the dimensionless surface temperature) and ξ^2 (the dimensionless radius-squared) to small changes in the physical parameters is as follows:

1. Define an offset value. For example, if the sensitivity of τ and ξ^2 to some arbitrary parameter P is under consideration, the notation for this offset value is ΔP ; the method of definition will be given later.
2. Define P_1 and P_2 where P_1 is fixed and $P_2 = P_1 + \Delta P$. Subsequently, P_3, P_5, P_7 , and P_9 will be defined. Note that the $(\bullet)_{odd}$ terms are referred to as primary values, and the $(\bullet)_{even}$ terms are the secondary values; thus the general method for computing the P_{even} values is $P_{even} = P_{odd} + \Delta P$. As mentioned earlier, the reason for defining five primary values was to see how the value of the physical parameter itself influenced the sensitivity.
3. The formula for the sensitivity of an arbitrary solution X to an arbitrary parameter P is given as $\Psi_P^X = P_{avg} \left| \frac{\partial X}{\partial P} \right|$ where Ψ_P^X is interpreted to read “the sensitivity of X to small changes in P .” For this thesis, the arbitrary solution X can be either τ or ξ^2 ; the arbitrary parameter can be any of the physical parameters examined in this thesis.

Since the solution was obtained numerically, the sensitivity was also evaluated numerically, viz.:

$$\psi_P^X = P_{avg} \left| \frac{X_{P+\Delta P} - X_P}{\Delta P} \right|$$

4. The offset value (ΔP) is taken as the average of the absolute difference of the P_{avg} value and the primary values, i.e.,

$$\Delta P = avg(|P_{avg} - P_i|)$$

where $i = 1, 3, 5, 9$, and P_{avg} is the average of the primary parameter values.

4.3. Results and Discussion

4.3.1. Sensitivity to the Gas Constant

Recall that the normalized gas constant, R , is defined by the expression $R W = R_u$ where R_u is the universal gas constant ($8.31434 \text{ kJ/kmol-K}$) and W is the molar mass of the substance (kg/kmol). Hence, if a substance has a large gas constant, then the substance must have a smaller molar mass. The following plots illustrate the sensitivity of the surface temperature and the radius-squared to the gas constant for $s \in [0, 3.0]$ where $\Delta R = 0.0447 \text{ kJ/kg-K}$.

The sensitivity of the surface temperature and the solution for the surface temperature are shown in Figure 2 and Figure 3, respectively. From Figure 2, there exists a very brief interval in which surface temperature has negligible sensitivity to the gas constant; this is the same interval in which the droplet experiences condensation (see Figure 5). Also, there is a reversal in the surface temperature sensitivity contours; at first a large value for gas constant induces a low sensitivity; then it induces a high sensitivity. This reversal occurs because the heat-up rate decreases, i.e., a larger value of the gas constant causes the surface temperature to reach its constant value faster. It is interesting to note that a large gas constant always induces a smaller temperature (Figure 2). Additionally, a large gas constant always corresponds to a smaller surface temperature derivative, i.e., a slower rate of change.

The sensitivity of the radius-squared and the solution for the radius-squared are shown in Figure 4 and Figure 5, respectively. Similar to the behavior of the surface temperature, the radius-squared initially experiences negligible sensitivity to the gas constant. Then there is a steady rise in sensitivity throughout the remainder of the evaporation process. However, there is a reversal, i.e., an instance where the value of the gas constant has an opposite effect on the sensitivity (see Figure 5). This reversal occurs because larger gas constant values allow the radius-squared to experience faster decay. However, the radius-squared grows progressively more sensitive to the gas constant for larger values of the gas constant. Additionally, a larger gas constant allows a smaller degree of condensation as well as faster evaporation.

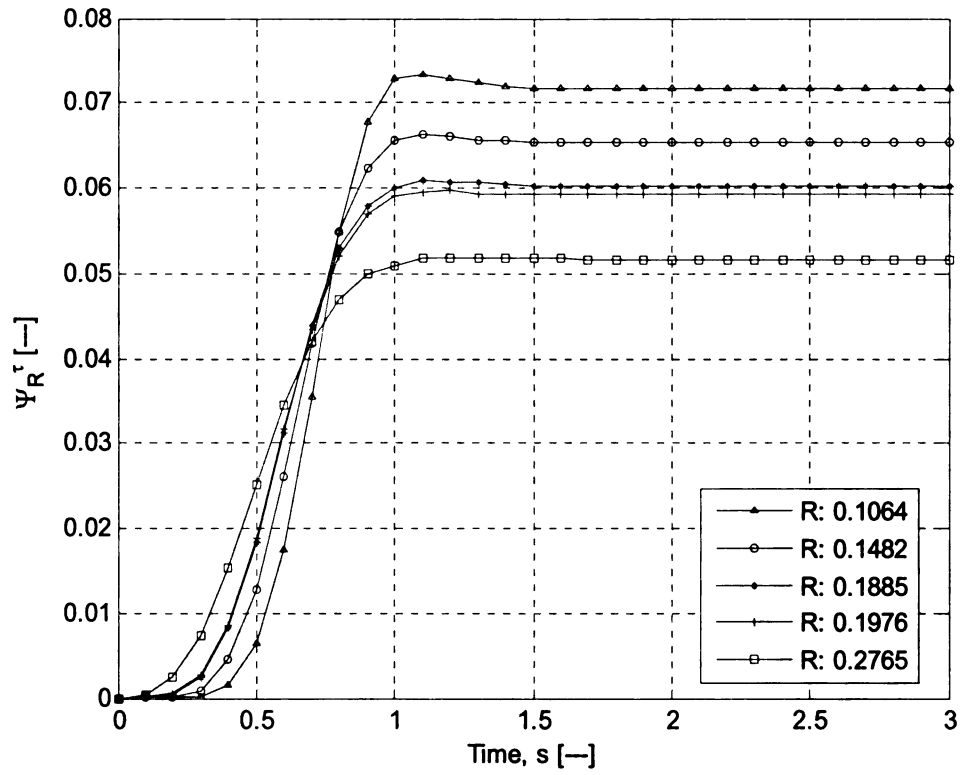


Figure 2. The sensitivity of the surface temperature to the gas constant.

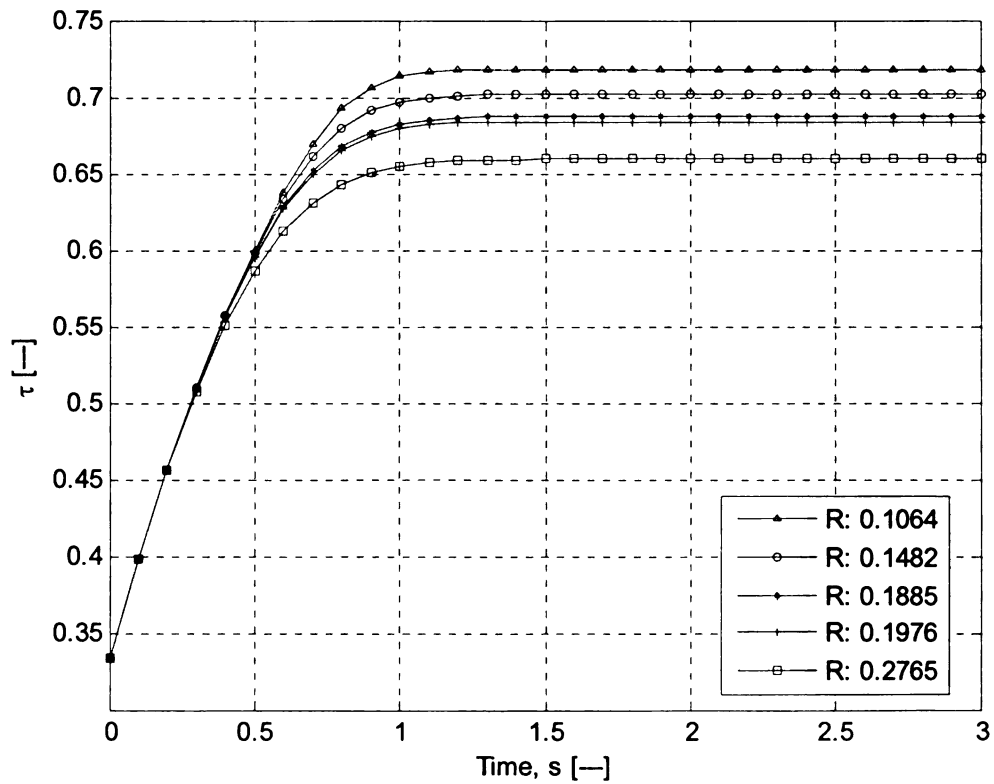


Figure 3. The surface temperature solution.

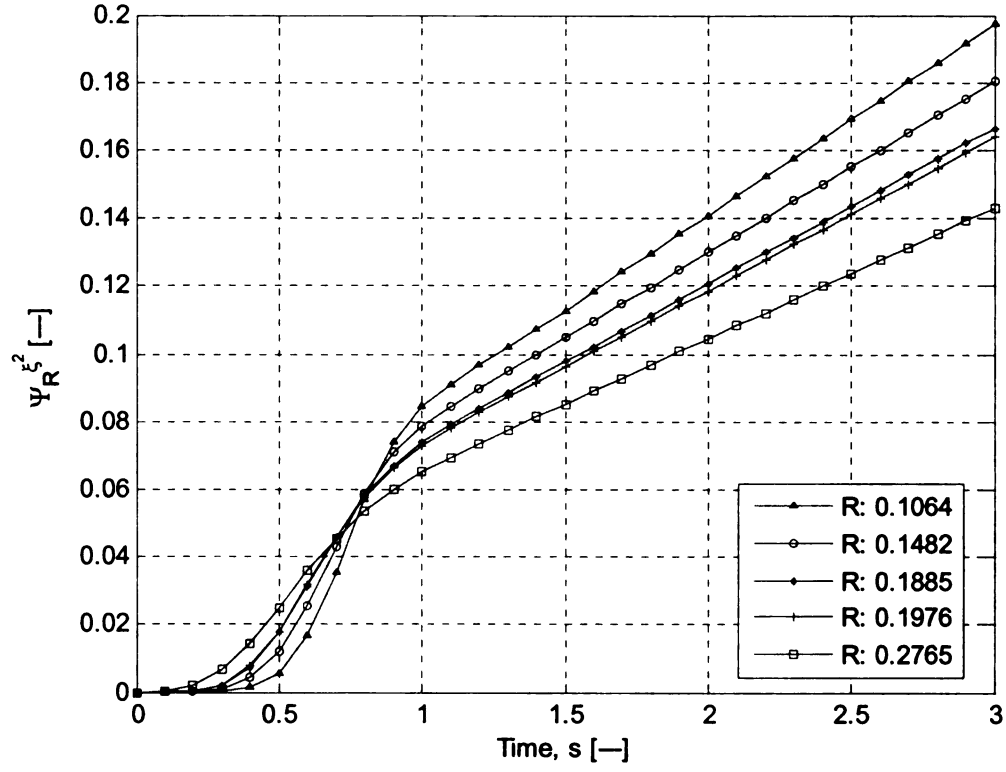


Figure 4. The sensitivity of the radius-squared to the gas constant.

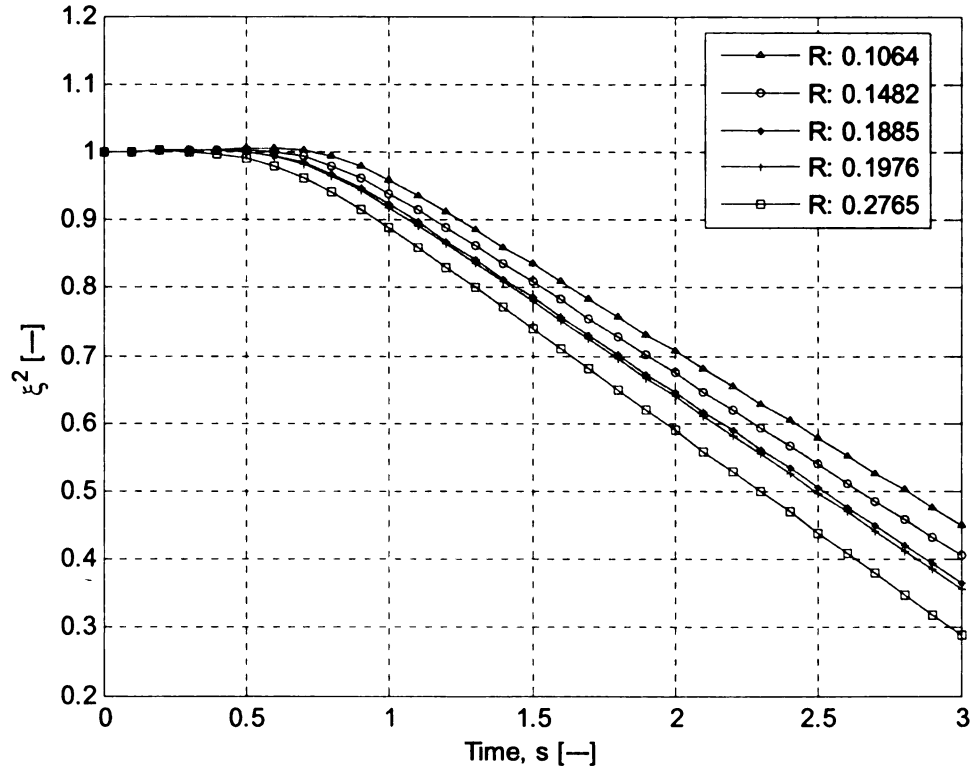


Figure 5. The radius-squared solution.

4.3.2. Sensitivity to the Latent Heat of Vaporization

Recall that the latent heat of vaporization is the amount of energy a substance needs to absorb in order to change from the liquid phase to the gas phase. The following plots illustrate the sensitivity of the surface temperature and the radius-squared to the latent heat of vaporization for $s \in [0, 3.0]$ where $\Delta L_v = 27.4 \text{ kJ/kg}$.

The sensitivity of the surface temperature and the solution for the surface temperature are shown in Figure 6 and Figure 7, respectively. It is apparent from Figure 6 that, overall, a large value of latent heat always induces a relatively low sensitivity in the surface temperature. Additionally, from Figure 7, a large latent heat allows the surface temperature to achieve a higher value. This stands to reason because if a substance has a large latent heat then that substance will require more energy in order to change phase. An interesting characteristic of the surface temperature sensitivity is the initial, steady increase in sensitivity, up to a peak; each contour has its own peak, and these peaks do not occur at the same instant. Specifically, these peaks occur when the contours of the derivative of surface temperature (equation (11.i)) reverse. Note that the derivative contours do not intersect at exactly the same instant, i.e., there is no “fixed point.” Specifically, on the LHS of the peaks, a large latent heat allows a faster rate of change in surface temperature, whereas on the RHS of the peaks, a large latent heat allows a slower rate of change.

The sensitivity of the radius-squared and the solution for the radius-squared are shown in Figure 8 and Figure 9, respectively. From Figure 8 and Figure 9, it can be seen that during the small condensation period, the radius-squared has negligible sensitivity to

latent heat. However, once the droplet starts to evaporate, the radius-squared becomes progressively more sensitive to changes in the latent heat, although a large value of latent heat induces less sensitivity. Additionally, a large latent heat always corresponds to a larger radius-squared, i.e., a large latent heat induces more condensation as well as a longer evaporation time.

Figure 10 and Figure 11 illustrate the variation of the sensitivity of the surface temperature and the radius-squared with the value of the latent heat for select instances of time. From these figures, it is apparent that when the latent heat has a lower value, both the surface temperature and the radius-squared experience lower levels of sensitivity for all time. It is also apparent that the radius-squared is more sensitive to the latent heat than is the surface temperature.

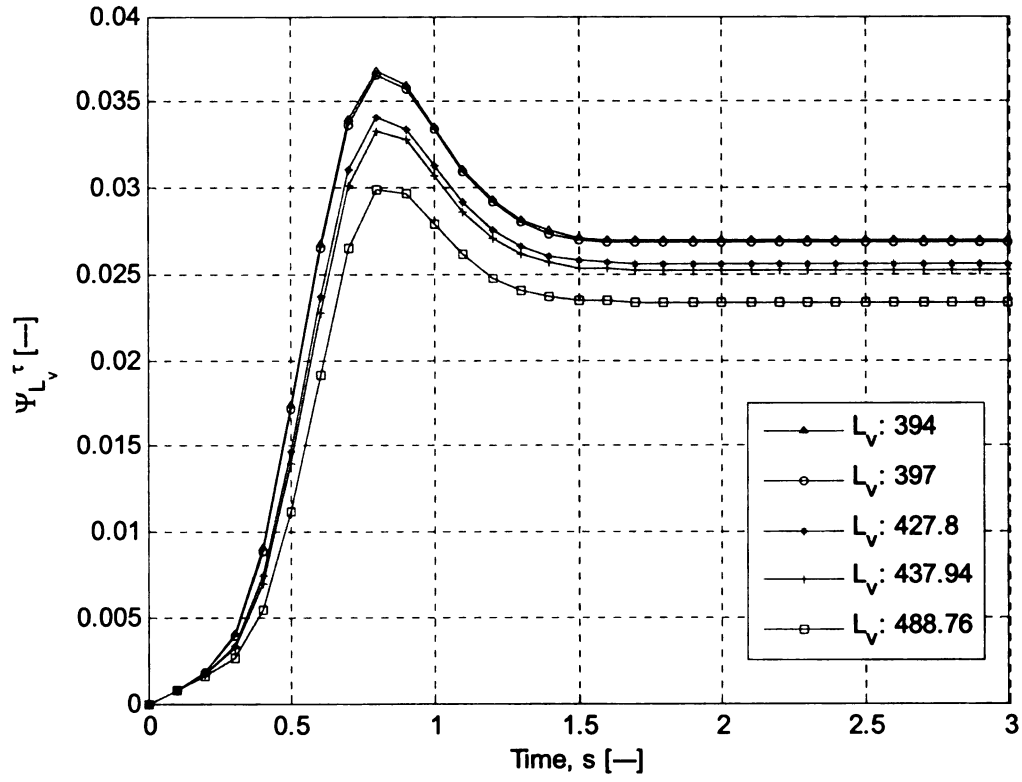


Figure 6. The sensitivity of the surface temperature to the latent heat of vaporization.

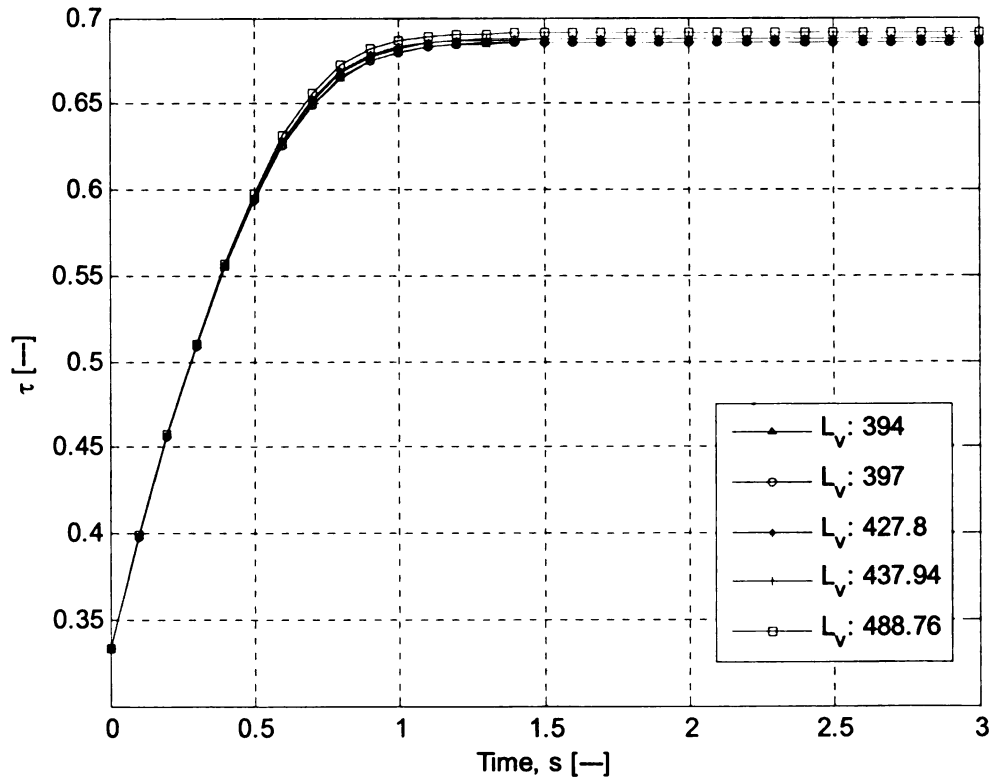


Figure 7. The surface temperature solution.

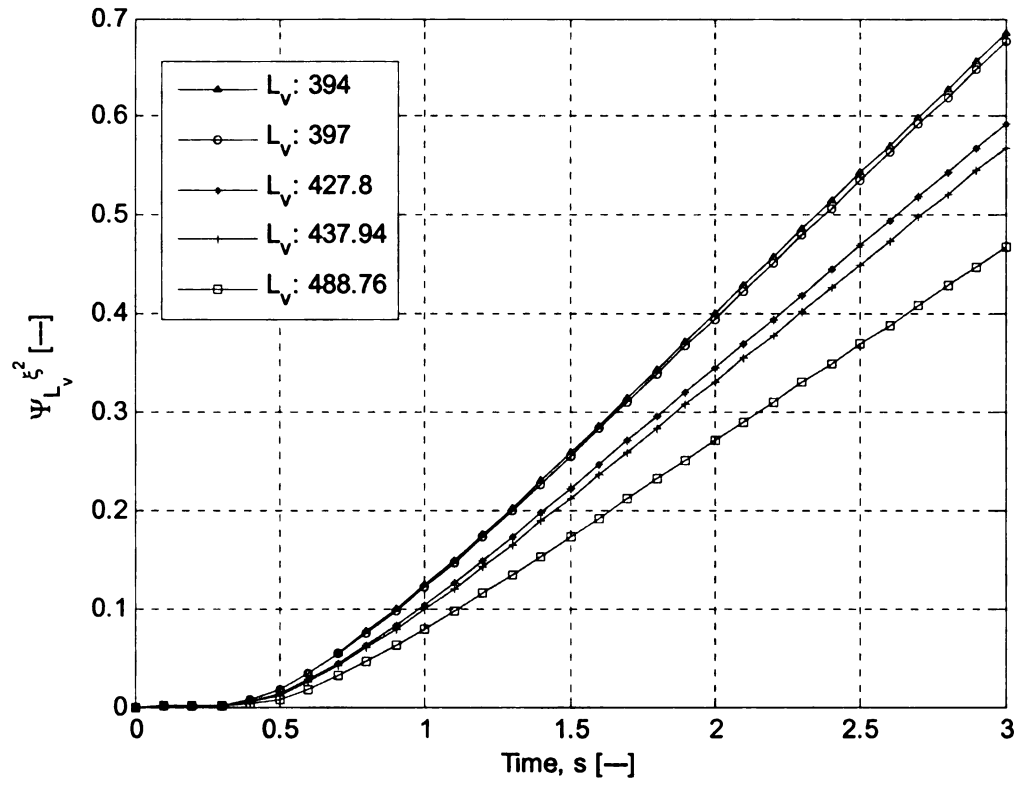


Figure 8. The sensitivity of the radius-squared to the latent heat of vaporization.

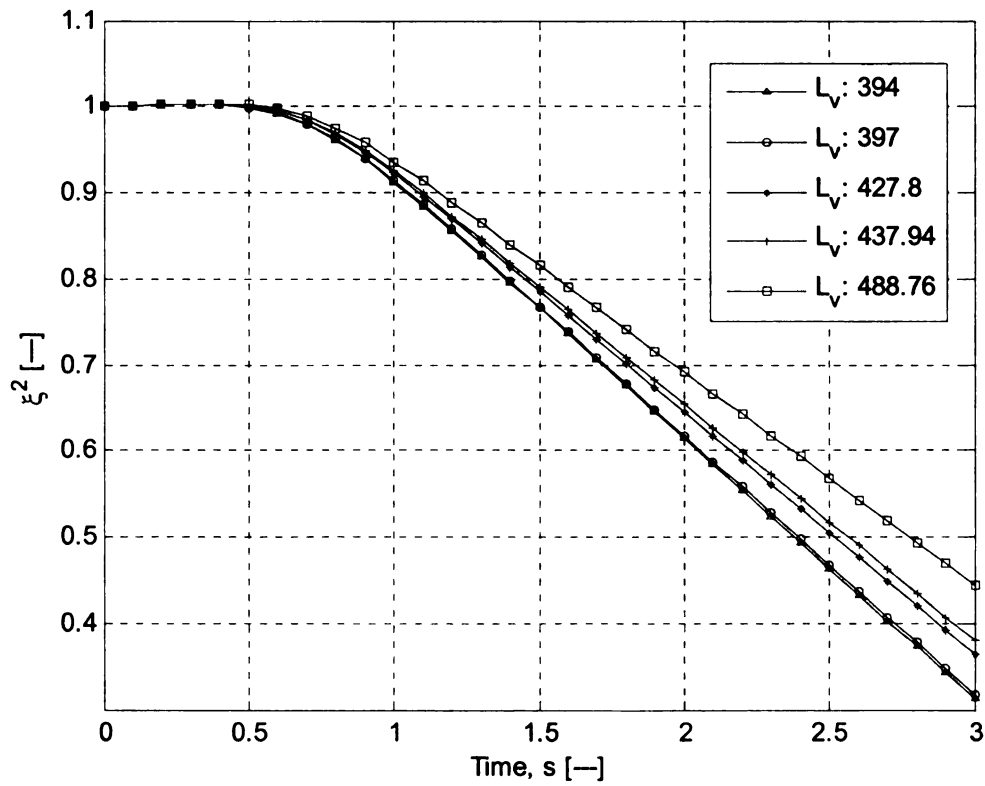


Figure 9. The radius-squared solution.

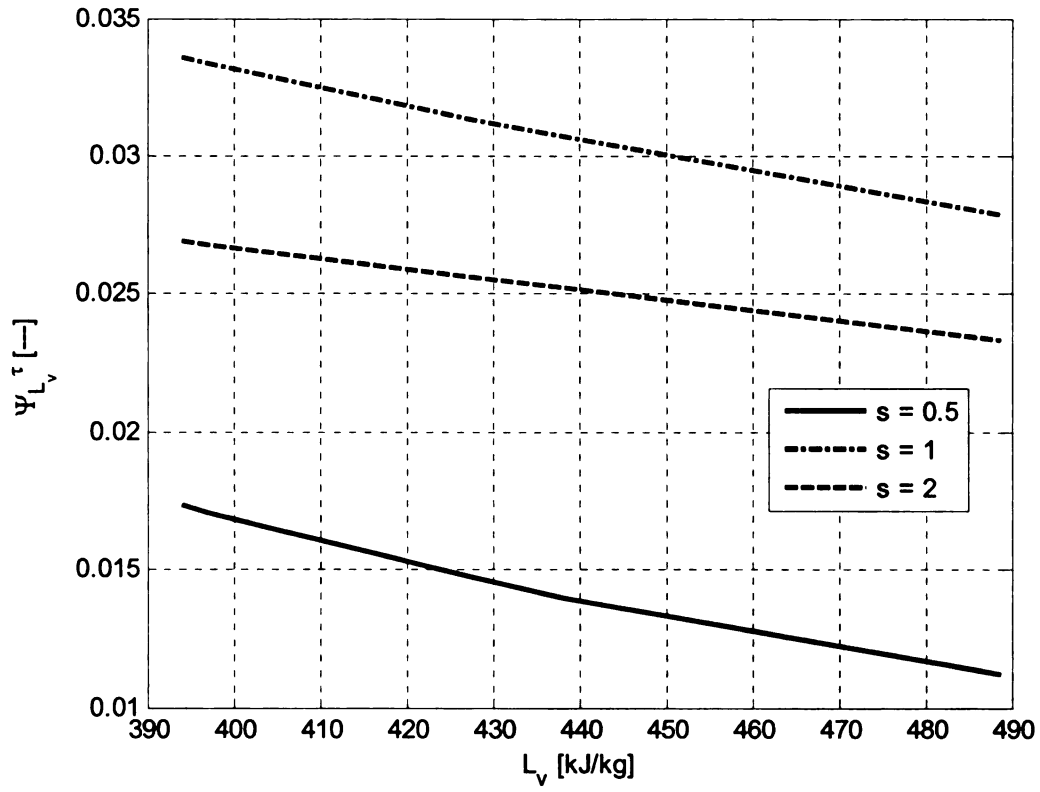


Figure 10. Variation of the surface temperature sensitivity with the latent heat at select instances of time.

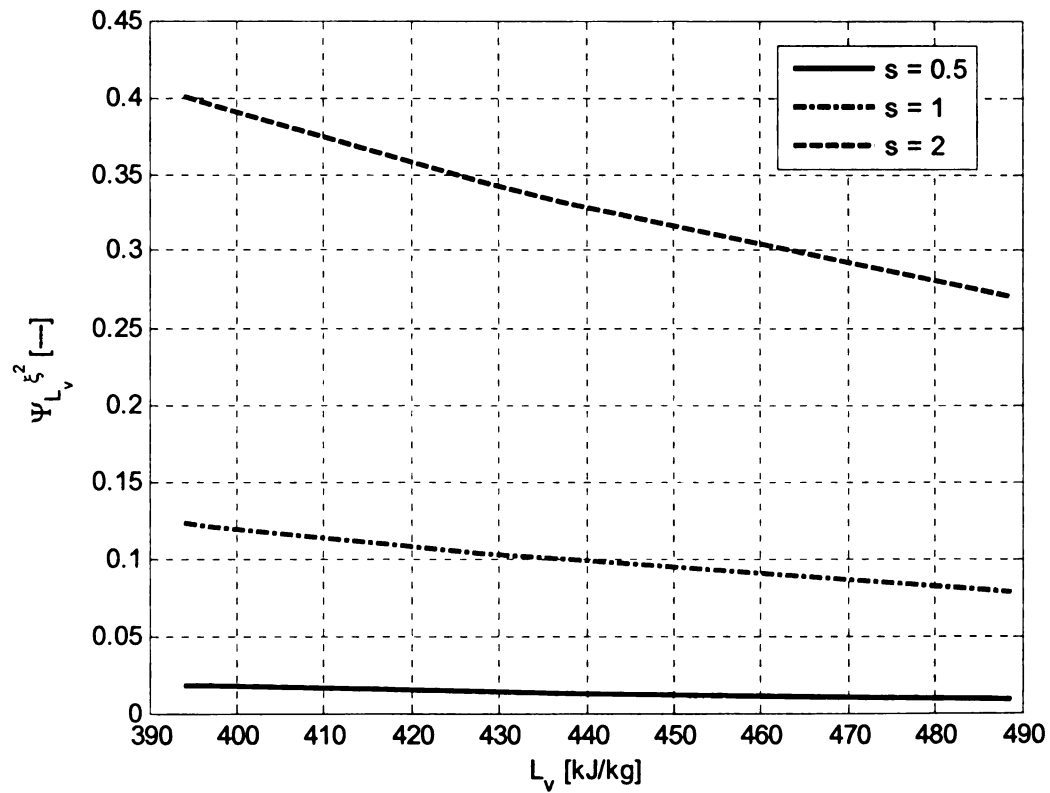


Figure 11. Variation of the radius-squared sensitivity with the latent heat at select instances of time.

4.3.3. Sensitivity to the Boiling Temperature

The boiling temperature of a liquid is that temperature at which the liquid changes to a gas at a solid interface. At atmospheric pressure, the boiling temperature of propane is 231.05 Kelvin, i.e., -42.1 °C. The following plots illustrate the sensitivity of the surface temperature and the radius-squared to the boiling temperature for $s \in [0, 3.0]$ where $\Delta T_b = 36\text{ K}$.

The sensitivity of the surface temperature and the solution for the surface temperature are shown in Figure 12 and Figure 13, respectively. There is a brief interval in which surface temperature has negligible sensitivity to the boiling temperature; this is the interval in which the droplet experiences a small amount of condensation – the longer the condensation process, the longer is the interval of negligible sensitivity. Furthermore, a large boiling temperature induces a lowered sensitivity in the surface temperature. It also allows the surface temperature to achieve a higher value. This characteristic stands to reason because a lower boiling temperature means that a substance does not require so much energy to boil.

The sensitivity of the radius-squared and the solution for the radius-squared are shown in Figure 14 and Figure 15, respectively. During the brief condensation phase, the sensitivity of the radius-squared is very similar to the sensitivity of the surface temperature in that during the condensation process, the radius-squared has negligible sensitivity to boiling temperature. However, once the droplet starts to evaporate, the radius-squared experiences a progressively larger degree of sensitivity until the droplet is completely evaporated. Additionally, a higher boiling temperature allows more

condensation to occur, thus a longer evaporation process, while at the same time allowing the radius-squared to be less sensitive to small changes in boiling temperature.

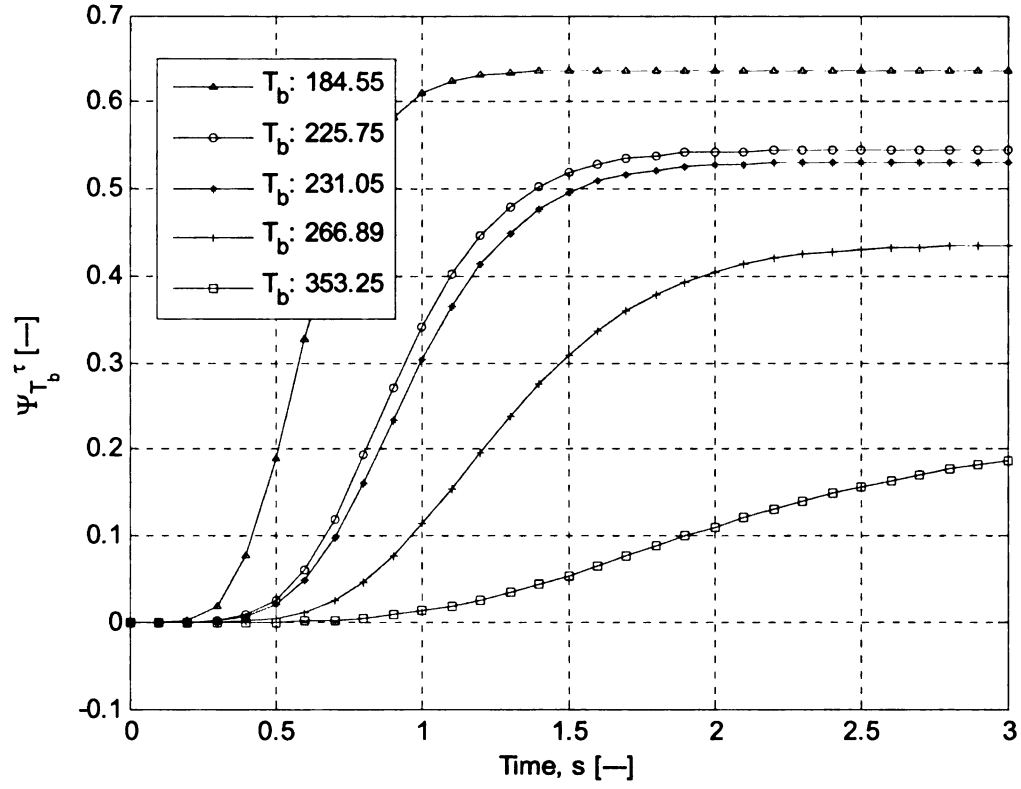


Figure 12. The sensitivity of the surface temperature to the boiling temperature.

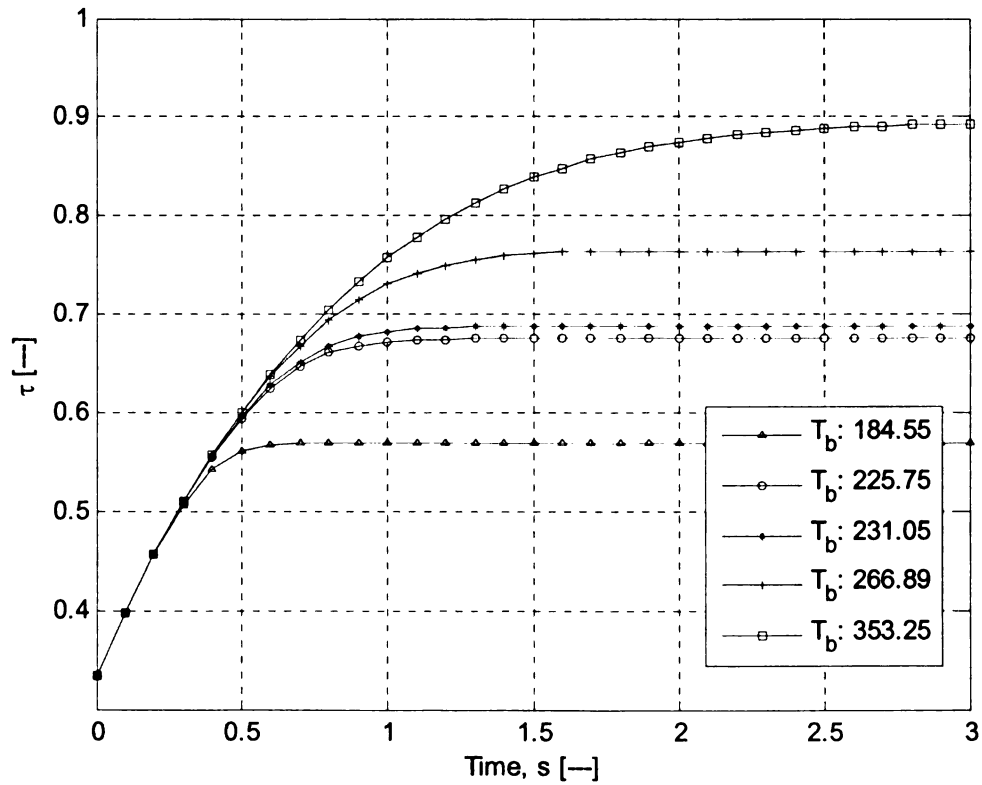


Figure 13. The surface temperature solution.

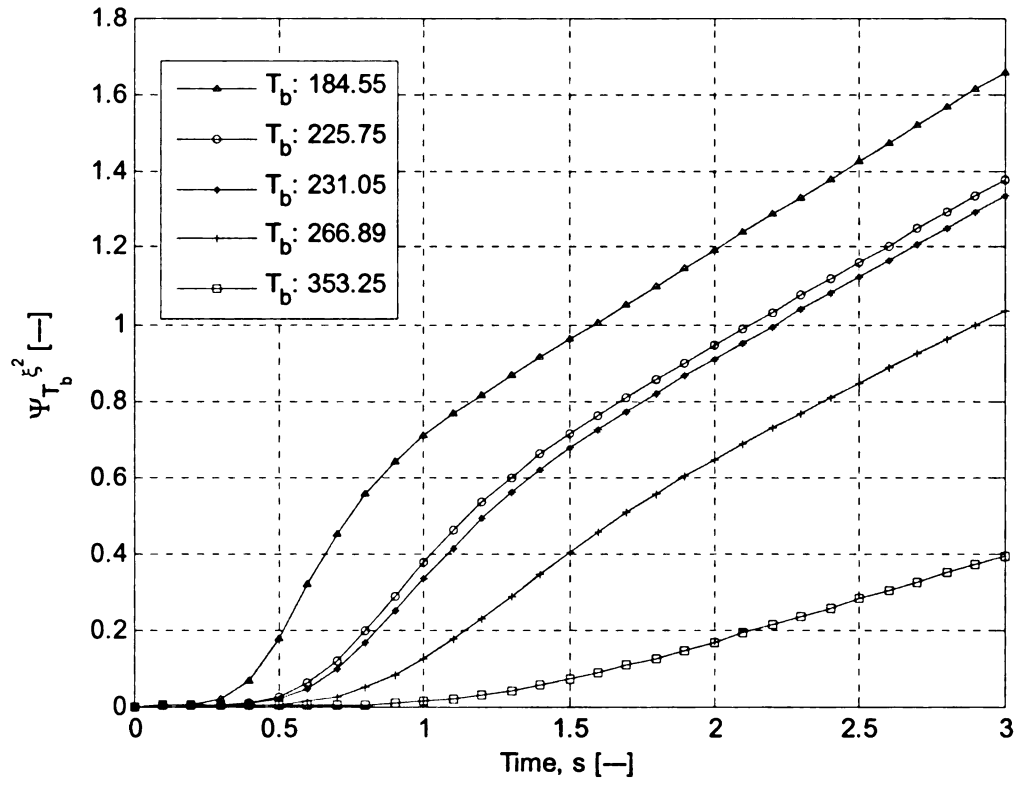


Figure 14. The sensitivity of the radius-squared to the boiling temperature.

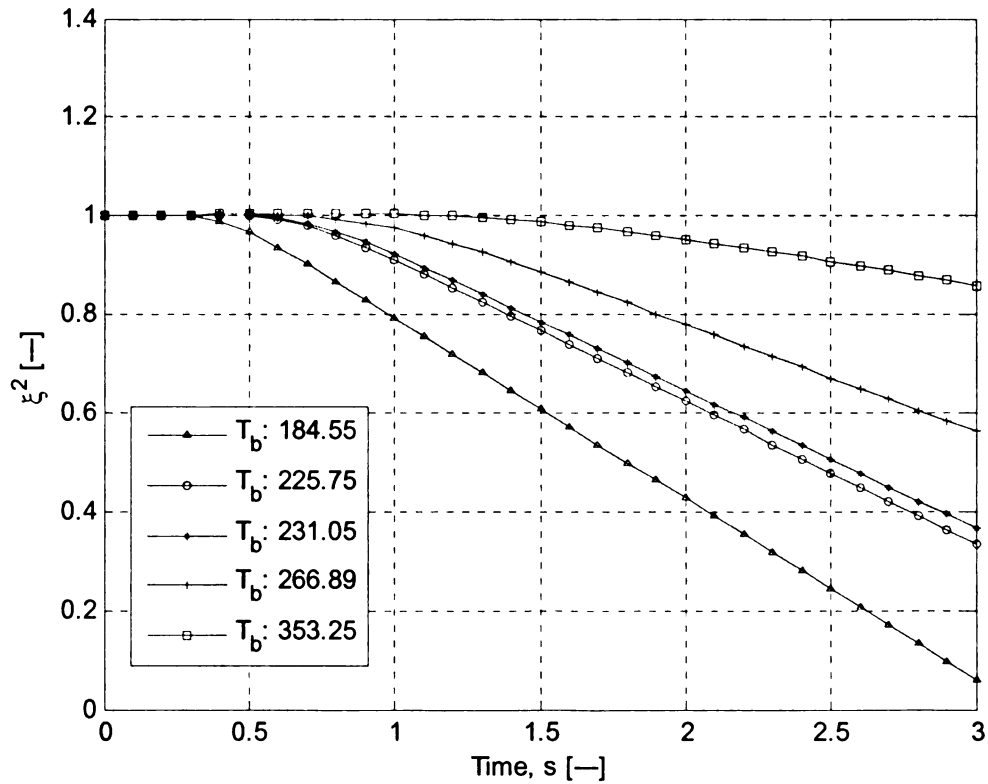


Figure 15. The radius-squared solution.

4.3.4. Sensitivity to the Ambient Temperature

The ambient temperature is the temperature of the medium in which the droplet is suspended. For this thesis, it was set at a nominal value of 300.15 Kelvin, i.e., 27 °C. The following plots illustrate the sensitivity of the surface temperature and the radius-squared to the ambient temperature for $s \in [0, 3.0]$ where $\Delta T_\infty = 12 \text{ K}$.

The sensitivity of the surface temperature and the solution for the surface temperature are shown in Figure 16 and Figure 17, respectively. The first noticeable characteristic is that the sensitivity decreases, with a larger ambient temperature inducing a larger decrease (see Figure 16). These relative minima do not occur at the exact same instant; rather they occur in the interval in which the contours of the derivative of the surface temperature intersect. Again, the derivative contours do not intersect at the exact same instant. Specifically, on the LHS of the sensitivity peaks, a larger ambient temperature induces a larger derivative; on the RHS, this behavior reverses. Although the contours of the surface temperature derivatives and the contours of the surface temperature sensitivity intersect, the contours of the surface temperature solution do not; in fact, a lower ambient temperature allows surface temperature to achieve a higher value for all time.

The sensitivity of the radius-squared and the solution for the radius-squared are shown in Figure 18 and Figure 19, respectively. During the brief condensation phase, the radius-squared has negligible sensitivity to changes in the ambient temperature (unlike the sensitivity of the surface temperature during this interval). However as soon as evaporation begins, the radius-squared grows progressively more sensitive until the

droplet has evaporated. Furthermore, the radius-squared has greater sensitivity to the ambient temperature when the ambient temperature is large; however, the radius-squared converges to the same amount of sensitivity regardless of the actual value of the ambient temperature. Additionally, a larger value for the ambient temperature allows less condensation, thus, a faster evaporation process.

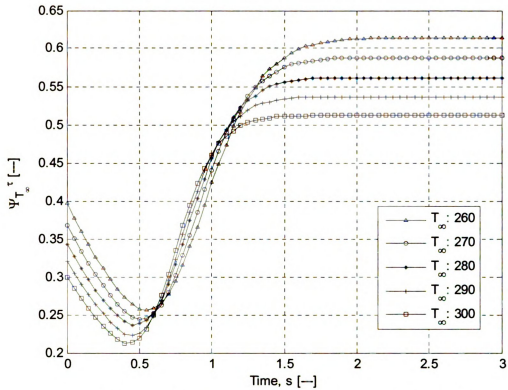


Figure 16. The sensitivity of the surface temperature to the ambient temperature.

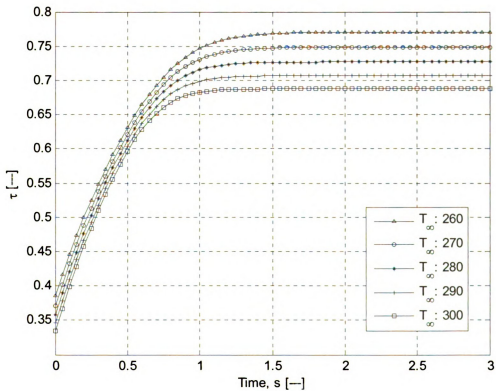


Figure 17. The surface temperature solution.

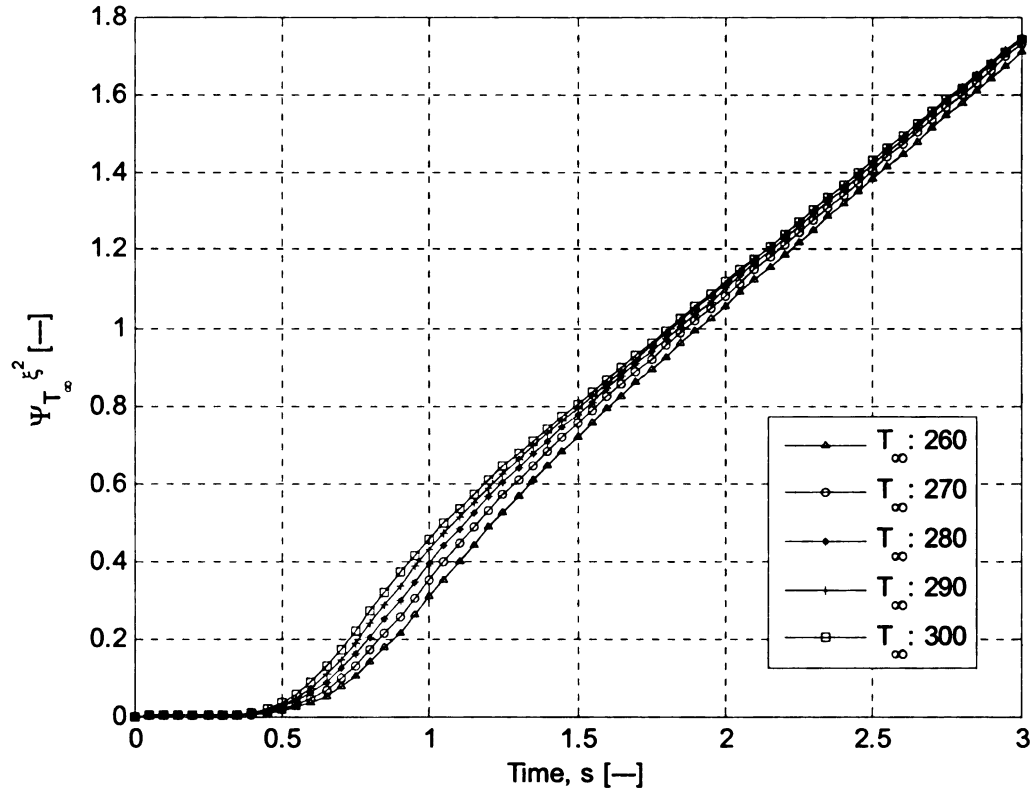


Figure 18. The sensitivity of the radius-squared to the ambient temperature.

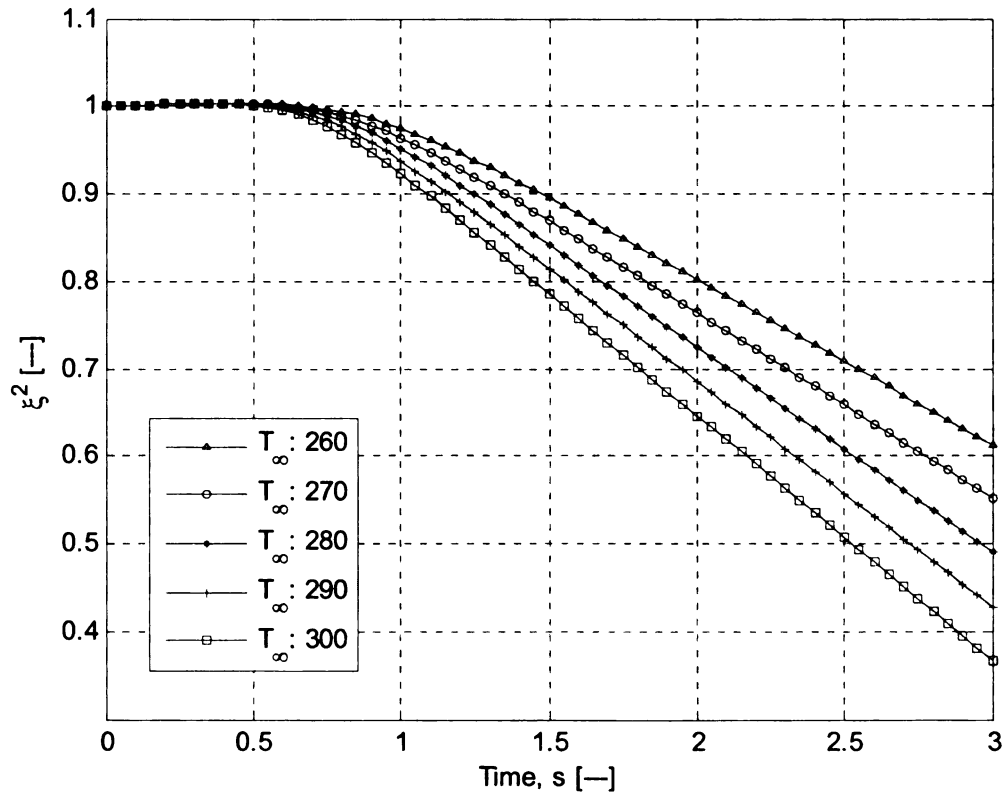


Figure 19. The radius-squared solution.

4.3.5. Sensitivity to the Initial Temperature

The initial temperature is the temperature of the droplet surface at time zero. For this thesis, it was set to a nominal value of 100.15 Kelvin, i.e., -173 °C. The following plots illustrate the sensitivity of the surface temperature and the radius-squared to the initial temperature for $s \in [0, 3.0]$ where $\Delta T_0 = 30 \text{ K}$.

The sensitivity of the surface temperature is given in Figure 20 and the solution for the surface temperature is given in Figure 21. At first, the surface temperature has relatively high sensitivity to its initial temperature, but this sensitivity quickly diminishes to zero. Additionally, a larger value of the initial temperature induces a quicker decay in the sensitivity. Additionally, the surface temperature becomes independent of initial temperature (unlike the behavior of the other parameters). Furthermore, the sooner the surface temperature reaches its constant-value behavior, the faster the sensitivity decays to zero.

The sensitivity of the radius-squared and the solution for the radius-squared are shown in Figure 22 and Figure 23. Between these figures, the radius-squared exhibits remarkable and unique behavior toward this parameter. During the condensation phase, there is a quick rise in the sensitivity of radius-squared. As the radius-squared approaches its linear decay regime, the sensitivity starts to level off to a constant value. This behavior is unique to this parameter in that such behavior does not show up in any of the other parameters. Furthermore, the sooner the radius-squared starts to decay, the more sensitive it is to the initial temperature.

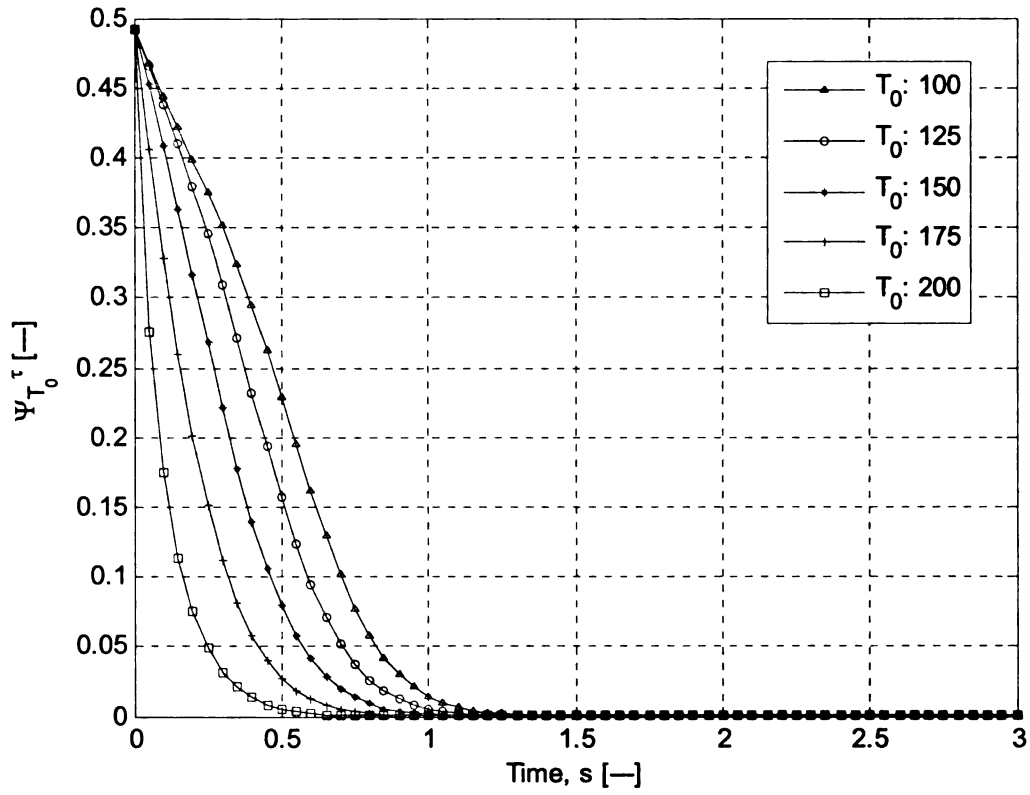


Figure 20. The sensitivity of the surface temperature to the initial surface temperature.

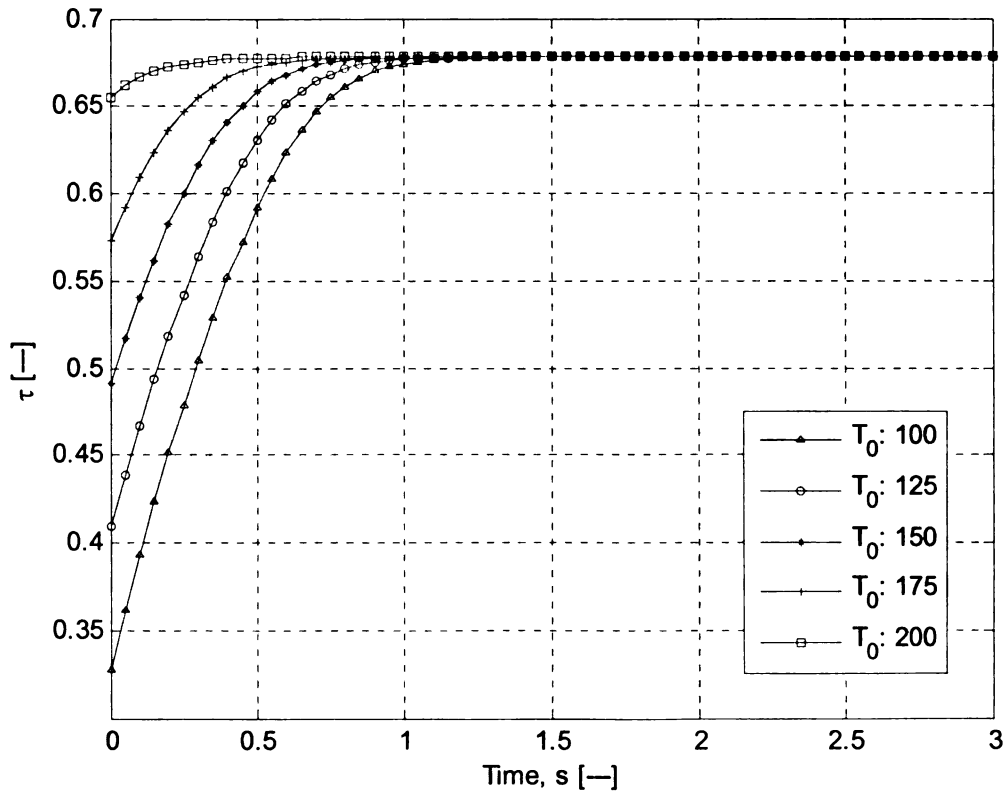


Figure 21. The surface temperature solution.

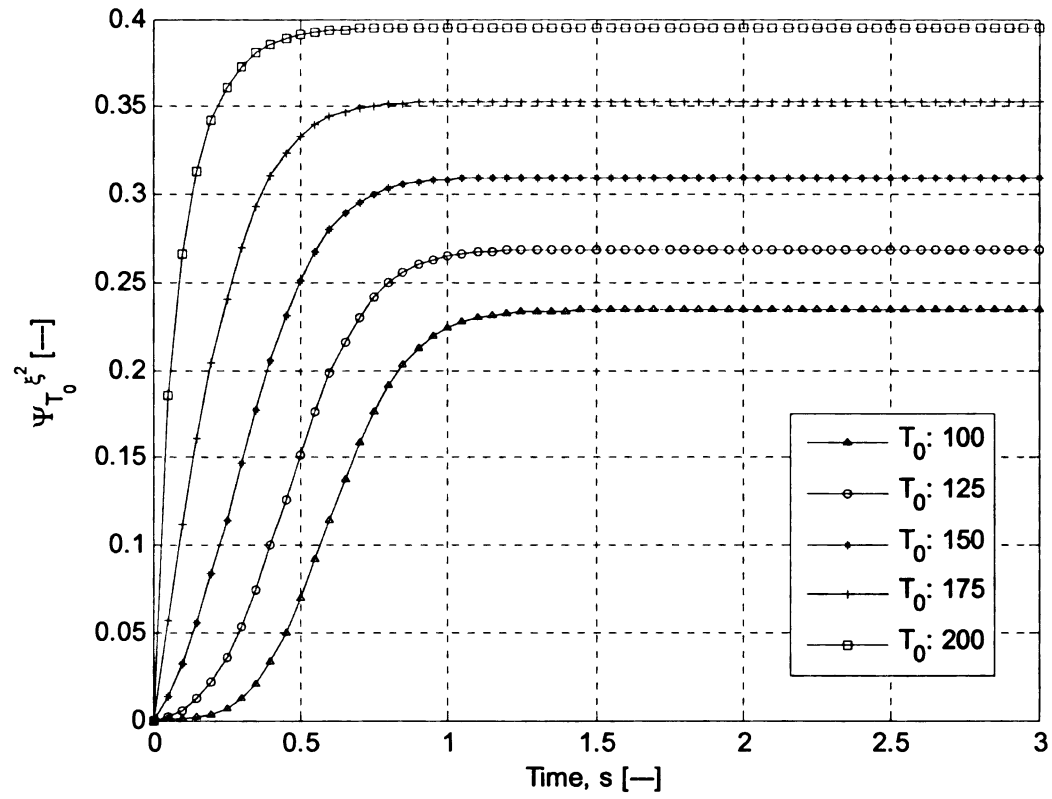


Figure 22. The sensitivity of the radius-squared to the initial surface temperature.

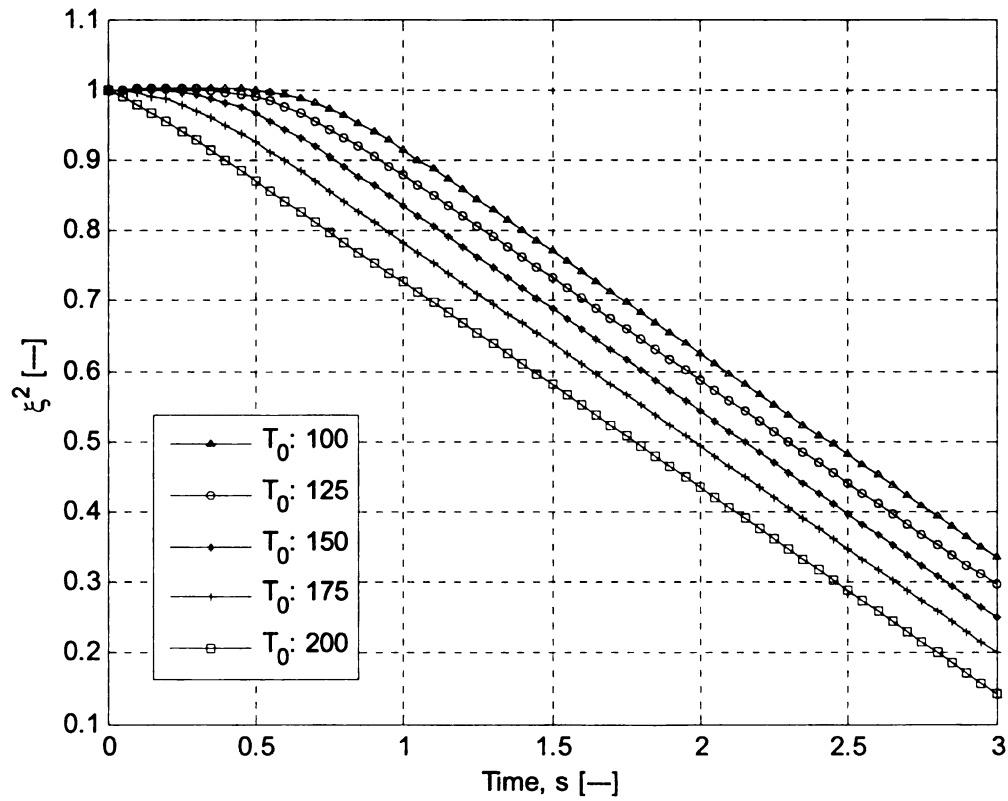


Figure 23. The radius-squared solution.

4.3.6. Sensitivity to the Specific Heat of the Droplet Vapor

The specific heat of the droplet vapor is the constant–pressure specific heat. At atmospheric pressure, the constant–pressure specific heat of propane is 1.6794 kJ/kg-K . The following plots illustrate the sensitivity of the surface temperature and the radius–squared to the vapor specific heat for $s \in [0, 3.0]$ where $\Delta C_p = 0.2263 \text{ kJ/kg-K}$.

The sensitivity of the surface temperature is given in Figure 24 and the solution for the surface temperature is given in Figure 25. From Figure 24, it is apparent that the surface temperature has very small sensitivity to the vapor specific heat, i.e., the sensitivity is always of the order of 10^{-3} . However, there are some noteworthy characteristics. The first is that a higher vapor specific heat always induces a smaller sensitivity in the surface temperature. Also, there exist “peaks” in the sensitivity. These contour peaks occur when the contours of the surface temperature derivative reverse; specifically, on the LHS of the peak, a larger vapor specific heat induces a smaller derivative. On the RHS of the peak, the reverse is true. At first, a large vapor specific heat induces a lower temperature (on the LHS of the peak); later, on the RHS of the peak, this characteristic has reversed. In fact, this reversal in the solution occurs at the instances the sensitivity contours have returned to zero. In the steady–state regime, a high vapor specific heat allows smaller sensitivity, although a higher value is allowed for the surface temperature. It must be noted that the derivative contours do not intersect at the exact same instant, thus the sensitivity contours do not peak at the exact same instant; this means that there is no fixed point in the behavior of the surface temperature.

The sensitivity of the radius-squared and the solution for the radius-squared are shown in Figure 26 and Figure 27 respectively. From Figure 26, it is apparent that the radius-squared is substantially more sensitive to changes in vapor specific heat than the surface temperature. Similar to the surface temperature sensitivity, a large vapor specific heat allows the radius-squared to be less sensitive to the vapor specific heat. However, the sensitivity contours also experience peaks. These peaks occur at the instances the contours of the derivative of radius-squared intersect. These derivative-intersections do not occur at the exact same instant, thus the sensitivity peaks do not occur at the exact same instant. The sensitivity contours all return to zero at the instances the solution contours intersect. Prior to this intersection, a large vapor specific heat allows less condensation to occur; after this intersection, a vapor specific heat corresponds to a longer evaporation time.

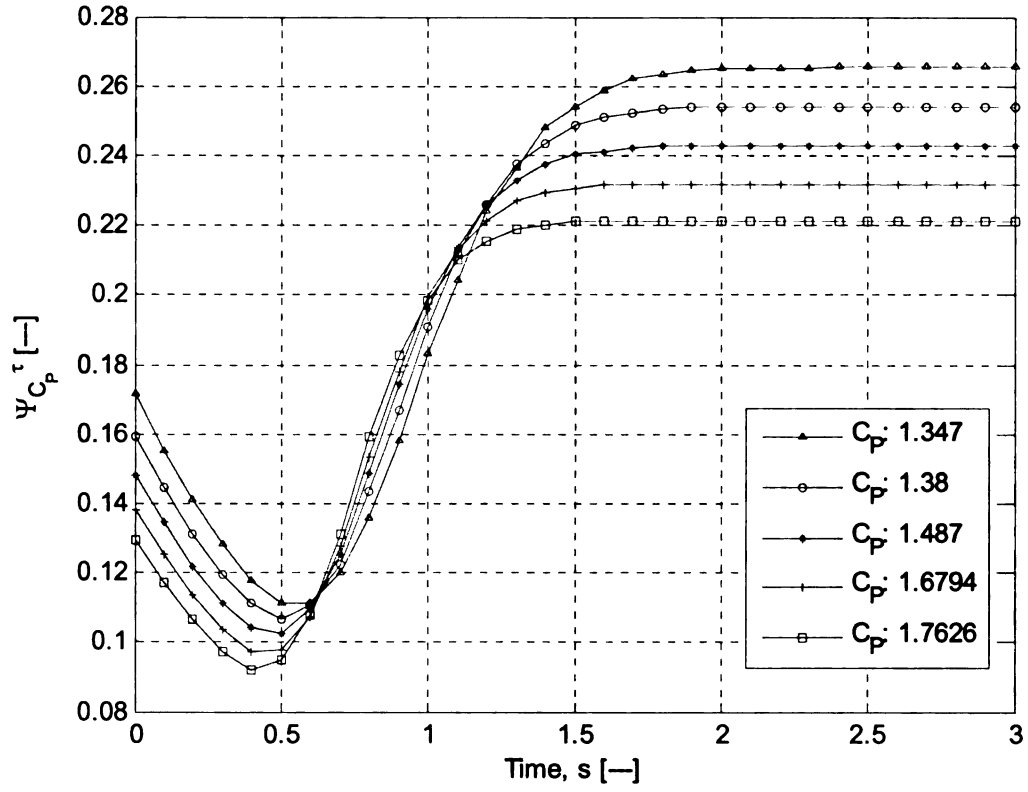


Figure 24. The sensitivity of the surface temperature to the specific heat of the droplet vapor.

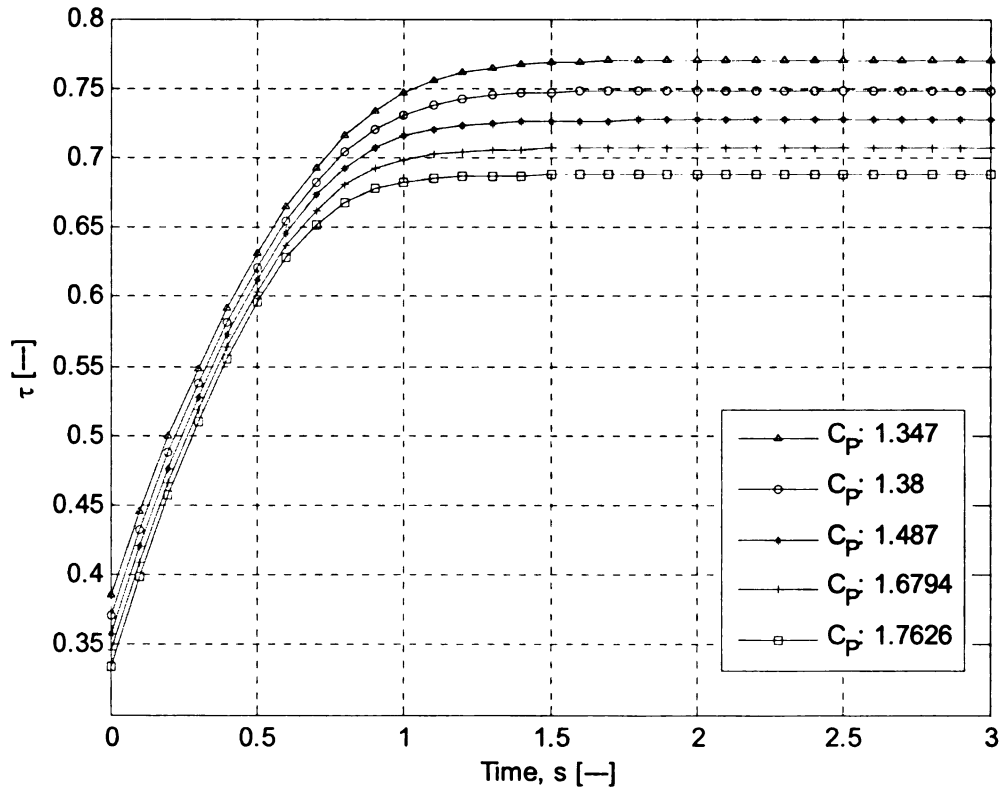


Figure 25. The surface temperature solution.

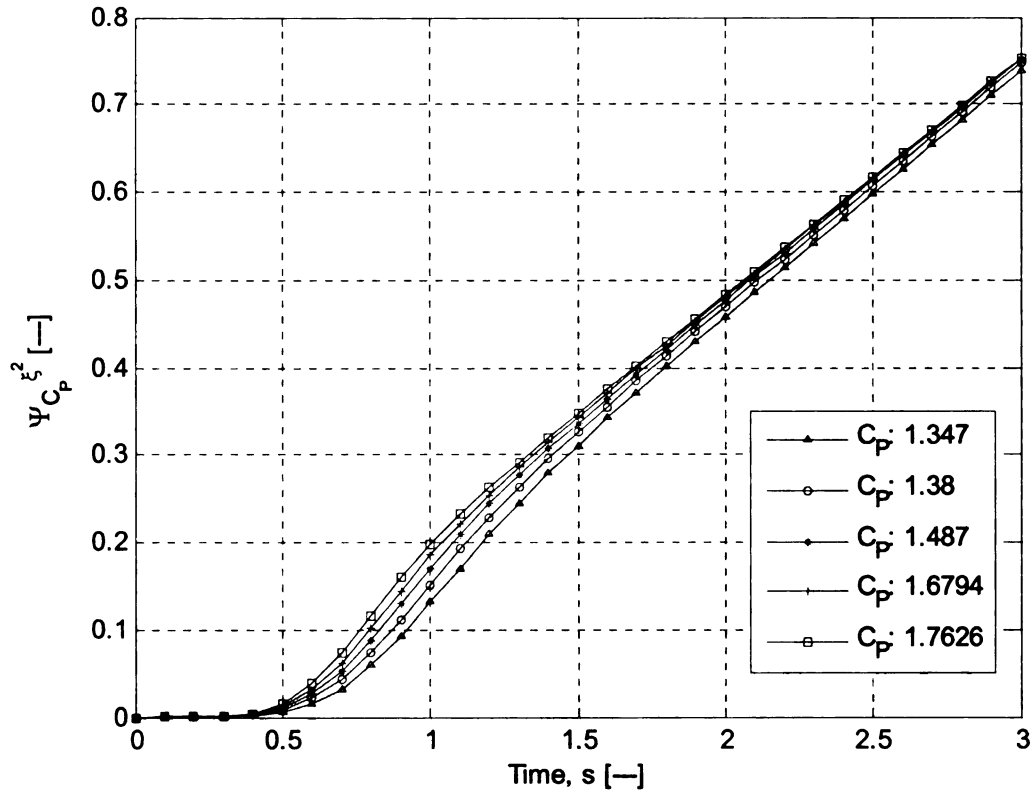


Figure 26. The sensitivity of the radius-squared to the specific heat of the droplet vapor.

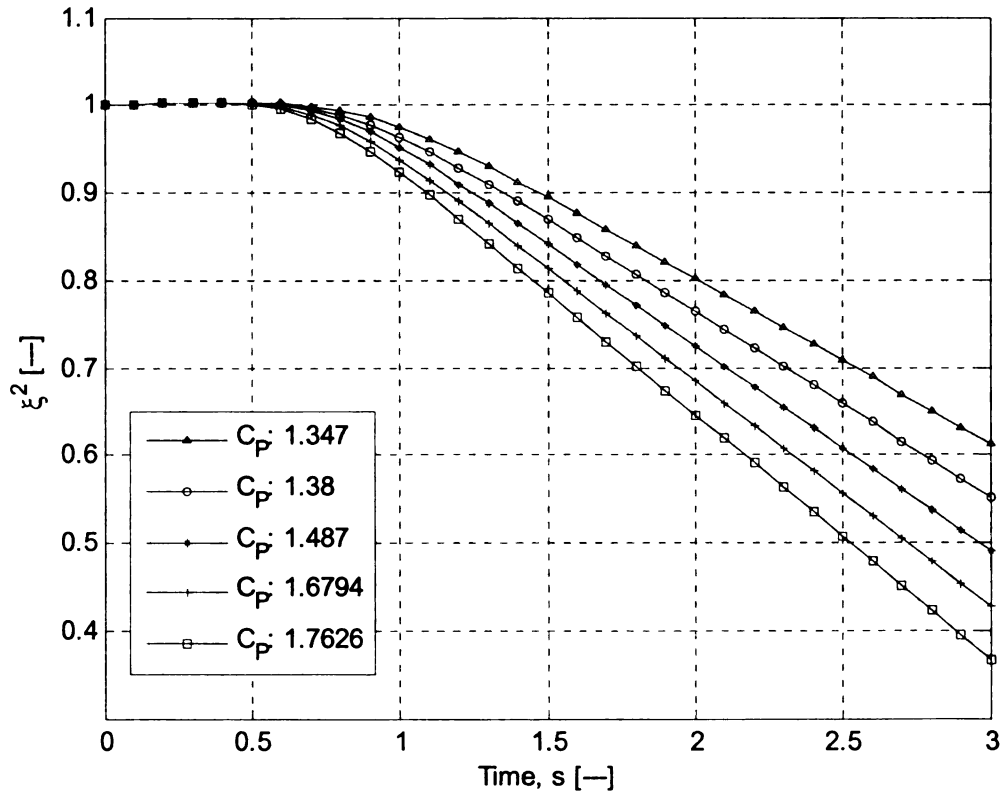


Figure 27. The radius-squared solution.

4.3.7. Sensitivity to the Specific Heat of the Liquid Comprising the Droplet

The specific heat of the liquid comprising the droplet is the constant–pressure specific heat. At atmospheric pressure, the constant–pressure specific heat of liquid propane is 2.25 kJ/kg-K . The following plots illustrate the sensitivity of the surface temperature and the radius–squared to the droplet specific heat for $s \in [0, 3.0]$ where $\Delta C_L = 0.12 \text{ kJ/kg-K}$.

The sensitivity of the surface temperature and solution for the surface temperature are shown in Figure 28 and Figure 29, respectively. Overall, the surface temperature is essentially insensitive to the droplet specific heat, since, from Figure 28, it is apparent that the sensitivity is always of the order 10^{-4} . However, even at this scale, there are some interesting characteristics. The first is that the surface temperature becomes insensitive to the droplet specific heat quite quickly. Also, there are two peaks in sensitivity, both of which occur when the derivative contours of the surface temperature intersect, although the intersections do not occur at the exact same instant. Thus, the contour peaks do not occur at exactly the same instant. The instant where the surface temperature has zero sensitivity to the droplet specific heat occurs at the instants where the droplet returns to its original dimensions. However, relative to the sensitivity of the radius–squared, the surface temperature has negligible sensitivity to the droplet specific heat.

The sensitivity of the radius–squared and the solution for the radius–squared is shown in Figure 30 and Figure 31, respectively. Similar to the behavior of the surface

temperature sensitivity, the sensitivity contours of the radius-squared return to zero when the droplet returns to its original dimensions. Although a large droplet specific heat induces more condensation, it also induces quicker evaporation. During the period of condensation, a high droplet specific heat allows the radius-squared to be more sensitive to the droplet specific heat, whereas when the droplet is evaporating, the radius-squared is less sensitive to changes in the droplet specific heat.

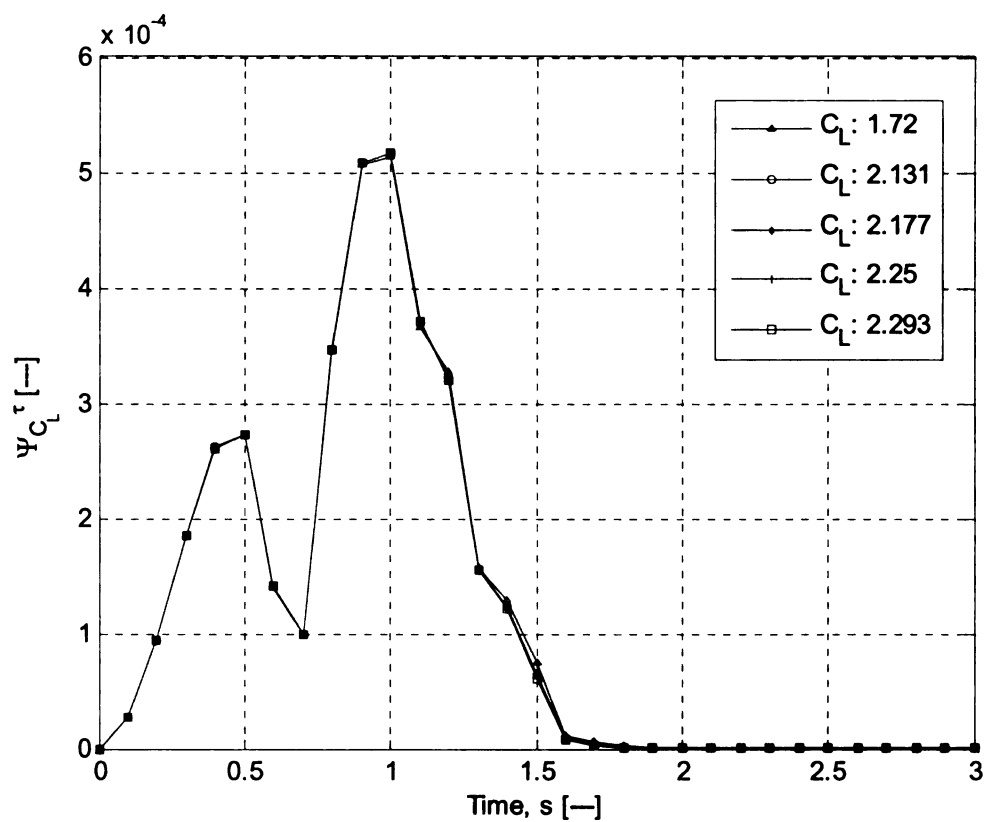


Figure 28. The sensitivity of the surface temperature to the droplet specific heat.

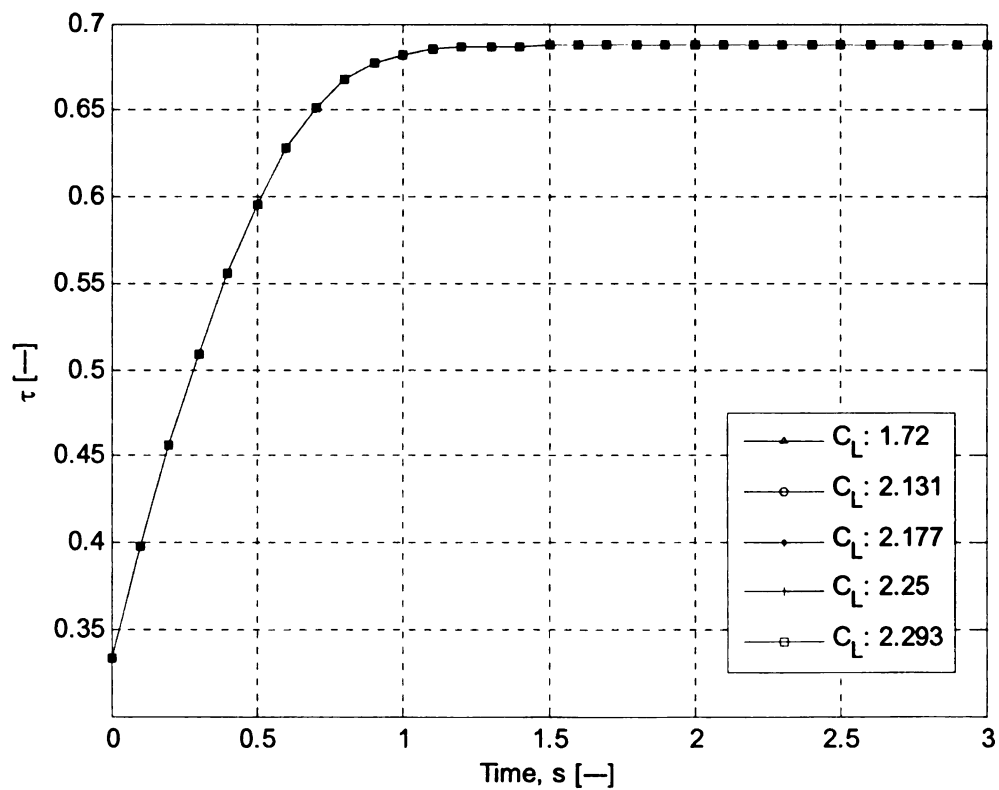


Figure 29. The surface temperature solution.

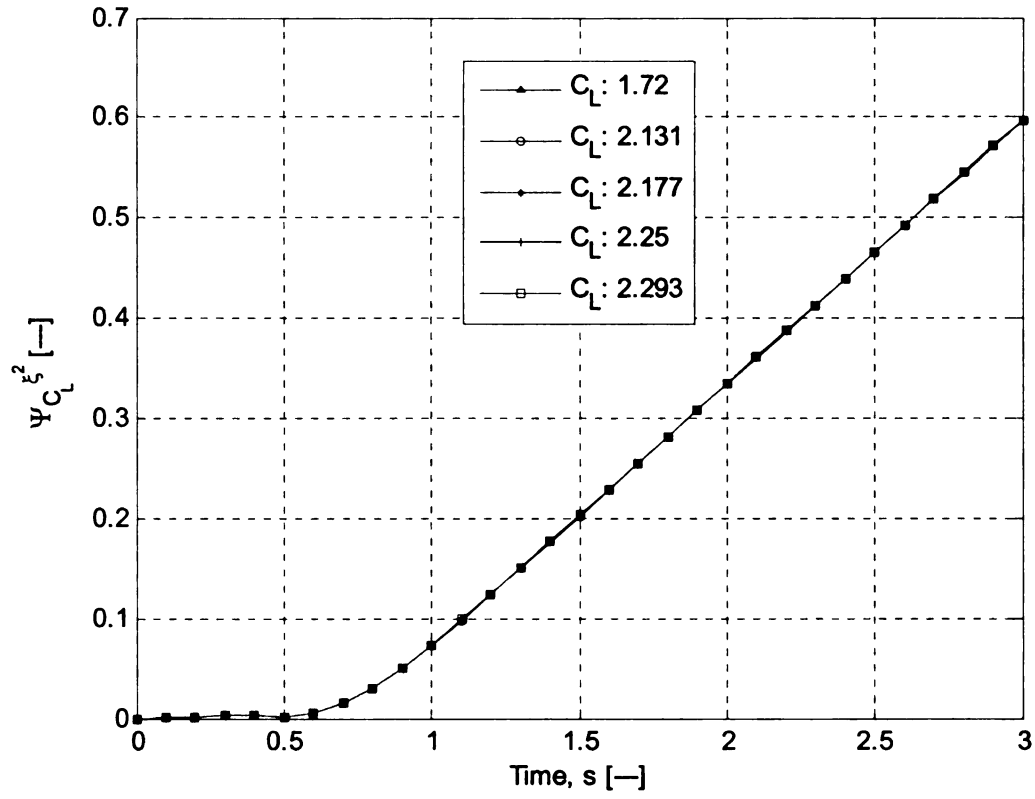


Figure 30. Sensitivity of the radius-squared to the droplet specific heat.

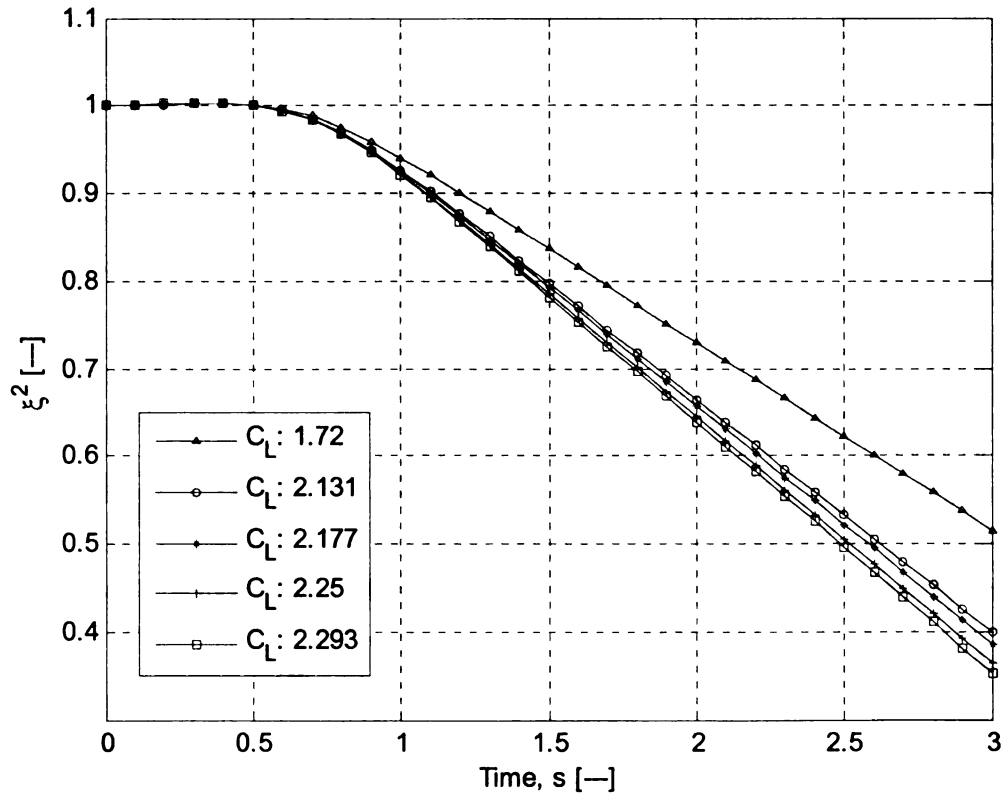


Figure 31. The radius-squared solution.

4.3.8. Sensitivity to the Lewis Number of the Fuel

The Lewis number is the ratio of the thermal diffusivity of the fuel to the mass diffusivity of the fuel. In most combustion-type problems, the Lewis number is of the order unity, which means that the mass is diffusing away from the droplet surface about as fast as heat is conducting toward the droplet surface. If thermal diffusivity is constant, then the Lewis number can only vary if the mass diffusivity varies. The following plots illustrate the sensitivity of the surface temperature and the radius-squared to the fuel Lewis number for $s \in [0, 3.0]$ where $\Delta Le_F = 0.1$.

The sensitivity of the surface temperature and the solution for the surface temperature is given in Figure 32 and Figure 33, respectively. There is a small peak in the sensitivity at the instant the contours of the surface temperature derivatives intersect; specifically, on the LHS of the peak, a lower Lewis number corresponds to a lower derivative (i.e., slower rate of change). On the RHS of the peak, this behavior reverses. Furthermore, a low Lewis number always allows the surface temperature to be more sensitive to changes in the Lewis number. The sensitivity returns to zero when the contours of the surface temperature solution contours intersect again. This intersection is significant since prior to the intersection, a low Lewis number corresponds to a higher surface temperature – a characteristic which reverses after the intersections occurred.

The sensitivity of the radius-squared and the solution for the radius-squared contours are given in Figure 34 and Figure 35, respectively. Some interesting behavior is that the solution contours intersect a few instances before the droplet returns to its original dimensions for a given Lewis number. This intersection is significant since a

low Lewis number corresponds to a larger amount of condensation as well as a faster evaporation. This phenomenon appears to correspond to the instances that the sensitivity returns to zero. Additionally, the sensitivity peaks occur slightly before the droplet attains its maximum size for a given Lewis number; note that radius-squared attains its maximum value when the derivative of radius-squared is zero. Specifically, the sensitivity peaks occur when the contours of the derivatives of the radius-squared intersect. It must be noted that the radius-squared solution contours do not intersect at the exact same instant, nor do the radius-squared derivative contours intersect at the exact same instant, nor do the radius-squared sensitivity contours intersect at the exact same instant; this means no “fixed point” exists in the radius-squared behavior.

Finally, a low Lewis number always allows the radius-squared to be more sensitive to changes in the Lewis number, and also allows a larger amount of condensation (as well as a faster evaporation). Similarly, a low Lewis number always allows the surface temperature to be more sensitive to changes in the Lewis number.

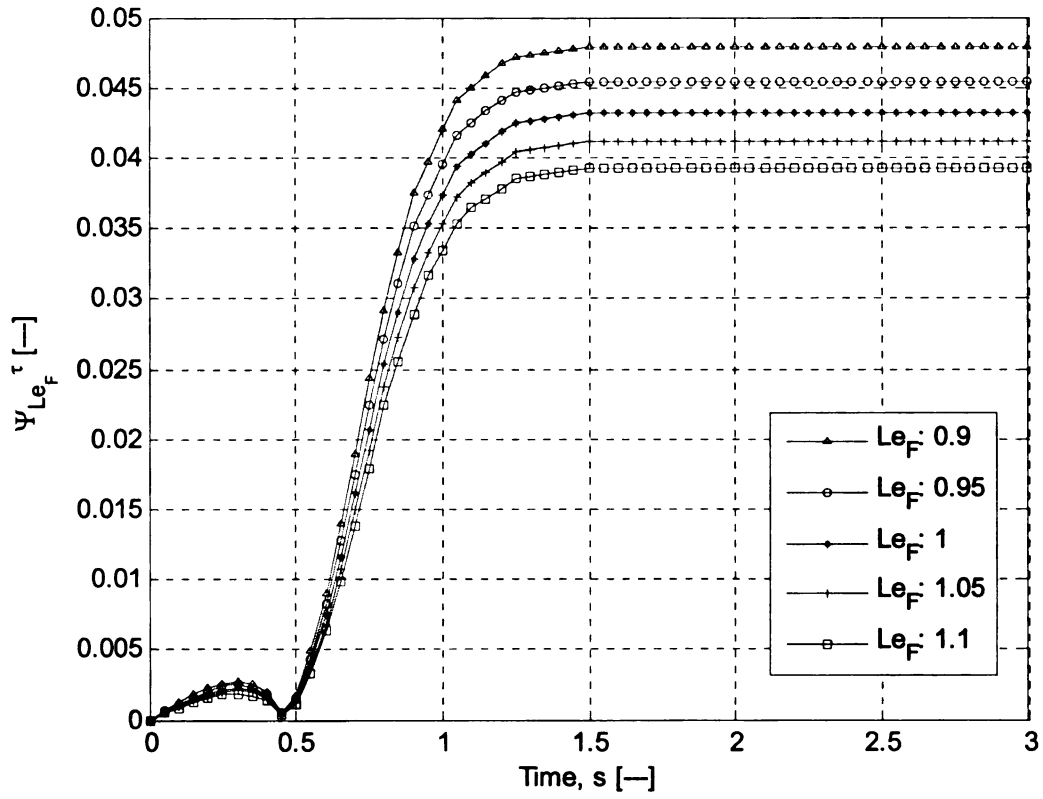


Figure 32. The sensitivity of the surface temperature to the fuel Lewis number.

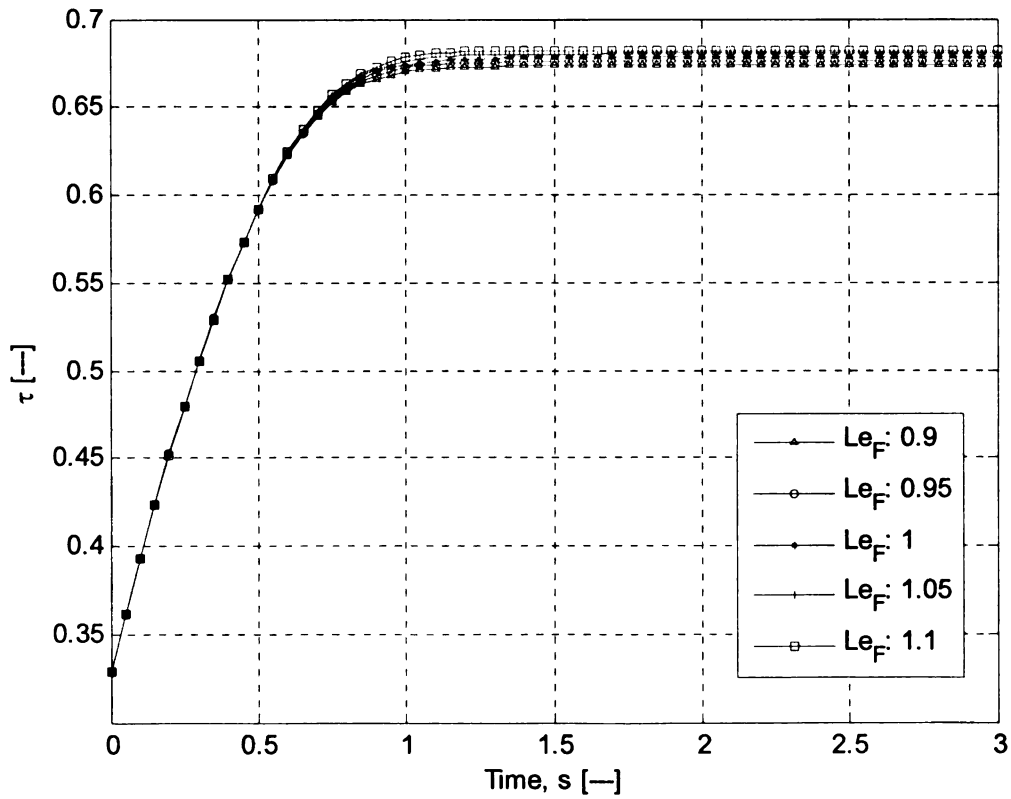


Figure 33. The surface temperature solution.

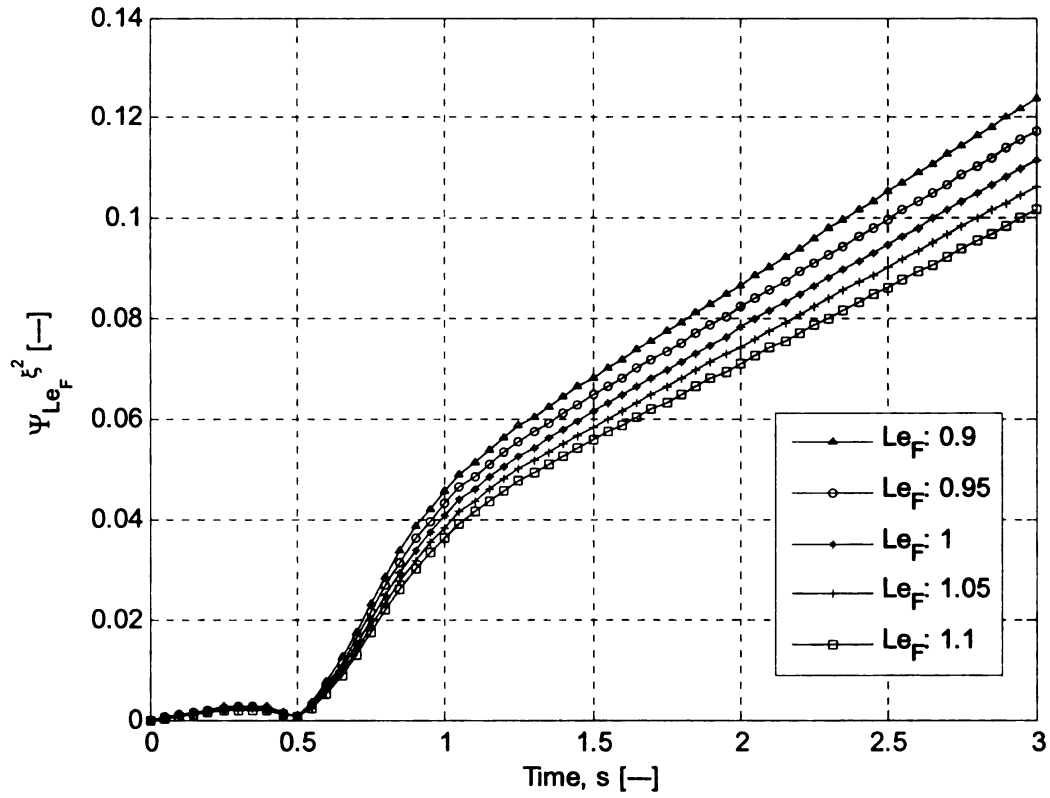


Figure 34. The sensitivity of the radius-squared to the fuel Lewis number.

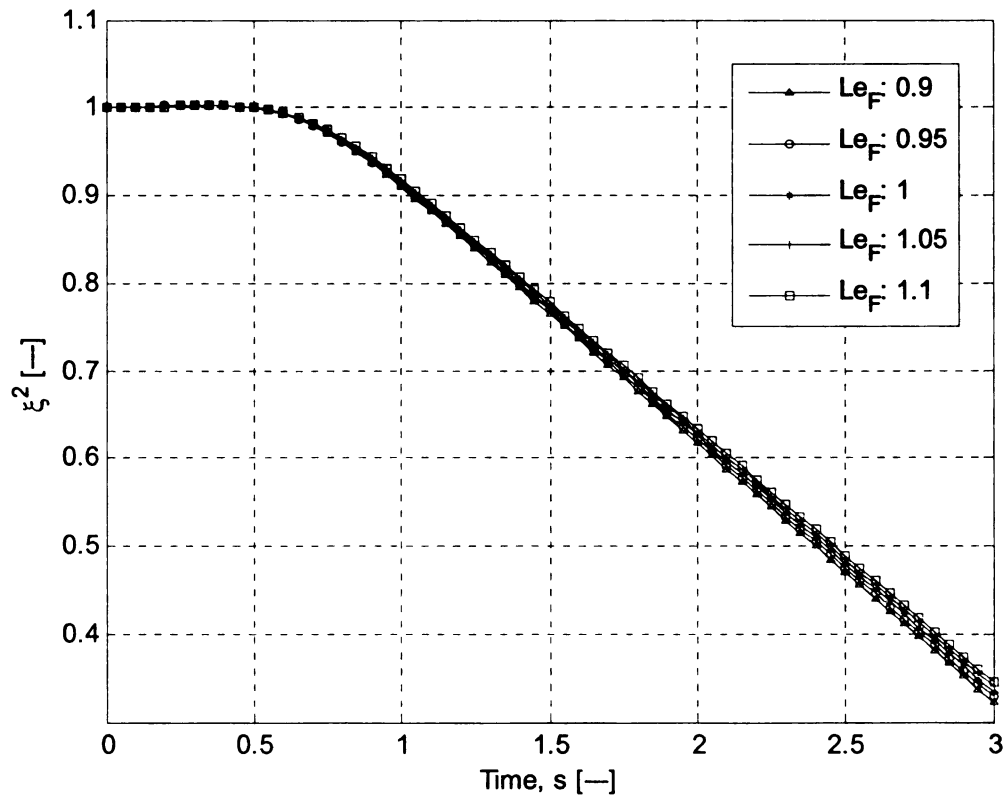


Figure 35. The radius-squared solution.

4.3.9. Sensitivity to the Ambient Mass Fraction

The ambient mass fraction of the fuel represents the portion of the fuel which is in the ambient; as such, it usually has a very small value. For this thesis, ambient mass fraction was set to a nominal value of 0.01. The following plots illustrate the sensitivity of the surface temperature and the radius-squared to the ambient mass fraction for $s \in [0, 3.0]$ where $\Delta Y_{F\infty} = 0.012$.

The sensitivity of surface temperature and solution of surface temperature is given in Figure 36 and Figure 37, respectively. Each sensitivity contour experiences a steady rise to a peak; then there is a steady decrease to constant-value behavior. However, before each sensitivity contour attains its peak, there is a reversal (Figure 36). Specifically, on the LHS of the reversal, a large $Y_{F\infty}$ -value induces greater sensitivity in the surface temperature; also, a large $Y_{F\infty}$ -value corresponds to a higher surface temperature, as well as a higher value for the derivative of the surface temperature. On the RHS of the reversal, a large $Y_{F\infty}$ -value induces a low sensitivity in the surface temperature which is maintained for all time. The sensitivity contours attain their respective peaks in the same interval in which the surface temperature derivative contours intersect one another, although the sensitivity contours peaks do not occur at the exact same instant nor do the derivative contours intersect at the exact same instant. For the entire evaporation process, a higher $Y_{F\infty}$ -value allows surface temperature to achieve a higher value.

The sensitivity of the radius-squared and the solution for the radius-squared are given in Figure 38 and Figure 38, respectively. From Figure 38, the radius-squared sensitivity has similar behavior to the surface temperature sensitivity. The sensitivity contours intersect one another just after the solution contours attain their respective peaks (i.e., before condensation reaches a maximum) and just before the solution contours return to unity. Prior to the intersection of the sensitivity contours, a high $Y_{F\infty}$ -value induces a high sensitivity in the radius-squared; afterward, a high $Y_{F\infty}$ -value induces a low sensitivity in the radius-squared which is maintained for the remainder of the evaporation. The first peaks (i.e., relative maxima) of the sensitivity contours occur in the same interval in which the respective radius contours return to unity. This is also the same interval in which the contours of the derivatives of the radius-squared intersect each other. On the LHS of the first sensitivity peaks, a high $Y_{F\infty}$ -value corresponds to higher derivative; on the RHS, a lower derivative. After the sensitivity contours have attained their respective peaks, the sensitivity contours of the radius-squared monotonically decrease until they reach their respective relative minima. These relative minima occur in the same interval in which the contours of the derivatives of the radius-squared intersect each other a second time.

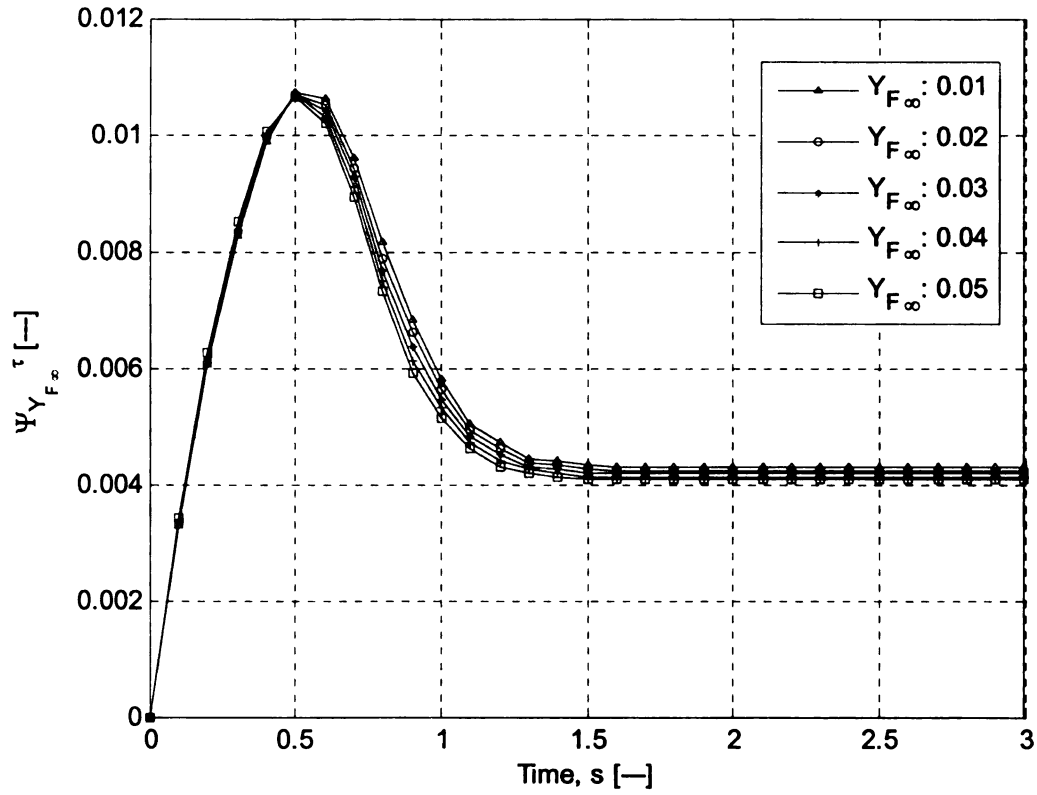


Figure 36. The sensitivity of the surface temperature to the ambient mass fraction.

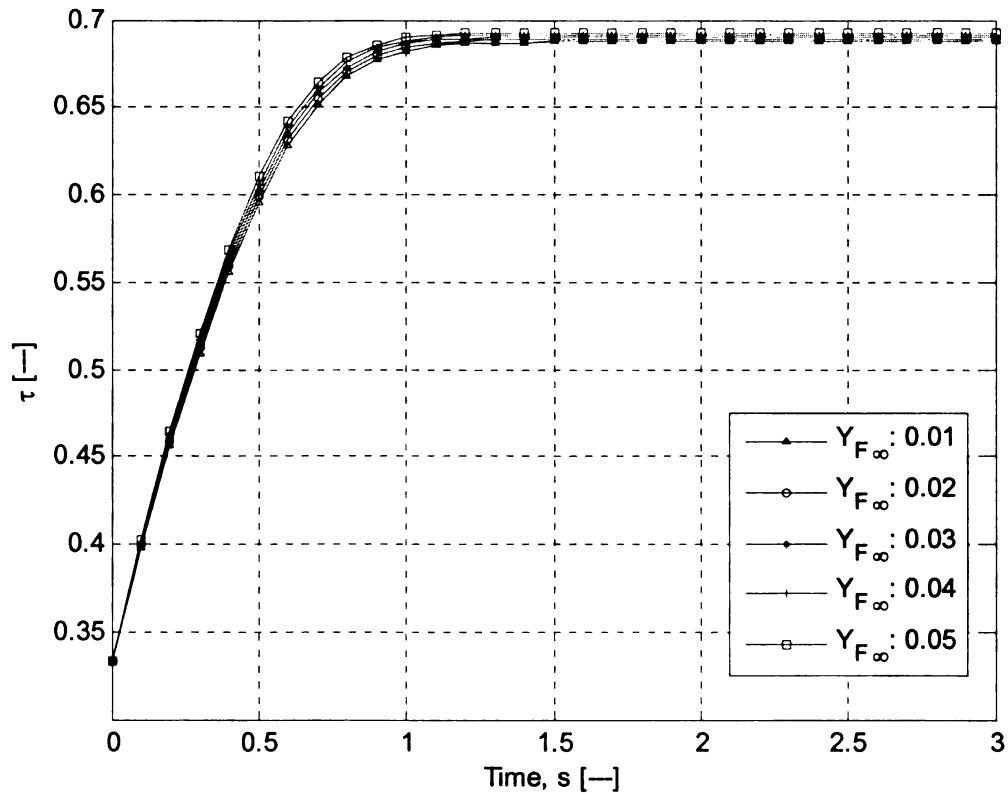


Figure 37. The surface temperature solution.

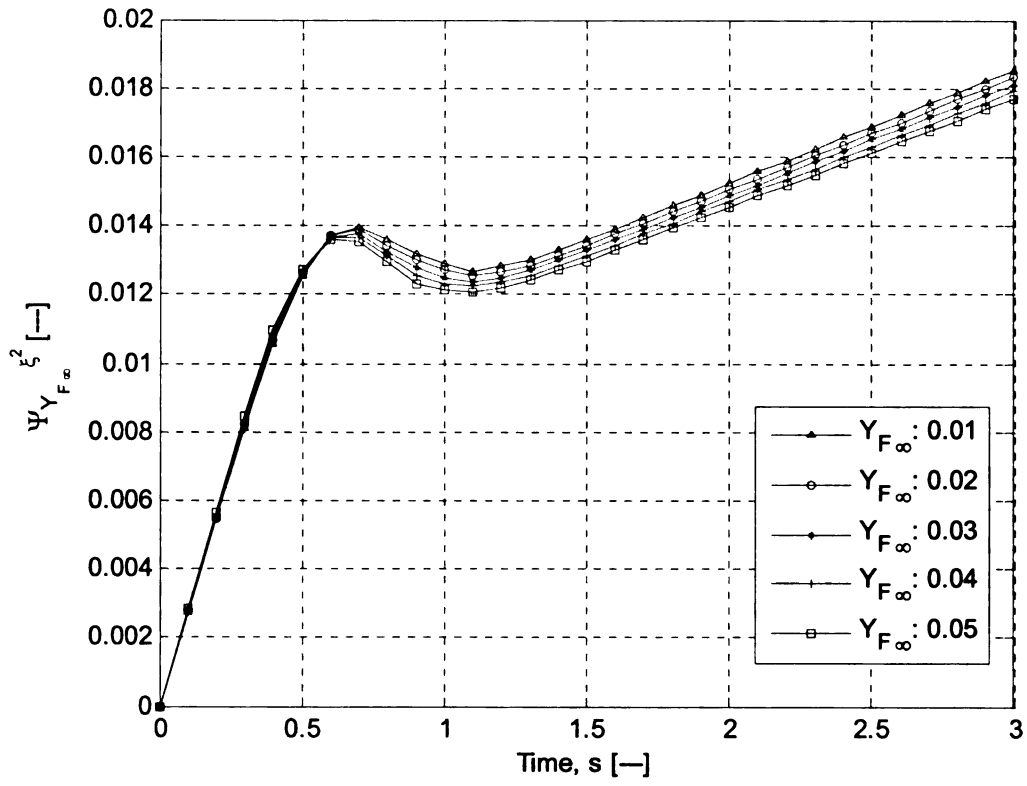


Figure 38. The sensitivity of the radius-squared to the ambient mass fraction.

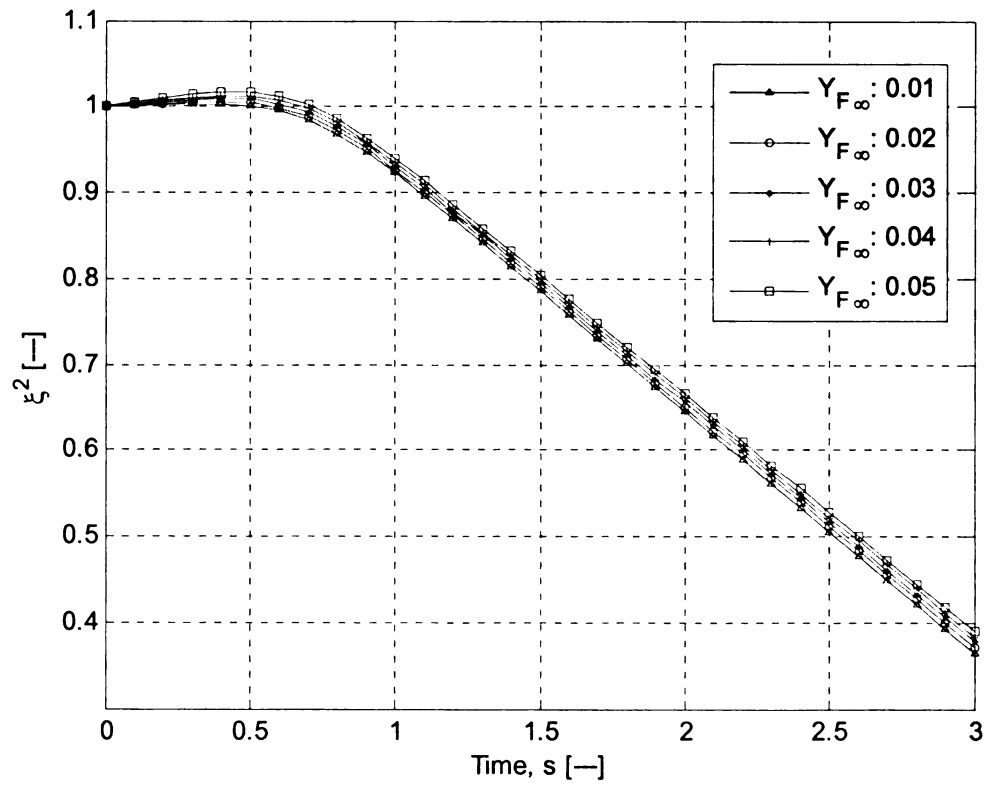


Figure 39. The radius-squared solution.

4.3.10. Sensitivity to the Mass Fraction above the Evaporated Surface

The mass fraction of the fuel above the droplet surface represents the portion of fuel that exists immediately above the droplet surface. As such, it is always of the order unity. For this thesis, the mass fraction above the droplet surface was assigned a nominal value of 0.9. The following plots illustrate the sensitivity of the surface temperature and the radius-squared to the mass fraction above the evaporated surface for $s \in [0, 3.0]$ where $\Delta Y_{Fb} = 0.06$.

The sensitivity of the surface temperature and the solution for the surface temperature are given in Figure 40 and Figure 41, respectively. At first, the surface temperature has negligible sensitivity to Y_{Fb} – this is the interval of condensation. Then there is a steady increase in sensitivity up to a steady state value. For all time, a large Y_{Fb} -value induces lower sensitivity in the surface temperature. Additionally, a large Y_{Fb} -value allows the surface temperature to achieve a lower value.

The sensitivity of the radius-squared and the solution for the radius-squared are given in Figure 42 and Figure 43 respectively. Similar to the surface temperature sensitivity, there is an interval in which the radius-squared has negligible sensitivity to Y_{Fb} . Then the radius-squared becomes progressively more sensitive for the remainder of the evaporation process. Also, a high Y_{Fb} -value induces lower sensitivity in the radius-

squared, as well as allows the radius-squared to achieve smaller values, i.e., a high Y_{Fb} -value corresponds to a smaller condensation, thus a shorter evaporation time.

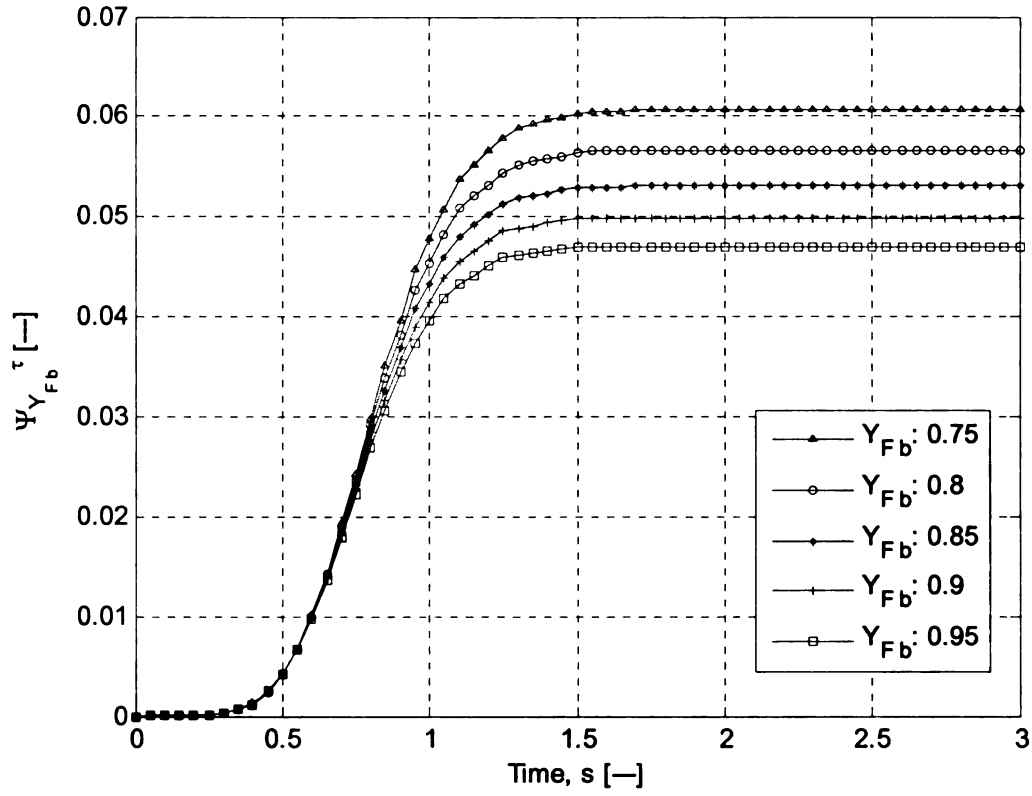


Figure 40. The sensitivity of the surface temperature to the evaporated mass fraction.

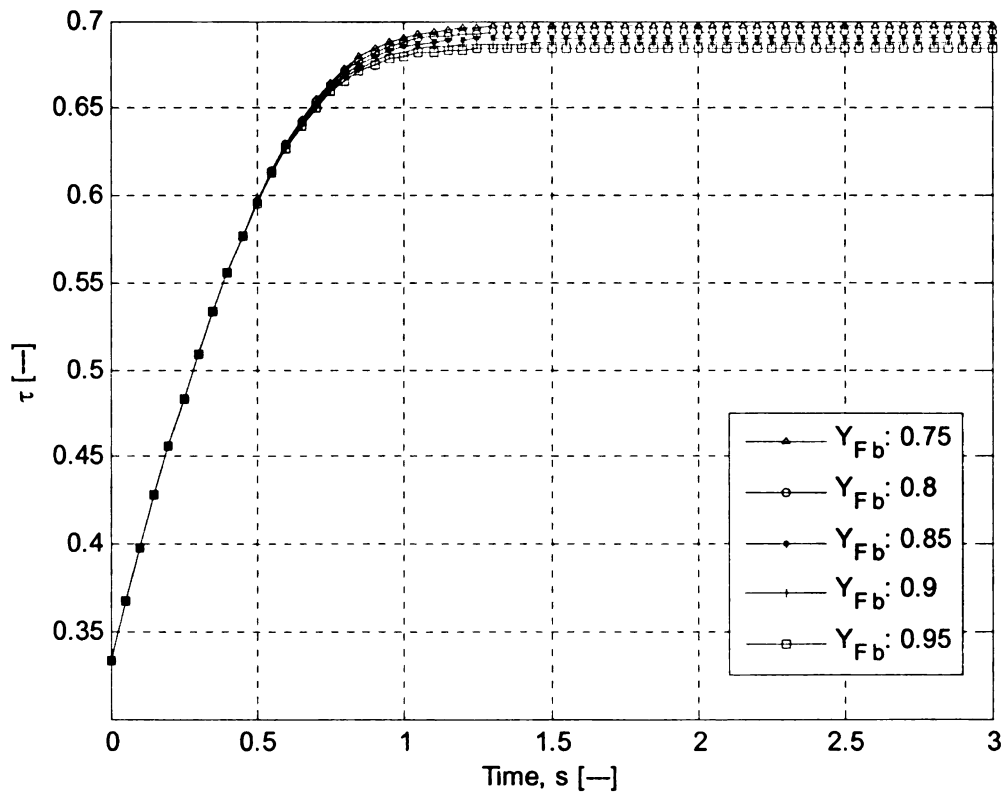


Figure 41. The surface temperature solution.

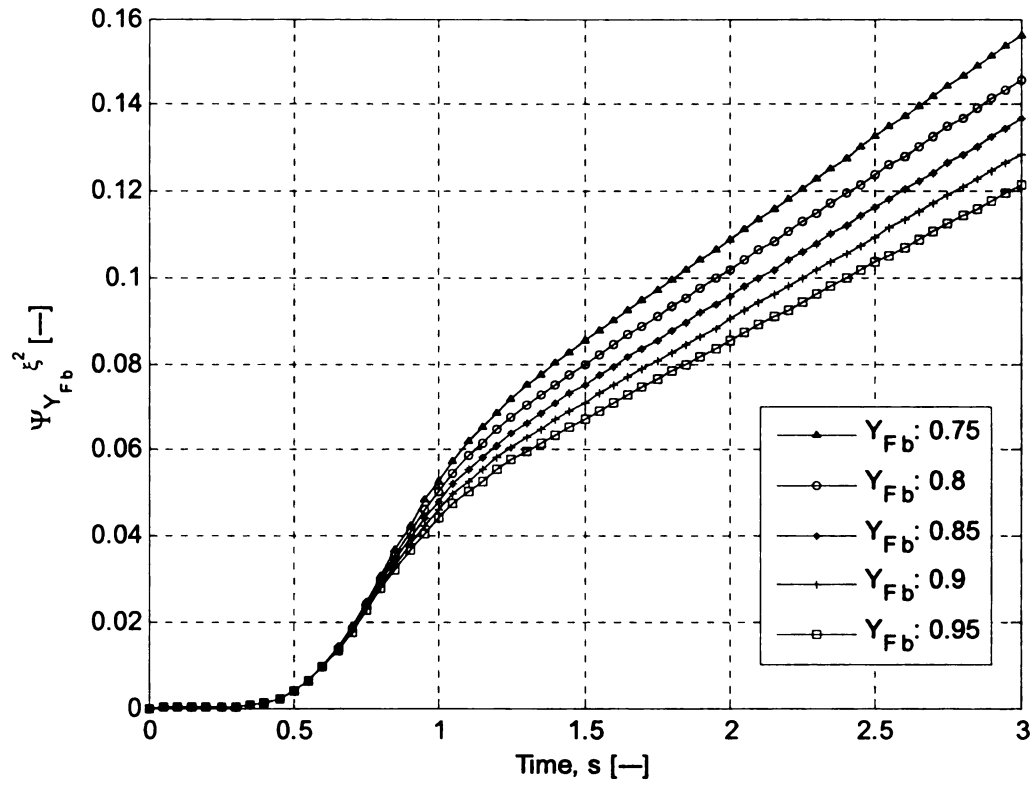


Figure 42. The sensitivity of the radius-squared to the evaporated mass fraction.

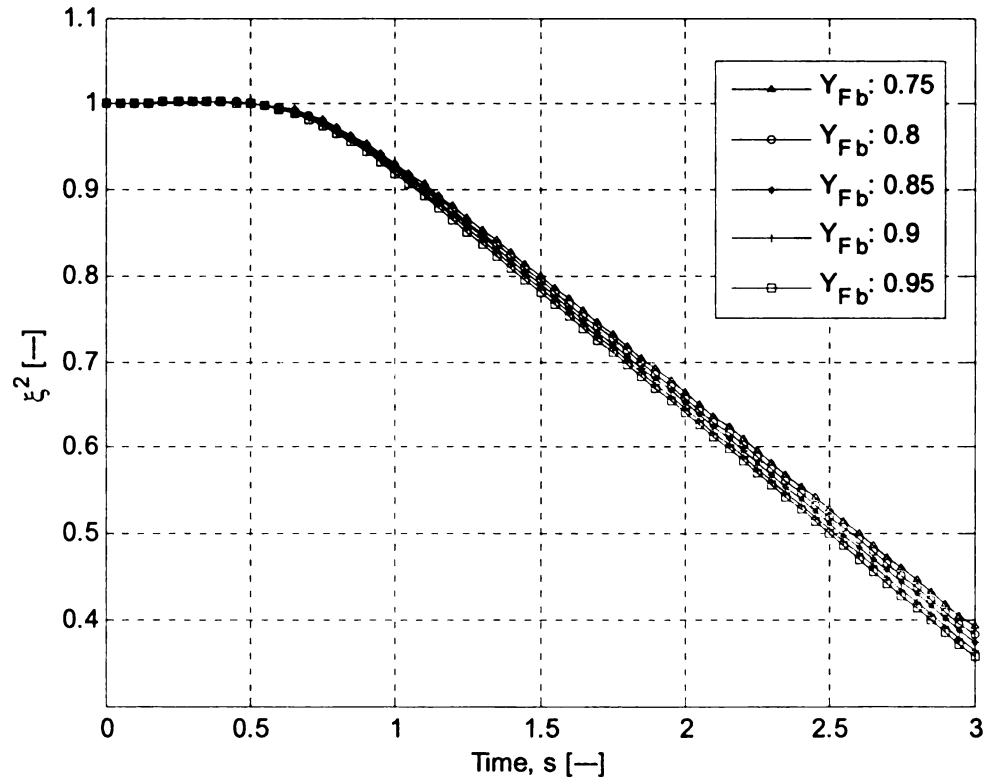


Figure 43. The radius-squared solution.

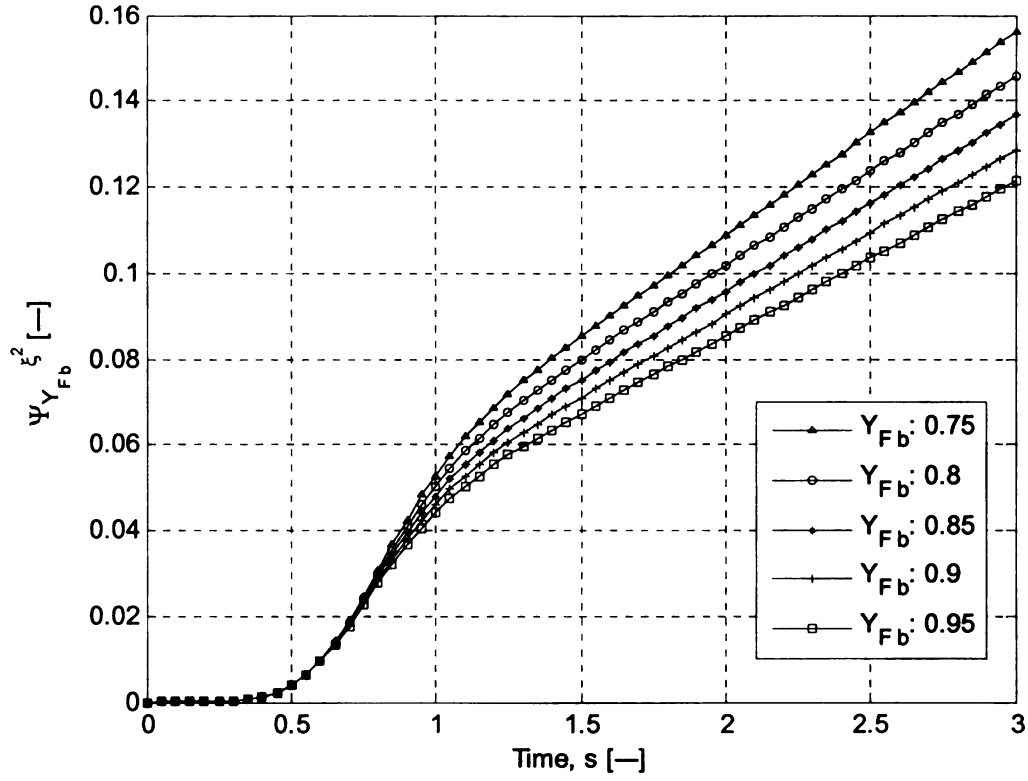


Figure 42. The sensitivity of the radius-squared to the evaporated mass fraction.

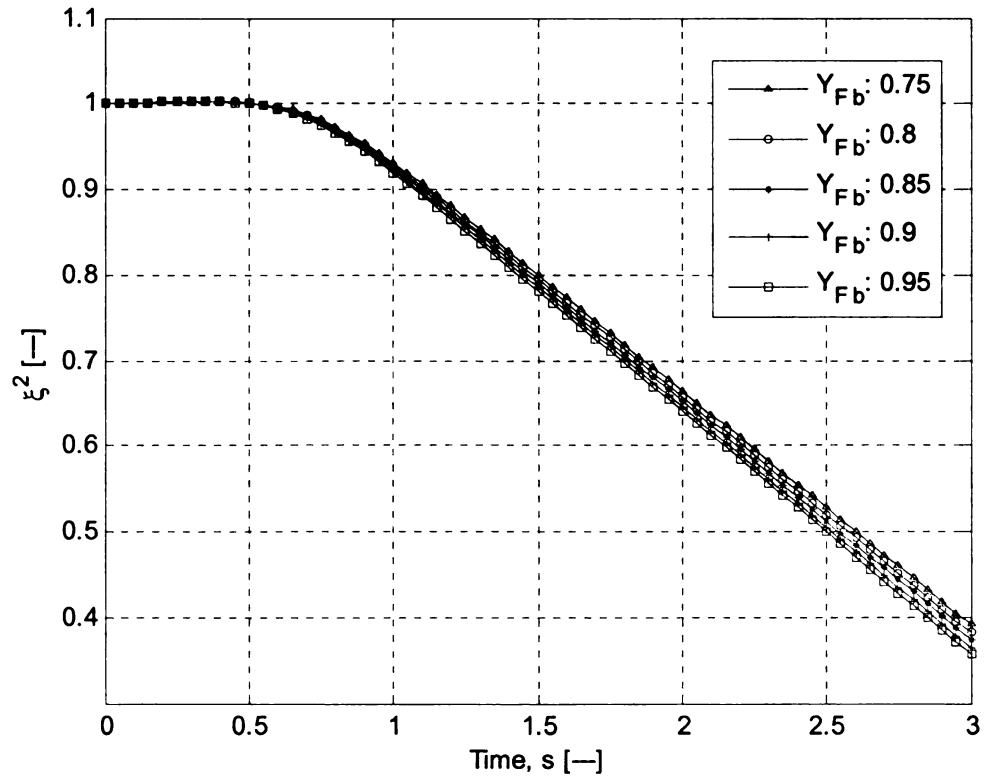


Figure 43. The radius-squared solution.

4.3.13. Final Conclusions for the Sensitivity Analysis

Essentially, both the sensitivity of the surface temperature and the sensitivity of the radius-squared follow the same pattern. For example, if the surface temperature sensitivity contours intersect, the radius-squared sensitivity contours also intersect. The first major difference is that the surface temperature sensitivity contours level off to constant values, whereas the radius-squared sensitivity contours progressively increase throughout the evaporation process.

The only parameter that defied this generality was the initial temperature. The surface temperature quickly became totally insensitive to the initial temperature of the droplet, whereas the radius-squared developed a constant sensitivity to the initial temperature. The second major difference was in the magnitude of the sensitivity – usually the radius-squared was substantially more sensitive to small changes in the parameters than surface temperature. The exceptions were the boiling temperature, the ambient temperature, the ambient mass fraction, and the evaporated-surface mass fraction. The surface temperature and the radius-squared had approximately equal sensitivity to these parameters.

Overall, the surface temperature experienced some interesting behavior with respect to certain parameters. The sensitivity of the surface temperature experienced reversals for the following parameters: the gas constant, the ambient temperature, and the ambient mass fraction. Specifically, large R and large $Y_{F\infty}$ at first induced more sensitivity in the surface temperature, whereas large T_∞ induced lower sensitivity (Figure

2, Figure 16, and Figure 36, respectively). The reversal was maintained for the gas constant and the ambient mass fraction for the remainder of the evaporation process. However, the ambient temperature induced another reversal in the surface temperature sensitivity (for a total of two reversals).

Although these parameters reversed their influence on the sensitivity of the surface temperature, they did not appear to reverse their influence on the surface temperature itself, i.e., large R and large T_∞ allowed the surface temperature to achieve smaller values (Figure 3 and Figure 17, respectively) for the entire evaporation process, and large $Y_{F\infty}$ -values allowed the surface temperature to achieve higher values (Figure 35).

The radius-squared tended to be relatively insensitive to all of the parameters during the condensation process. The exceptions to this were the initial temperature (Figure 22) and the ambient mass fraction (Figure 38), both of which saw an immediate increase in the sensitivity. After the condensation process ended and the evaporation started, the radius-squared grew progressively more sensitive to the parameters for the remainder of the evaporation process.

Concerning an overall “sensitivity magnitude,” the surface temperature is sensitive to the following parameters (from lowest sensitivity to highest): T_0 , C_L , $Y_{F\infty}$, L_v , C_p , Le_F , Y_{Fb} , R , T_∞ , T_b . The radius-squared is sensitive to the following parameters (from lowest sensitivity to highest): $Y_{F\infty}$, Le_F , Y_{Fb} , R , C_p , T_0 , C_L , L_v , T_b , T_∞ .

Another interesting characteristic was the presence of “peaks” in the sensitivity contours; these contour peaks occurred as either relative maxima or relative minima. Specifically, these contour peaks occurred for the following parameters: the gas constant, the latent heat of vaporization, the ambient temperature, the vapor specific heat, the droplet specific heat, the fuel Lewis number, and the ambient mass fraction. The contour peaks always occurred in the same interval in which the surface temperature derivative contours or the radius-squared derivative contours intersected – the derivative contours never intersected at the exact same instant, thus the sensitivity contours never peaked at the exact same instant. Figure 44 is a plot of equation (11.i) for contours of constant latent heat of vaporization; Figure 45 is a close-up of Figure 44 in the vicinity of the contour intersections. The purpose of these figures is to illustrate that there is no “fixed point” in the governing equations.

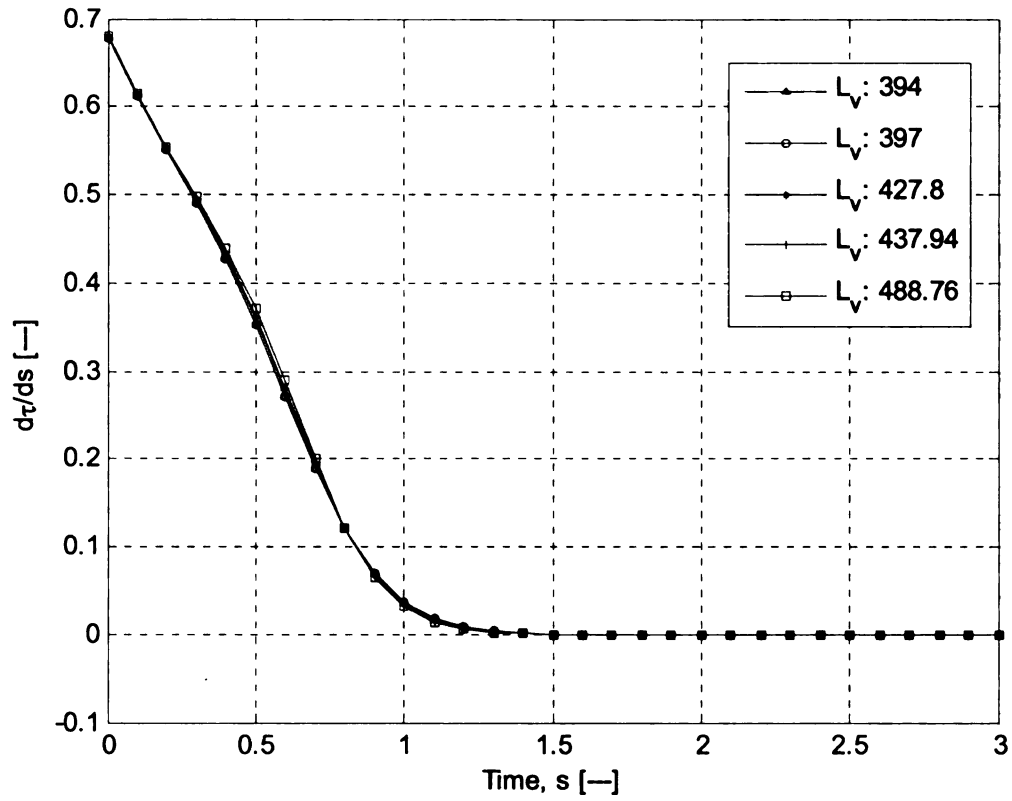


Figure 44. A plot of eqn. (11.i) for contours of constant latent heat.

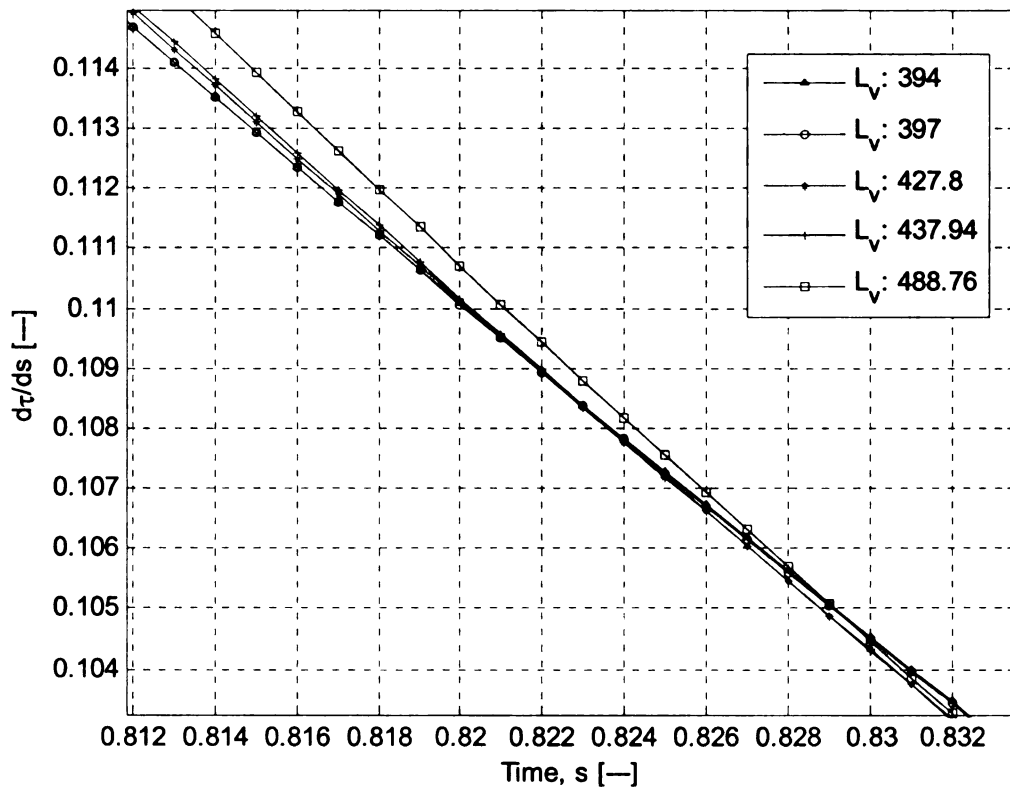


Figure 45. A close-up of Figure 44 in the vicinity of the contour intersections.

Chapter 5: The Optimization Study

5.1. Overview

This part of this thesis is concerned with parameter optimization. For this portion of the study, the HEEDS®² software package was utilized. Since this software was developed to find optimal designs based on certain constraints, the parameter optimization study can be considered as finding a hydrocarbon fuel that possesses these optimized parameters. In a HEEDS® parameter optimization study, optimized designs are sought by iteratively changing the values of certain variables, executing the defined analyses, and evaluating the responses of each design candidate. New design candidates are generated based on the various mathematical search algorithms in HEEDS®. Primarily, the SHERPA³ search algorithm was utilized since it is a particularly effective method for most parameter optimization problems. During a single search, this method uses multiple search algorithms simultaneously as opposed to sequentially. Furthermore, the SHERPA method is capable of learning about the design space and adaptively navigating many types of design spaces.

² Acronym for **H**ierarchical **E**volutionary **E**ngineering **D**esign **S**ystem

³ Acronym for **S**ystematic **H**ybrid **E**xploration that is **R**obust, **P**rogressive, and **A**ddaptive.

The parameters to be optimized are the relevant physical constants (e.g. latent heat, boiling temperature, etc.); they are optimized in order to minimize s_b , where s_b is the dimensionless instant of time that the droplet disappears. At this condition, we have $\xi^2(s_b) = 0$. For this study, all values for these parameters are restricted to those of hydrocarbon fuels. In other words, the range of the parameter space of the governing parameters is restricted to that which corresponds to hydrocarbon fuels. For all of the parameter optimization runs, the following items will be shown: an agent response plot, a table containing the *best* designs, and a table containing the parameter ranges.

For this study, a *good* design is one in which the burn-out time is less than the baseline as well as one in which the parameters lie within the specified range. The baseline hydrocarbon is propane; the baseline parameter values are given in section 3.6.

5.2. Computational Methodology

This optimization study is done in two parts. The first part is the necessary background analysis work, viz., solving the governing equations based on the given values for the physical parameters; this part is done in the C++ programming language. The governing equations are solved with the classical 4th order Runge-Kutta method, the form of which is given in equation (14).

$$x(t+h) = x(t) + \frac{1}{6}(K_1 + 2K_2 + 2K_3 + K_4) \quad (14.i)$$

$$K_1 = h f(t, x) \quad (14.ii)$$

$$K_2 = h f\left(t + \frac{h}{2}, x + \frac{K_1}{2}\right) \quad (14.iii)$$

$$K_3 = h f\left(t + \frac{h}{2}, x + \frac{K_2}{2}\right) \quad (14.iv)$$

$$K_4 = h f\left(t + h, x + K_3\right) \quad (14.v)$$

Note that the function $f(t, x)$ refers to the ordinary differential equation or system thereof. Since we have a system of two ordinary differential equations, we can write them in vector form as follows:

$$\dot{\vec{x}} = \vec{f}(t, \vec{x}(t))$$

This algorithm was validated by comparing its results to those acquired by MATLAB®; there is agreement between the two usually to the second or the third decimal place.

The second part is the optimization process, which is conducted in HEEDS®. It is necessary to explain some of the terms that are found in a HEEDS® optimization study. All HEEDS® projects, regardless of type, have the following elements: at least one *process* which contains at least one *analysis*; a set of project *variables*; a set of project *responses*; and at least one *agent* [28]. In this thesis, the analysis solves the governing equations in order to determine the instant at which the droplet is completely evaporated. A process is the analysis (or set of analyses) that are performed by an agent to fully evaluate a particular design. Some evaluations may require a single analysis, while other evaluations may require several analyses and use different analysis tools. The project variables are the quantities that are varied – here, the variables are the

physical parameters. The project response is simply the value of s_b , i.e., the dimensionless instant of time that total evaporation has occurred. Finally, an agent executes and controls the design exploration. In this application, a *design evaluation* is simply the burn-out time. In other words, the computation of a new value for the burn-out time, given new parameter values, constitutes a design evaluation.

For this particular study, HEEDS® requires three items from the user: an input file, an executable file, and an output file. The input file contains a list of values for the physical parameters, or the *baseline* design, which is used by HEEDS® as a starting point for the optimization process. As mentioned earlier, propane was chosen as the baseline design. The executable file is created when the C++ source code is compiled. Finally, the output file is created when the executable file is run (or executed).

Finding the instant that the radius-squared goes to zero makes this a root-finding problem. The derivative of ξ^2 is known from the governing equations (equation (11.ii)), so ξ^2 itself is needed in order to utilize the Newton-Raphson method, the general form of which is the following:

$$t_{n+1} = t_n - \frac{F(t_n)}{F'(t_n)}$$

A subtle point about all root-finding methods is the choice of an initial guess for the root. This means that if the initial guess is “close” to the actual root, then the method will converge to that root. For the Newton-Raphson method, a quadratic convergence rate exists for an initial guess which is sufficiently close to the root.

In this particular study it is known *a posteriori* that ξ^2 develops a linear decay. Also, the Newton–Raphson method converges in exactly one iteration if $F(t)$ is linear, i.e., if $F(t)$ has the form $F(t) = a + bt$. Thus, for this study, the burn–out time, s_b , is calculated via equation (15).

$$s_b = s_{b,initial} - \frac{\xi^2}{(-\lambda\chi)} \quad (15)$$

The algorithm is as follows:

1. Compute θ until θ is about constant; if $\theta > 1$, evaporation is present so the algorithm can proceed.
2. Check for condensation. If $\xi^2 > 1$ at $s = h$, i.e., the next time step, then condensation is present. Thus a critical time (s_c) can be calculated ($s_c \equiv$ instant where ξ^2 returns to unity). The current code will return $s_c - h$. This is acceptable since s_c is ONLY used for computing an initial guess for s_b , which is $s_{b,initial} = 2.0*s_c$. It is known *a posteriori* that the factor of 2.0 moves the evaluation far enough into the linear region of ξ^2 such that the single-iteration N-R method returns reasonable results.
3. If condensation is not present, then the slope of ξ^2 must be considered in order to determine an initial guess for s_b . The slope is first computed at $s = h/10$; then the slope is computed a second time at $s = h$ (note that h has been fixed at 0.001). Then

these results are passed to a pretest loop where subsequent slopes are computed. When two consecutive slopes are within 1.0×10^{-8} of each other, the loop stops since the slope of ξ^2 is sufficiently linear. The initial guess to s_b is taken as the s – value where the most recent slope was computed.

5.3. Results and Discussion

5.3.1. Optimization of the Gas Constant, the Latent Heat of Vaporization, the Boiling Temperature, the Vapor Specific heat, the Droplet Specific Heat, the Vapor Thermal Conductivity, and the Droplet Density

For this optimization run, the following parameters are optimized in order to minimize the burn-out time: the gas constant, the latent heat of vaporization, the boiling temperature, the vapor specific heat, the droplet specific heat, the thermal conductivity, and the droplet density. For this study the parameter domain is given by Table 1. These ranges were selected since they are representative of common hydrocarbon fuels such as ethane and benzene. The computed burn-out time per evaluation (agent response plot) is given in Figure 46. The top-ranking designs (from worst down to best) are given in Table 2. The units of the parameters are given in section 3.6.

Table 1. Parameter ranges for those that are varied.

	R	L_v	T_b	C_P	C_L	k_g	ρ_L
Minimum	0.072783	300	180	1.2	1.7	0.0136	546.49
Baseline	0.1885	427.8	231.05	1.6794	2.25	0.0151	581
Maximum	0.2765	500	400	1.823	3.11	0.148	680.5

Table 2. Top – ranking designs.

s_b	R	L_v	T_b	C_P	C_L	$k_g (10^{-4})$	ρ_L
2.50135	0.1441	492	186.6	1.5987	2.024	1.22	671.1193
1.91127	0.0769	304	224	1.4617	2.433	0.19	638.9569
1.63547	0.0728	500	180	1.2000	3.110	1.48	680.5
1.19067	0.0728	300	180	1.2000	3.110	1.48	680.5
1.18933	0.1054	300	180	1.2000	3.110	1.48	680.5
1.18578	0.1013	300	180	1.2000	3.110	1.48	680.5

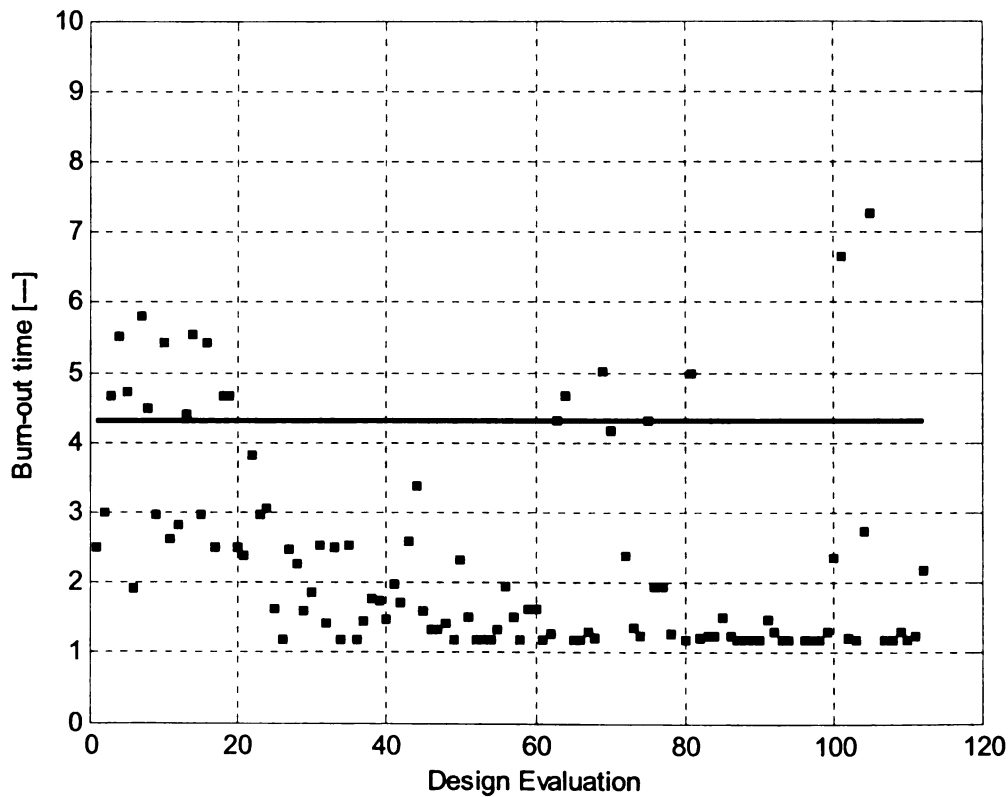


Figure 46. Burn-out time per design evaluation. The horizontal line represents the burn-out time for a propane droplet, i.e., the baseline design.

From Figure 46, it is apparent that in about the first twenty evaluations, HEEDS© has found about as many “bad” designs as good designs; this is because the SHERPA method is randomly sampling the design space in order to acquire an understanding of the design space. However, by the 30th evaluation, HEEDS© has essentially converged. The presence of the outliers is due to the fact that the SHERPA method never stops searching the design space for an even better design.

From the Table 1 and Table 2, we see that the optimal gas constant is between the minimum allowable value and the baseline, albeit closer to the minimum; the optimal latent heat is consistent at its minimum allowable value as is the optimal boiling temperature. The vapor specific assumed its minimum allowable value whereas the liquid specific heat assumed its maximum allowable value. The thermal conductivity and liquid density both assumed their maximum allowable values.

Intuitively, a fuel droplet will experience the quickest evaporation if the droplet has a low latent heat of vaporization and a low boiling temperature (thus the droplet must absorb a smaller amount of energy in order to change phase). Also, vapor with a low heat capacity will serve to accelerate evaporation.

A minimal gas constant indicates a large molar mass (recall section 3.2 and 4.3.1). A larger molar mass would aid in evaporation since it would allow the substance to have a higher heat capacity. Thus it follows that a droplet with a large heat capacity would serve to accelerate evaporation since a large specific heat essentially means that the droplet “holds” a large quantity of heat that aids in the evaporation of near-surface molecules.

To optimize k_g and ρ_L may not yield reliable results since it is known from the sensitivity analysis that both the surface temperature and the radius-squared are completely insensitive to these parameters.

5.3.2. Optimization of the Gas Constant, the Latent Heat of Vaporization and the Boiling Temperature

For this optimization run, the following parameters are optimized in order to minimize the burn-out time: the gas constant, the latent heat of vaporization, and the boiling temperature. For this study the parameter domain is given by Table 3. These ranges were selected since they are representative of common hydrocarbon fuels such as ethane and benzene. The computed burn-out time per evaluation (agent response plot) is given in Figure 47. The top-ranking designs (from worst down to best) are given in Table 4. The units of the parameters are given in section 3.6.

Table 3. Parameter ranges for those that are varied.

	R	L_v	T_b
Minimum	0.072783	300	180
Baseline	0.1885	427.8	231.05
Maximum	0.2765	500	400

Table 4. Top – ranking designs.

s_b	R	L_v	T_b
33.06541	0.1278	462	380.2
14.97371	0.0789	396	318.6
7.828994	0.2419	396	303.2
3.184831	0.1033	378	191
3.131561	0.1033	404	182.2
2.561621	0.0728	300	180
2.556044	0.0769	300	180
2.553503	0.0789	300	180
2.54645	0.0932	300	180
2.545874	0.0911	300	180
2.545723	0.0893	300	180

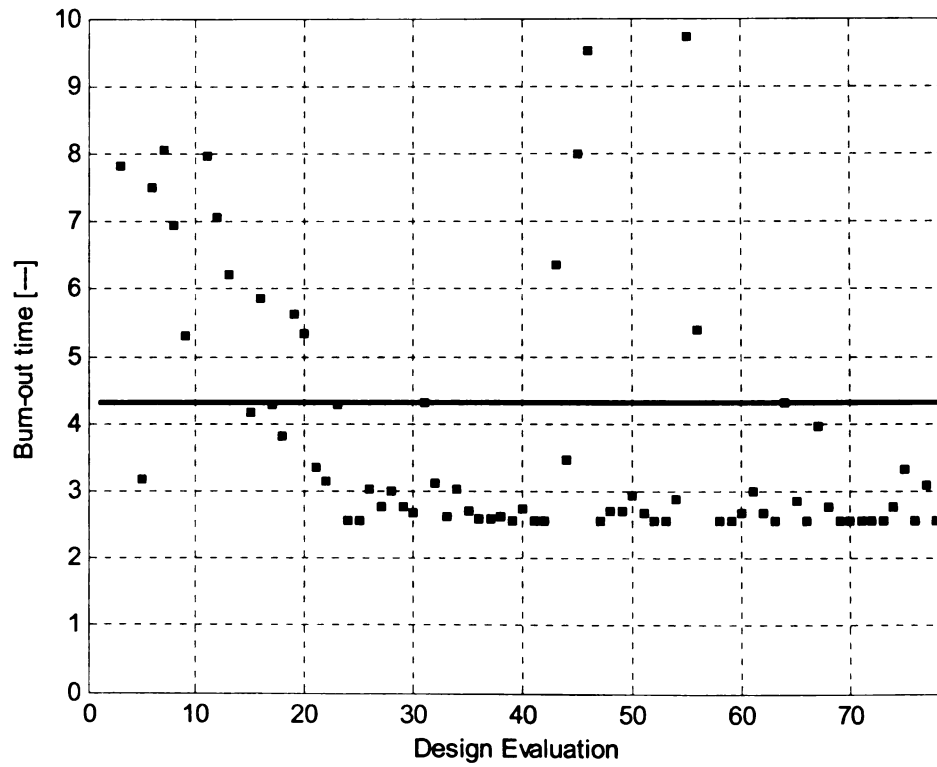


Figure 47. Burn-out time per design evaluation. The horizontal line represents the burn-out time for a propane droplet, i.e., the baseline design.

From Figure 47, it is apparent that in about the first twenty evaluations, HEEDS© found about as many “bad” designs as good designs, but by the 30th design, HEEDS© has converged. However, the minimal burn-out time for this run is not as small as for the previous run.

Between Table 3 and Table 4, the optimal gas constant is close to the minimum allowable value; the optimal latent heat is equal to the minimum allowable value; the optimal boiling temperature is also equal to the minimum allowable value. These results seem physically plausible for the reasons given in the previous section.

From the sensitivity analysis, it is known that the radius-squared exhibits a high level of sensitivity to the boiling temperature and a smaller level of sensitivity to the gas constant. Such a characteristic might explain why the gas constant required more evaluations to converge to its optimal value, whereas the boiling temperature converged to its optimal value relatively quickly.

5.4. Final Conclusions

Unfortunately, there was only sufficient time to thoroughly investigate two optimization runs. However, the results from the two runs seem to suggest a certain pattern which supports the sensitivity analysis.

Between the two optimization runs, the radius-squared was relatively insensitive to some parameters and sensitive to other parameters. The order of the radius-squared sensitivity is given in section 4.3.13. For the insensitive parameters (i.e., the parameters to which the radius-squared had relatively no sensitivity), HEEDS© seemed to converge

to their optimal values rather quickly. For the sensitive parameters (i.e., the parameters to which the radius-squared was sensitive), HEEDS© seemed to require slightly more evaluations to converge to their optimal values (if indeed optimal values exist). This stands to reason because if the radius-squared is insensitive to a given parameter, then that parameter would have minimal effect on the burn-out time; thus, that parameter could be assigned almost any value. Of course, this is only suggested by the current studies; more optimization studies would be necessary to verify this pattern.

Chapter 6: The Asymptotic Analysis

Due to the non-linearity of the governing equations, they must be solved numerically. However, if we consider a hypothetical fuel that possesses a high activation energy, i.e., $l_v \gg O(1)$, then it is possible to conduct an asymptotic analysis that might be analytically tractable. The purpose of the asymptotic analysis is to remove all but the most essential elements of a system so that the system is simplified but still illustrates the relevant physics.

When $l_v \gg O(1)$ (say that $l_v \sim 100$) and while the surface temperature (τ) is still increasing, it can be shown that the χ parameter is about constant. This would constitute the first interval in which the asymptotic analysis is conducted. As the surface temperature approaches the transition to its constant-value behavior, χ is still about constant; this is the second interval for the asymptotic analysis. These intervals are quantified in Figure 48. In this figure are plots of τ (the dimensionless surface temperature), ξ^2 (the dimensionless radius-squared) and the χ -parameter for a large l_v -value. For the remainder of this section, the dimensionless parameters take the following values:

$$\tau_0 = 0.3337; \tau_b = 0.7698; l_v = 97.21; \Omega = 10.91; \lambda = 0.893; \gamma = 1.126.$$

$$C \approx 0.009; K \approx 0.01; J \approx 1.005; B \approx 111.4; m \approx 112; U \approx -0.306.$$

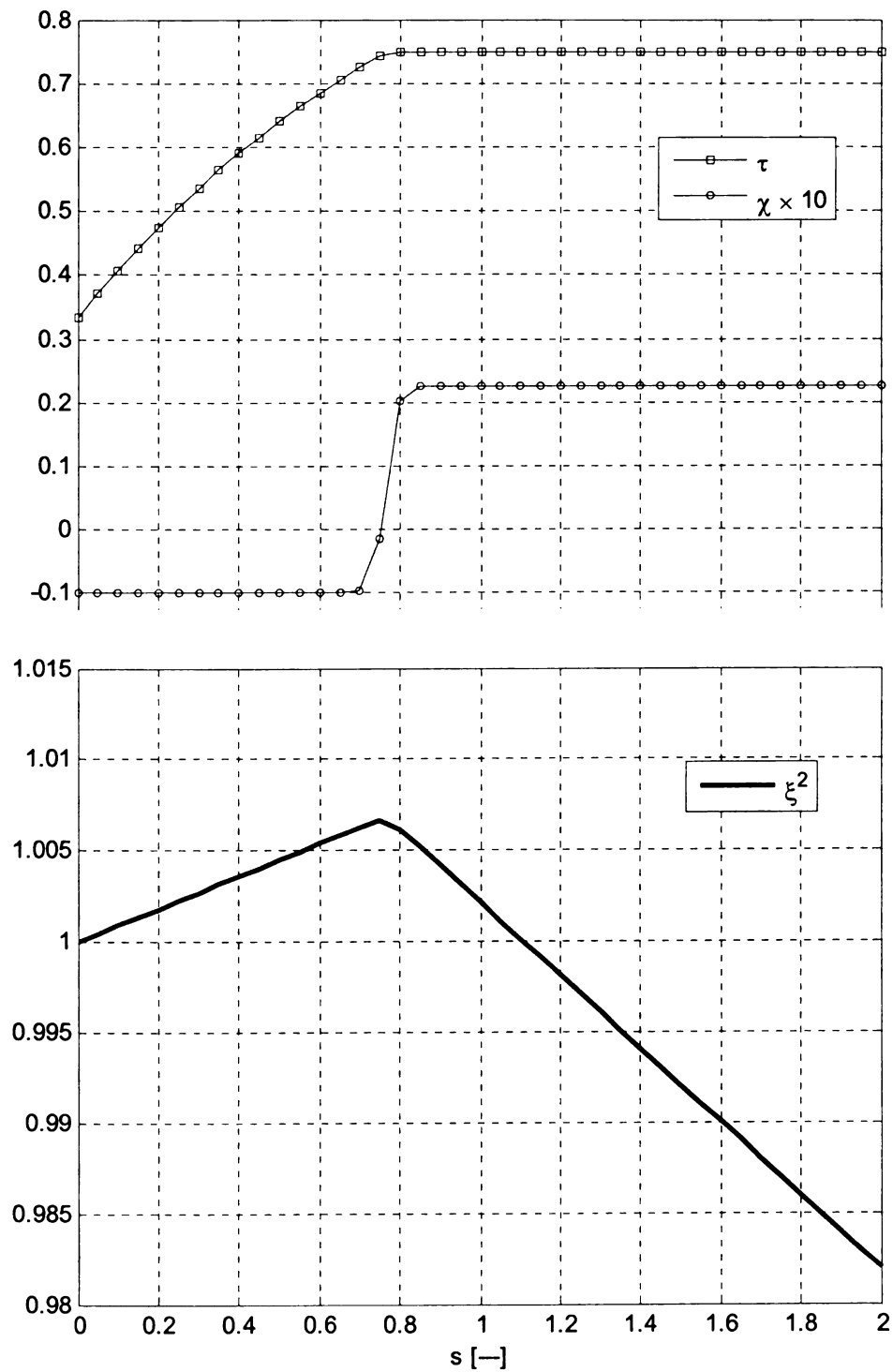


Figure 48. Solutions for the surface temperature, the radius-squared and the χ -parameter for a large latent heat. Note χ is 10 times larger for illustration purposes.

The first interval of the asymptotic analysis extends from $s = 0$ to just before ξ^2 attains its maximum value. The second interval extends from there to just before τ attains its constant-value behavior.

In the first interval of this limiting case, we have $\chi \approx -0.0101$. If we define $\chi = -K$ in this particular interval, and substitute this definition into equation (11.ii), then the solution for the dimensionless radius-squared is:

$$\xi^2 = 1 + Cs$$

On substitution of this expression into equation (11.i), the ordinary differential equation (which is now linear) is:

$$\frac{d\tau}{KB - J\tau} = \frac{ds}{1 + Cs}$$

Here, $C = \lambda K$, $B = \frac{1}{1 - e^{-K}} + \Omega$, $J = \frac{K}{1 - e^{-K}}$. It can be shown that the solution for the dimensionless surface temperature is:

$$\tau = \frac{KB}{J} \left\{ 1 - (1 + Cs)^{-2m} \right\} + \tau_0 (1 + Cs)^{-2m}$$

Here, $m = J/C$. These two solutions suggest that the dimensionless time variable, s , be scaled with C^{-1} , i.e., $\eta = Cs$; also, that the dimensionless surface temperature be scaled, i.e., $\Phi = \left(\frac{J\tau}{KB} \right)$. Thus, the radius-squared and the surface temperature can be expressed in the following ways:

$$\xi^2 = 1 + \eta$$

$$\Phi = 1 + U \xi^{-2m}$$

Here, $U = \left(\frac{J \tau_0}{K B} \right) - 1$. Figure 49 illustrates these two asymptotic solutions. From inspection, it is clear that as $s \rightarrow \infty$, $\Phi \rightarrow 1$. From Figure 46, the first interval extends to about $s = 0.6$. From the definition of η , the corresponding η -value is about 0.0054.

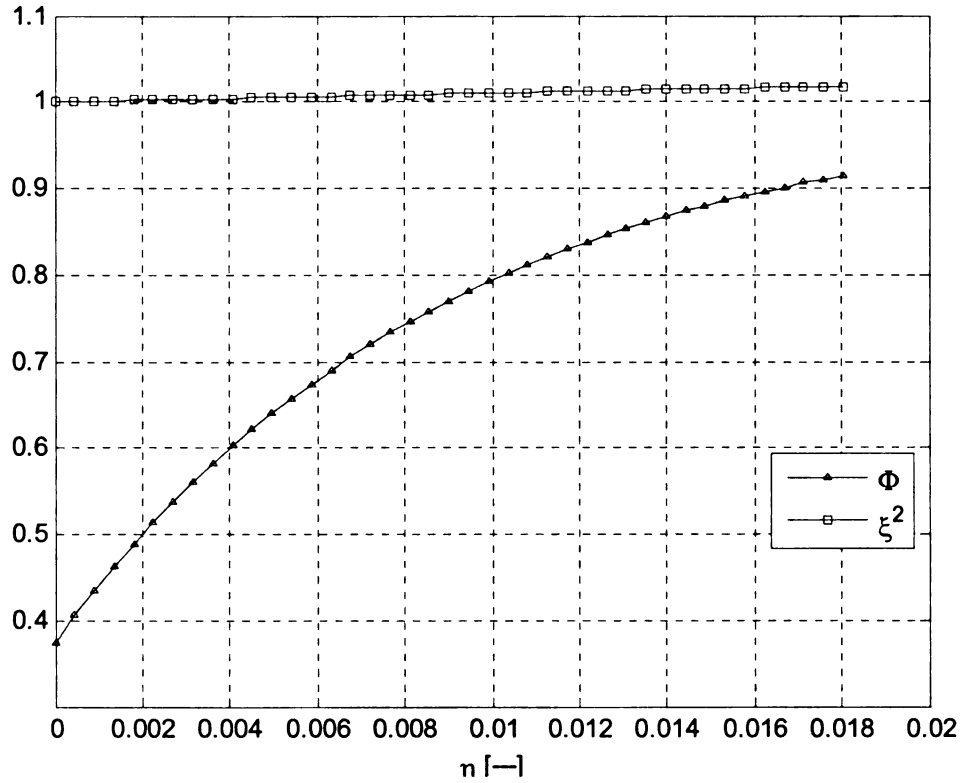


Figure 49. Asymptotic solutions for the interval of increasing surface temperature and radius-squared.

As the dimensionless surface temperature approaches its constant-value behavior, this first asymptotic analysis breaks down. Thus we start the second analysis in the next interval which begins at the instant ξ^2 attains its maximum value; at this instant, χ is still about equal to $-K$. In this particular analysis, $\xi^2(s_c \approx 0.75) = \xi_{max}^2 \approx 1.007$. We make the following definition:

$$\tau = l - \frac{\sigma}{l_v}$$

In the above expression, $\sigma = \sigma_0 + \frac{\sigma_1}{l_v} + \frac{\sigma_2}{l_v^2} + \dots$. Also, we expand s in the neighborhood of s_c , viz., $h = l_v(s - s_c)$. Thus, with the $\chi = -K$ approximation, and assuming l_v is large, we can integrate equation (11.ii) from $\xi^2(s_c)$ to $\xi^2(s)$; then we substitute the definition for h . The solution for ξ^2 is now the following:

$$\xi^2 - \xi_{max}^2 = \frac{\lambda K}{l_v} h$$

If we define $g(h) = h$, we can extract the following differential equations:

$$\frac{d\sigma}{dh} = \frac{\chi}{\xi_{max}^2} \left\{ \frac{\sigma}{l_v(1 - e^\chi)} + \Omega \right\}$$

$$\frac{dg}{dh} = -\frac{\chi}{K}$$

One advantage that the above system offers over the original system (equations (11.i-ii)) is that the σ -equation has no explicit dependence on the g -function. Additionally, it is clear from the definition of $g(h)$ that $g(0) = 0$; and that this occurs at the instant the radius-squared attain its maximum value. In order to acquire an initial condition for the σ -equation, we note that $\sigma = l_v(l - \tau)$. Thus, $\sigma(h = 0) = l_v(l - \tau(s = s_c))$. Consistent with the numerical values of the other parameters, $\sigma(0) \approx 25$. If the asymptotic definition of τ is substituted into equations (12.i-iii), we can approximate the χ -parameter with the following expression:

$$\chi = \frac{l}{Le_F} \ln \left(\frac{l - Y_{F\infty}}{l - Y_{Fb} e^{-\beta}} \right)$$

$$\beta = \left\{ \sigma / \tau_b - \left[l_v(l - \tau_b) / \tau_b \right] \right\}$$

The asymptotic solutions are shown in Figure 50, Figure 51, and Figure 52. From Figure 48, this analysis only applies from $s = 0.75$ to about $s = 0.85$; from the definition of the h -variable, the corresponding h -value is about 10.

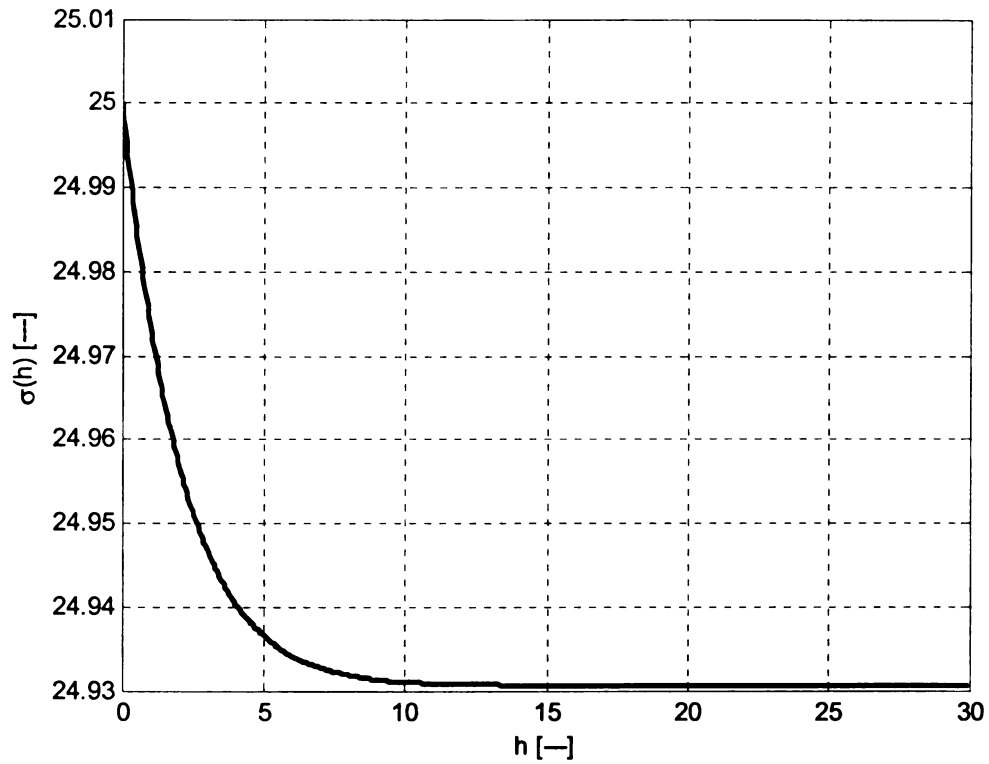


Figure 50. Asymptotic solution for the surface temperature in the vicinity of the maximum radius-squared.

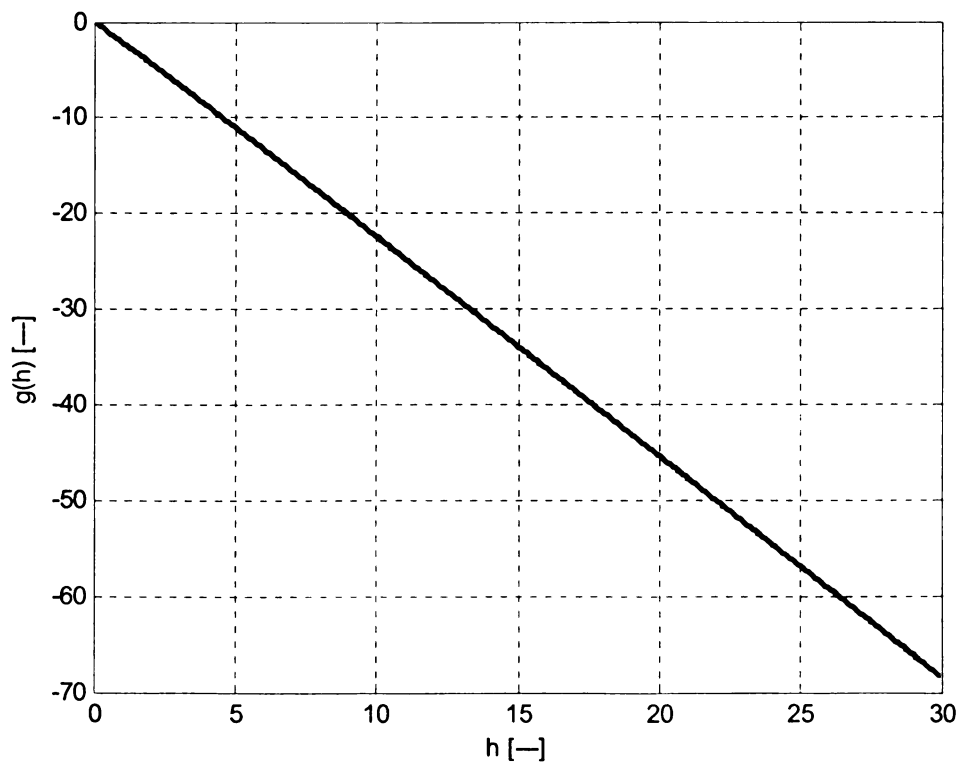


Figure 51. Asymptotic solution for the radius-squared in the vicinity of the maximum radius-squared.

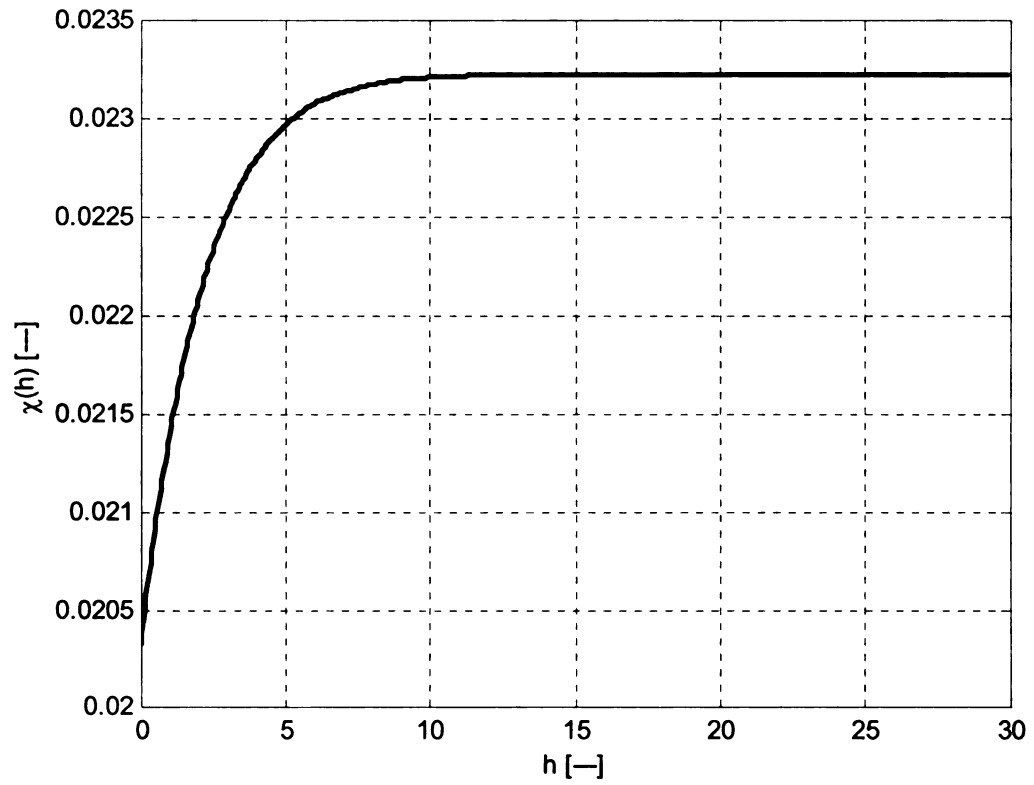


Figure 52. Asymptotic solution for the χ -parameter in the vicinity of the maximum radius-squared.

Chapter 7: Notes concerning the Computational Algorithms

The first issue that was problematic to this study was not realizing the importance of the θ parameter in the evaporation process. Essentially, if θ becomes greater than unity at some point in time, then evaporation is present. Specifically, it is the constant portion of θ that has the greatest relevance to the evaporation process.

The second issue was setting a final time, s_{final} , in order to provide a time interval in which the governing equations would be solved. At first, s_{final} was set to a value of 6 since the surface temperature reached its constant-value behavior around this time in many simulations. Then it seemed to be a simple matter to check if $\theta(s_{final}) > 1$; if so, then evaporation was present. However, it was discovered that for certain values of the physical parameters, total evaporation occurred before $s_{final} = 6$! This created havoc with the algorithm. This was resolved by setting an s -window from 0 to 400. Then, θ was computed until it reached its constant-value behavior.

The last noteworthy issue was that θ had two constant-value regions under certain conditions. Typically, the first constant-value region was less than unity. As the then-current algorithm was written, this first constant-value region of θ indicated to the rest of the algorithm that no evaporation was present when in fact evaporation was present! Thus, the algorithm was modified to read:

1. Compute $\theta_1 = \theta(s = 0)$.
2. Compute $\theta_2 = \theta(s = h)$.
3. Compute $\Delta\theta = \theta_2 - \theta_1$.
4. If $\Delta\theta \leq \Delta\theta_{max}$, then there is “flat behavior” toward the start of θ .
 - 4.a. $\theta_2 = \theta_1$; continue until $\Delta\theta > \Delta\theta_{max}$.
 - 4.b. At the instant $\Delta\theta > \Delta\theta_{max}$, $\theta_2 = \theta_1$.
 - 4.c. Continue on in computing θ_1 and θ_2 until $\Delta\theta > \Delta\theta_{tolerance}$.
5. If $\Delta\theta > \Delta\theta_{max}$, then there is no flat spot, so go to step 4.c.

Bibliography

- [1] Cengel, Y.A. & Boles, M.B. (2002) Thermodynamics: An Engineering Approach 4th ed. McGraw Hill Book Co.
- [2] Cheney, W. & Kincaid, D. (2004) Numerical Mathematics & Computing 5th ed. Thompson-Brooks/Cole
- [3] Dai, M., Perot, J.B., & Schmidt, D.P. (2002, September) “Heat Transfer within Deforming Droplets” Proceedings of ASME: Internal Combustion Engine Division, New Orleans
- [4] Dash, S. K., Sengupta, S. P., & Som, S. K. (1991) “Transport Processes & Associated Irreversibilities in Droplet Evaporation” J. Thermophysics & Heat Trans. Vol. 5, No. 3, pp. 366–373
- [5] Digilov, R., & Reiner, M. (2004) “Trouton’s rule for the law of corresponding states” Eur. J. Phys. Vol. 25, pp. 15–22
- [6] Ebbing, D.D. (1996) General Chemistry 5th ed. Houghton Mifflin Co.
- [7] Elperin, T. & Krasovitev B. (2006) “Transient Analysis for Sub-critical Evaporation of Fuel Droplet in Non-isothermal Stagnant Gaseous Mixtures: Effects of Radiation & Thermal Expansion” J. Heat and Mass Transfer Vol. 42, pp. 427–436
- [8] Ghassemi, H., Baek, S., & Khan, Q. (2006) “Experimental Study on Binary Droplet Evaporation at Elevated Pressures and Temperatures” Combust. Sci. and Tech. Vol. 178, pp. 1031–1053
- [9] Ha, V. & Lai, C. (2000) “The Onset of Stationary Marangoni Instability of an Evaporating Droplet” Proceedings of the Royal Society of London, pp. 885–909
- [10] Hegseth, J. J., Rashidnia, N., & Chai, A. (1996) “Natural Convection in Droplet Evaporation” Physical Review E, Vol. 54, Issue 2, pp. 1640–1644

- [11] Hiwase, S.D., Datta, A., & Som, S.K. (1998) "Entropy Balance & Exergy Analysis of the Process of Droplet Combustion" J. Phys. D: Applied Physics Vol. 31, pp. 1601–1610
- [12] Hornbeck, R.W. (1975) Numerical Methods Quantum Publishers, Inc.
- [13] Incropera, F.P. & DeWitt, D.P. (2002) Introduction to Heat Transfer 4th ed. John Wiley & Sons
- [14] Kays, W. M. (1966) Convective Heat & Mass Transfer McGraw Hill Book Co.
- [15] Kozyrev, A.V. & Sitnikov, A.G. (2001) "Evaporation of a Spherical Droplet in a Moderate-pressure Gas" Uspekhi Fizicheskikh Nauk., Vol. 44, pp. 725–733
- [16] Poinso, T. & Veynante, D. (2001) Theoretical and Numerical Combustion R.T. Edwards, Inc.
- [17] Potter, M.C. & Wiggert, D.C. (2002) Mechanics of Fluids 3rd ed. Thompson-Brooks/Cole
- [18] Sherwood, T.K., Pigford, R.L., & Wilke, C.R. (1975) Mass Transfer McGraw Hill Book Co.
- [19] Sirignano, W.A. (1999) Fluid Dynamics & Transport of Droplets & Sprays Cambridge University Press
- [20] Som, S. K., & Dash S. K. (1993) "Thermodynamics of Spray Evaporation" J. Phys D: Appl. Phys. Vol. 26, pp. 574–584
- [21] Spalding, D. B. (1959) "A Standard Formulation of the Steady Convective Mass Transfer Problem" Int. J. Heat Mass Transfer, Vol. 1, pp. 192–207
- [22] Turns, S.R. (2000) An Introduction to Combustion: Concepts and Applications 2nd ed. McGraw Hill Book Co.

- [23] Vargaftik, N. B., Vinogradov, Y. K., & Vargion, V. S. (1996) Handbook of Physical Properties of Liquids and Gases 3rd ed. Begell House, INC

- [24] Wichman, I.S. Notes on Droplet Combustion Dept. of Mechanical Engineering, Michigan State University

- [25] Williams, F.A. (1985) Combustion Theory 2nd ed. The Benjamin/Cummings Publishing Company, INC.

- [26] Tseng, C. C. & Viskanta, R. (2004) "Effect of Radiation Absorption on Fuel Droplet Evaporation" Combustion Science & Technology, Vol. 177, No. 8, pp. 1511–1542

- [27] Zhu, G. S. & Aggarwal, S.K. (2002) "Fuel Droplet Evaporation in a Supercritical Environment" J. Engineering for Gas Turbines and Power, Vol. 124, pp. 762–770

- [28] HEEDS User Manual
(MSU UNIX path: /opt/soft/heeds-4.1/manuals/usersman.pdf)
Red Cedar Technology, 4572 S. Hagadorn Rd., Suite 1- E, E. Lansing, MI 48823,
www.redcedartech.com

- [29] Gunnar Norman's homepage <http://www4.tsl.uu.se/~norman>
The Svedberg Laboratory, Box 533, S-75121 Uppsala, Sweden

- [30] <http://www.princeton.edu/~fldryer/nasa.dir/backgrnd.htm>
"General Background for Spherically Symmetric Isolated Droplet Combustion"
Dr. Frederick L. Dryer, Dept. of Mechanical and Aerospace Engineering, D-316
Engineering Quadrangle, Princeton University, Princeton, NJ 08544

MICHIGAN STATE UNIVERSITY LIBRARIES



3 1293 02845 6758